THE DESIGN AND CONTROL OF ACTIVE ANKLE-FOOT ORTHOSES

BY

KENNETH ALEXANDER SHORTER

DISSERTATION

Submitted in partial fulfillment of the requirements
for the degree of Doctor of Philosophy in Mechanical Engineering
in the Graduate College of the
University of Illinois at Urbana-Champaign, 2011

Urbana, Illinois

Doctoral Committee:

Associate Professor Elizabeth Hsiao-Wecksler, Chair
Professor William Durfee, University of Minnesota
Professor Karl Rosengren
Associate Professor Srinivasa Salapaka
Dr. Geza Kogler, Georgia Institute of Technology

Abstract

Ankle foot orthoses (AFOs) can be used to ameliorate the impact of impairments to the lower limb neuromuscular motor system that affect gait. Existing AFO technologies include passive devices with fixed and articulated joints, semi-active devices that modulate damping at the joint and active devices that make use of a variety of technologies to produce power to move the foot. Emerging technologies provide a vision for fully powered, untethered AFOs. In this dissertation, a novel portable powered ankle-foot orthosis (PPAFO) cabable of providing un-tethered assistance during gait is presented. The PPAFO provides both plantarflexor and dorsiflexor torque assistance via a bi-directional pneumatic rotary actuator. The system uses a portable pneumatic power source (compressed CO2 bottle) and embedded electronics to control the motion of the foot. Experimental data from two impaired and five healthy subjects were collected to demonstrate design functionality. The impaired subjects had bilateral impairments to the lower legs that caused weakness to the plantarflexors, in one case, and to the dorsiflexors in the other. Data from the healthy walkers demonstrated the PPAFO's capability to provide correctly timed plantarflexor and dorsiflexor assistance during gait. The results from the impaired subjects demonstrated the PPAFO's ability to provide functional assistance during gait. Additionally, this dissertation presented a modeling and control approach to address limitations present in the PPAFO through the introduction of a new hardware configuration and new control architecture. A combined model consisting of both the PPAFO and the human foot and shank segments was first derived and validated. Next, the current and the new PPAFO system

configurations were evaluated both in simulation and experimentally during three simplified functional gait tasks: (1) motion control of the foot at the start of the gait cycle, (2) plantarflexor torque assistance during late stance, and (3) dorsiflexor position control of the foot during swing. The resulting analysis showed that the new system configuration both outperformed and was more efficient than the current PPAFO configuration. The stringent design requirements of light weight, small size, high efficiency and low noise make the creation of daily wear assist devices challenging, but once such devices appear they will present new opportunities for clinical treatment of gait abnormalities.

Dedication

To Kira, Adelynn and my fantastic family!

Acknowledgements

This work was supported by National Science Foundation grant #0540834 and the Center for Compact and Efficient Fluid Power, an NSF Engineering Research Center. I would also like to thank Professor Andrew Alleyne, Professor Eric Loth, Professor Tim Bretl, Kira Barton, Yifan (David) Li, Emily Morris, Aaron Becker, Henry Kohring, Jason Thomas, Joel Gilmer, Anastasia Borok, Richard Kessler, Enric Xargay, Dave Hoelzle, Louis DiBerardino, my HDCL lab mates, my committee members, and the investigators in the Comparative Neuromechanics Laboratory at Georgia Tech (Prof. Young-Hui Chang, Megan Toney, and Jasper Yen) for their assistance with this work.

Table of Contents

LIST OF TABLES……ix

LIST OF FIGURES……xi

CHAPTER 1 INTRODUCTION 1

1.1 Motivation 1

1.2 Dissertation Overview 3

CHAPTER 2 TECHNOLOGIES FOR POWERED AFOS: POSSIBILITIES AND CHALLENGES* 5

2.1 Introduction 5

2.2 Motivation 6

2.3 Normal and Pathological Gait 7

2.4 Existent Passive and Active AFO Designs 11

2.4.1 Passive AFO Designs 11

2.4.2 Active and Semi-Active AFO Designs 18

2.5 Discussion 28

CHAPTER 3 A PORTABLE POWERED ANKLE-FOOT ORTHOSIS FOR REHABILITATION* 35

3.1 Introduction 35

3.2 Methods 38

3.2.1 PPAFO System Description 39

3.2.2 Empirical Testing of PPAFO Functional Performance during Gait 46

3.3 Results 49

3.3.1 PPAFO System Performance Characteristics 49

3.3.2 Functional Walking Results 52
3.4 Discussion 56
3.5 Conclusion 60
CHAPTER 4 EXPERIMENTAL EVALUATION OF THE PPAFO 62
4.1 Introduction 62
4.2 Methods 64
4.2.1 System Description Hardware and Control 64
4.2.2 Subject Information 65
4.2.3 Experimental Procedure and Data Collection 66
4.2.4 Data Analysis 68
4.3 Results 73
4.3.1 Results from the Healthy Walkers 73
4.3.2 Results from ISubPF 83
4.3.3 Regions of Deviation Analysis 86
4.3.4 Results from ISubDF 88
4.4 Discussion 92
4.5 Conclusion 96
CHAPTER 5 MODELING, ANALYSIS AND CONTROL OF A POWERED ANKLE-FOOT ORTHOSIS 97
5.1 Introduction 97
5.2 Modeling, System Identification, and Model Validation 100
5.2.1 PPAFO System Hardware 100
5.2.2 Modeling of the PPAFO-Leg System 102
5.2.3 PPAFO-Leg Model Validation 112
5.3 Model-Based System Analysis and Control Design 114
5.3.1 Description of Functional Tasks Required for Gait 115
5.3.2 PPAFO Control Design 118
5.3.3 Experimental and Simulation Results 120
5.4 Discussion 125
5.5 Conclusion 126

CHAPTER 6 CONCLUSIONS AND FUTURE DIRECTION 128

6.1 Conclusions 128

6.2 Future Work 131

6.2.1 Improving the Efficiency of the Current System 132

6.2.2 The Next Generation PPAFO System 132

6.2.3 Improved Control of the PPAFO 133

6.2.4 Continued Subject Testing 135

LIST OF REFERENCES 136

List of Tables

Table 2.1 *A comparison of weight, torque, advantages, disadvantages, performance metrics, and effectiveness of the novel passive AFO designs described in Section 2.4.* 33
Table 2.2 *A comparison of weight, torque, advantages, disadvantages, performance metrics, and effectiveness of the novel Active and Semi-Active AFOs designs described in Section 2.4*.....34
Table 4.1 *Healthy subject joint range of motion, mean (and standard deviation), for each speed and footwear condition. N unitless ROM symmetry index (SI) between the bilateral joint pairs was calculated for each joint pair. A negative SI indicates that the parameter value for the left side was greater than the right.* 74
Table 4.2 *Healthy subject, mean (and standard deviation), values for step length, cycle time, stance time, and step width for all speed and footwear conditions. A unitless symmetry index (SI) was also calculated for the bilateral parameters. A negative SI indicates that the parameter value for the left side was greater than the right.* 75
Table 4.3 *Peak moment and powers and associated % gait cycle timing for the left ankle joint.* 76
Table 4.4 *Peak moment and powers and associated % gait cycle timing for the right ankle joint.*.....77
Table 4.5 *Mean (and standard deviation) values of complexity and variability separated by body segment, side of the body, and footwear condition at the normal walking speed.* 81
Table 4.6 *Mean (and standard deviation) values of complexity and variability separated by body segment, side of the body, and walking speed for shoe walking.* 82
Table 4.7 *Mean (and standard deviation) values of complexity and variability separated by body segment, side of the body, and walking speed for PPAFO assisted walking*.....83
Table 4.8 *ISubPF joint range of motion, mean (and standard deviation), for shoe and PPAFO footwear conditions. A symmetry index (SI) between the bilateral joint pairs was calculated for each joint. A negative SI indicates that the parameter value for the left side was greater than the right*.....84

Table 4.9 *ISubPF mean (and standard deviation), values for step length, cycle time, stance time, and step width for shoe and PPAFO footwear conditions. A symmetry index (SI) was also calculated for the bilateral parameters. A negative SI indicates that the parameter value for the left side was greater than the right.* 84
Table 4.10 *Mean (and standard deviation) values of complexity and variability separated by body segment, body side, and footwear condition for the plantarflexor impaired subject (ISubPF).* 88
Table 4.11 *ISubDF joint range of motion, mean (and standard deviation), for shoe and PPAFO footwear conditions. A symmetry index (SI) between bilateral joint pairs was calculated. A negative SI indicates that the parameter value for the left side was greater than the right.*.....89
Table 4.12 *ISubDF mean (and standard deviation), values for step length, cycle time, stance time, and step width for shoe and PPAFO footwear conditions. A symmetry index (SI) was also calculated for the bilateral parameters. A negative SI indicates that the parameter value for the left side was greater than the right.*.....89
Table 5.1 *Proportional valve PID gains for the three task controllers.* 119
Table 5.2 *Performance of the proportional and solenoid valves during the three functional tasks*.....120

List of Figures

Figure 1.1 *A commercially available passive AFO from Becker Orthopedic [3]. This device restricts the motion of the foot and provides structure and support for the user during gait.*.....2

Figure 2.1 *A gait cycle is defined from heel strike to heel strike and further divided into multiple phases defined by functional tasks [1]. Ankle-foot orthoses assist gait by controlling motion during stance and swing (dorsiflexor assistance) or by providing assistive torque during stance (plantarflexor propulsive torque).*.....8

Figure 2.2 *Healthy sagittal-plane power generation (positive) and absorption (negative) at the ankle, knee, and hip joints normalized to body weight and percentage of the walking cycle. Solid lines are normalized inter-subject averages, while dotted lines show one standard deviation about the average [8].* 9

Figure 2.3 *Passive AFO designs. (A) Metal and leather AFO; (B) Posterior leaf spring AFO; (C) Hybrid AFO with a linear spring and thermoplastic AFO; (D) Pneumatically assisted Pumaflex AFO. From [3, 16-18].*.....12

Figure 2.4 *Energy harvesting passive AFO designs. (A) The Illinois power-harvesting AFO; (B) The Osaka University AFO; (C) Kanagawa Rehabilitation Center AFO. From [22-24].*.....16

Figure 2.5 *Semi-active AFO designs. (A) The Oksaka magneto rheology (MR) damper AFO and torque amplifying mechanical linkage; (B) The Halmstad magneto rheology (MR) damper AFO;-(C) The MIT Active AFO powered by a series elastic actuator. (D) The Arizona State AFO powered by a modified series elastic actuator. From [28-31].*.....20

Figure 2.6 *Tethered active AFO designs. (A) University of Michigan AFO powered by pneumatic muscles; (B) Arizona State University Robotic Gait Trainer with spring over muscle pneumatic actuators; (C) A mechanical drawing of the hydraulically powered CIRRIS AFO; (D) MIT AnkleBot shown with the two front mounted DC-motor-powered linear actuators. From [41-44].*.....27

Figure 3.1 *First prototype of the PPAFO. The rotary actuator is powered using a compressed CO_2 bottle (far right) worn by the subject on the waist.* 37

Figure 3.2 *The cycle is divided into multiple phases defined by functional gait tasks [1]. The Portable Powered Ankle-Foot Orthosis (PPAFO) assists gait by providing assistive dorsiflexor torque at heel strike to prevent foot slap (1. darker grey shading), plantarflexor torque during stance to assist propulsion (3. Lighter grey shading), and dorsiflexor torque during swing to control foot motion (4. Darker grey shading). No assistance from the PPAFO is provided during mid stance (2. White shading).* 39

Figure 3.3 *PPAFO force sensor data are used to identify the current gait event. The initiation of the event determines the corresponding valve configuration, which dictates the type and direction of torque assistance.* 43

Figure 3.4 *(A): Experimental determination of output torque generation of the PPAFO system as a function of input pressure. Pressure was increased in 5 psig (0.034 MPa) increments (denoted as* X*) to 90 psig (0.621 MPa) and then decreased in 5 psig increments from 95 psig (0.655 MPa) (denoted as* O*). The torque increased linearly with pressure as noted by slope $K_{actuator}$. (B): Positional step response of the PPAFO system. Valve activation (t_0), initiation of rotation (t_1), and the cessation of rotation (t_2) are shown in the plot. Average response of the unloaded (solid) and load (dashed) system. (C): Average footplate force sensor data (78 cycles) from a healthy subject. Data were normalized to percent gait cycle with toe off occurring at 60% of the cycle.* 51

Figure 3.5 *Averaged data (25 gait cycles) from a healthy walker at self-selected walking speed with a peak assistive torque of 9.2 Nm from an operating pressure of 90 psig. The data were normalized to stance and swing with toe off occurring at 60%.* 53

Figure 3.6 *Averaged data (25 gait cycles) for the tibialis anterior from a healthy walker at self-selected walking speed with and without assistance. The subject walked with 90 psig plantarflexor assistance and 30 psig dorsiflexor assistance. A visible decrease in activation level is present in the EMG data from the sensor placed on the tibialis anterior. The data were normalized to stance and swing with toe off occurring at 60%.* 54

Figure 3.7 *One gait cycle from the impaired subject with a peak assistive torque of 9 Nm from an operating pressure of 90 psig. The data were normalized to percent gait cycle.*.....55

Figure 4.1 *Mean sagittal plane joint angle data for the ankle, knee, and hip. Data were collected from the healthy subjects at their normal, fast, and slow walking speeds. Data from the 30 second walking trials from each subject for each condition were first normalized and then*

averaged over the five subjects. For the normal trial, right and left toe off occur at 65% of the cycle. For the fast trial, right toe off occurs at 63% and left toe off at 64% of the cycle. For the slow trials, right toe off occurs at 67% and left occurs at 68% of the cycle. 70
Figure 4.2 *Representative phase portraits from Healthy Subject 05. Sagittal plane foot, shank, and thigh segment angles and velocities from the three footwear conditions at normal walking speeds are shown. Only five of the 20 consecutive cycles are shown for clarity.* 72
Figure 4.3 *Healthy walker average left ankle moments and powers for the three footwear conditions and three walking speeds.* 76
Figure 4.4 *Healthy walker average right ankle moments and powers for the three footwear conditions and three walking speeds.* 77
Figure 4.5 *Left Panels: SROD values for the healthy subjects' during the shoe walking trials that illustrate normative levels of asymmetry in the joint angle data. Right Panels: SROD values during the PPAFO assisted walking trials. These plots illustrate the asymmetries in the joint angle data of the healthy subjects during PPAFO assisted walking.* 79
Figure 4.6 *Left and right IROD values for the normal, fast, and slow PPAFO assisted trials*.....80
Figure 4.7 *Average anterior-posterior (AP), medial-lateral (ML), and vertical ground reaction force (GRF) data for ISubPF during PPAFO assisted and shoe walking trials. Positive AP-GRF data indicates forces directed towards the anterior direction, while negative ML-GRF data indicates forces directed towards the right side of the subject. Average toe off for each condition is indicated by a circle.*.....85
Figure 4.8 *Average right ankle moments (Top) and powers (Bottom) for the assisted and shoe walking trials for ISubPF. Positive moment values are in the plantarflexion direction. Average toe off for each condition is indicated by a circle.* 86
Figure 4.9 *ISubPF Symmetry ROD values calculated for the ankle joint during shoe and PPAFO assisted walking*.....87
Figure 4.10 *Average left and right ankle IROD values for the shoe walking and PPAFO assisted trials for the subject with the impaired plantarflexors (ISubPF), bottom left and bottom right respectively. The subject's average left and right ankle joint angles are plotted against normative data for comparison in the top left and right plots.* 87
Figure 4.11 *Average right and left ankle joint angles for the shoe walking and PPAFO assisted trials for subject ISubDF, top and bottom respectively.* 90
Figure 4.12 *ISubDF Symmetry ROD values calculated for the ankle joint during shoe and PPAFO assisted walking*.....91

Figure 4.13 *Average left and right ankle IROD values for the shoe walking and PPAFO assisted trials for subject ISubDF, bottom left and bottom right respectively. The subject's average left and right ankle joint angles are plotted against normative data for comparison in the top left and right plots.* 91

Figure 5.1 *The portable powered ankle-foot orthosis (PPAFO). The rotary actuator (A) is powered using a compressed CO_2 bottle (B) worn by the subject on the waist. Onboard electronics (C), force sensors (D), and an angle sensor (E) are used to control the solenoid valves (F). A second pressure regulator (G) is used to modulate the magnitude of the dorsiflexor assistance.* 98

Figure 5.2 *Current binary control scheme used with the solenoid valves. PPAFO sensor data are used to identify the current gait event and open/close the corresponding valve.* 99

Figure 5.3 *The PPAFO pneumatic actuation system included a dual-vane rotary actuator, a solenoid or proportional valve, pneumatic lines, and the AFO footplate (not shown). The solid lines in the valve indicate the connected configuration. Port 1 is connected to the source (regulated CO_2 bottle) Port 2 is connected to atmosphere. Pneumatic pressure builds in chamber 1, while chamber 2 remains at atmospheric pressure. The resulting pressure differential creates rotational actuator torque (clockwise). Hard stops prevent the vane from rotating more than 90 degrees. Leakage occurs between chambers ($\dot{m}_{leak}$). Additional symbols are defined in the text.* 104

Figure 5.4 *Left panel: experimental determination of $K_{actuator}$. Measurements were taken as the pressure in the actuator chamber was increased by 5 psig (0.034 MPa) increments (denoted as X) to 90 psig (0.621 MPa) and then decreased by 5 psig increments back to 0 psig (denoted as O). The average of three sets of measurements was used to determine $K_{actuator}$. Right panel: experimental determination of rotary damping ratio β. The ratio between the angular acceleration and the angular velocity is proportional to β,* i.e., $\alpha/\omega = -\beta / I_{zz}$, *where α is angular acceleration and ω is angular velocity.* 108

Figure 5.5 *The two-link rigid body leg model is coupled to the PPAFO through the applied external torque T_{ex}.* 111

Figure 5.6 *Simulated and experimental open-loop coupled PPAFO-Leg system response to a step function with the proportional valve. (A) The vane angle increased through the actuator's full range of motion (110 deg); (B) the pressure differential driving the actuator; (C) the pressure response in the first chamber (P_1); (D) the pressure (P_2) in the second chamber fell as the vane rotated. Experimental and simulated results compare well.* 113

Figure 5.7 *Proposed control architecture that makes use of separate PID controllers to accomplish three functional gait tasks by tracking different variables.* 115
Figure 5.8 *The coupled model was used to compare the performance and efficiency of PPAFO hardware configurations and associated control algorithms during three functional tasks: (A) prevention of foot slap, (B) propulsive torque assistance, and (C) prevention of foot drop.* 117
Figure 5.9 *Experimental and simulation results during functional task 1, motion control of the foot during initial contact to prevent foot slap. The proportional valve (bottom panel) significantly outperformed the solenoid valve (top panel) during this task. Note that simulated results capture the behavior of the system and are comparable to the experimental results.* 122
Figure 5.10 *Experimental and simulation results for both valve configurations during the second task, propulsive torque assist during stance. The system configured with the proportional valve (bottom panel) tracked the reference trajectory better than the solenoid valve (top panel), particularly during the initial ramp. The simulated results for both valve configurations agree well with the experimentally collected data.* 123
Figure 5.11 *Experimental and simulation results for the third functional task, motion control of the foot during swing to prevent foot drop. The solenoid valve (top panel) was not able to track this reference input. The proportional showed some difficulties, as evident by the large overshoot and long settling time, but had much better performance as compared to the solenoid valve. Both the modeled systems show good agreement with the experimental results.* ... 124

Chapter 1
INTRODUCTION

1.1 Motivation

For most people, walking is a fundamental part of one's daily routine and a key component in overall quality of life. The efficiency and effectiveness of gait depends on joint mobility and muscle activity, which are both selective in terms of timing and intensity [1]. The forces and motions generated during gait are attributed to three main functional tasks: weight acceptance, single limb support, and limb advancement. Weight acceptance and single limb support occur during stance when the foot is in contact with the ground, whereas limb advancement takes place during swing when the foot is off the ground. The ability to walk can be impaired by injuries, as well as numerous neurological and muscular pathologies [1]. In the United States alone, sizable populations exist with these impairments: stroke (4.7M), polio (1M), multiple sclerosis (400k), spinal cord injuries (100k), and cerebral palsy (100K) [2]. These types of lower limb impairments are frequently treated with ankle-foot orthoses (AFOs) as a means of improving functionality during gait.

An AFO is an external device worn on the lower leg and foot to support the ankle and control the motion of the foot. AFOs can be divided into three groups: passive, semi-active, and active. Figure 1.1 shows an example of a traditional passive AFO commonly used in clinical rehabilitation applications. Passive devices do not contain electronics or active control mechanisms. However, they do often have mechanical elements such as springs or dampers,

which enable motion control of the ankle joint during gait. Semi-active AFOs use computer control to vary the compliance or damping of the joint in real-time. Fully active AFOs typically have onboard or tethered sources of power, one or more actuators to move the joint, sensors, and a computer or onboard electronics used to control the application of assistance during gait.

Figure 1.1 *A commercially available passive AFO from Becker Orthopedic [3]. This device restricts the motion of the foot and provides structure and support for the user during gait.*

Passive AFOs are generally characterized as being customizable, lightweight, compact, and relatively inexpensive devices. As a result, passive AFOs make up the majority of the devices prescribed by clinicians to treat weakness at the ankle joint complex. Despite their popularity, the inability to provide assistive torque during gait limits the functional benefit of passive AFOs. To address this limitation, current research efforts are now being directed towards the development of active AFOs. Recent advances in electronics, sensing, and other enabling technologies have contributed to the growth of active AFOs in existence today. Despite noticeable improvements in functional assistance, active AFOs exhibit a limitation in that they

currently only exist in laboratory or clinical settings where they are tethered to off-board power sources and computers.

The development of a lightweight, compact, efficient, powered, untethered AFO has the potential to yield significant advancements in orthotic control mechanisms and new clinical treatment strategies for rehabilitation and daily assistance. The goal of the work presented in this dissertation was to develop, test, and evaluate a novel ***untethered*** active AFO to assist the gait of individuals with below the knee muscle weakness.

1.2 Dissertation Overview

The body of the dissertation is divided into five chapters (2-6). Chapter 2 motivates the need for AFOs, describes current state-of-the-art AFO technology, and identifies technological challenges facing the development of an untethered active AFO. The conclusions from this chapter highlight a few key technological advances necessary for the creation of an untethered AFO capable of providing active assistance in a variety of walking conditions. Specifically, the design must be aimed at reducing the size and weight of the device, while simultaneously increasing the efficiency of the power supply and actuators. These objectives directly motivated the work in the remaining chapters.

Chapter 3 introduces the design of a novel portable powered ankle-foot orthosis (PPAFO) capable of providing untethered assistance during gait. The PPAFO provides both plantarflexor and dorsiflexor torque assistance via a bi-directional pneumatic rotary actuator. The system uses a portable pneumatic power source (compressed CO_2 bottle) and embedded electronics to control the actuation of the foot. Pilot experimental data from one impaired and three healthy subjects demonstrated functionality, as well as the ability to provide functional plantarflexor assistance.

Chapter 4 further characterizes the performance of the PPAFO with experimentally collected data from both healthy and impaired subjects. Data from a subject with a dorsiflexor impairment and two additional healthy subjects were added to the data set from Chapter 2. This larger data set and an expanded set of gait analysis metrics were used to examine the biomechanical effect that the PPAFO had on the gait of both healthy and impaired walkers. Additionally, the performance of the PPAFO during changing gait speeds is examined in this chapter.

Chapter 5 presents simplified models of both the orthosis and the lower leg (shank and foot) to assist in the development of improved control schemes and the design of future devices. The PPAFO provided both motion control and external torque assistance at the ankle via a binary, event-based control scheme that used solenoid valves. While stable, this design approach limited the overall performance of the system. The use of computational models of the PPAFO-Leg system, combined with the introduction of a proportional valve and new control architecture, resulted in performance and efficiency improvements for the PPAFO. Finally, Chapter 6 discusses concluding thoughts and ideas about the future direction of the work presented in this dissertation.

Chapter 2

TECHNOLOGIES FOR POWERED AFOS: POSSIBILITIES AND CHALLENGES*

2.1 Introduction

Ankle-foot orthoses (AFOs) can be used to ameliorate the impact of impairments to the lower limb neuromuscular motor system that affect gait. Existing AFO technologies include passive devices with fixed and articulated joints, semi-active devices that modulate damping at the joint, and active devices that make use of a variety of technologies to produce torque for motion control and propulsive assistance. Emerging technologies provide a vision for fully powered, untethered AFOs. However, stringent design requirements such as lightweight, small size, high efficiency, and low noise present significant engineering challenges that must be met before such devices can be realized. Once such devices appear, they will present new opportunities for clinical treatment of gait abnormalities.

This remainder of this chapter motivates the need for ankle-foot orthotic devices, introduces state-of-the-art passive, semi-active, and active AFO systems, and finally presents a discussion of enabling solutions to technological barriers currently preventing the creation of a portable powered AFO system.

*This chapter is based on reference [54].

2.2 Motivation

Biomechanical deficits of the lower extremities and their related pathologies affect joint mobility and muscle activity. The work in this dissertation focuses on the treatment of lower limb deficiencies with ankle-foot orthoses (AFOs). More specifically, the purpose of this chapter is to present the background and rationale for developing new technologies for use in fully powered, untethered AFOs.

AFOs can be divided into three groups: passive, semi-active, and active. Passive devices contain no active control or onboard electronics, but can have mechanical elements such as springs or dampers to help direct the motion of the ankle joint during gait. Semi-active devices use computer control to vary the compliance or damping of the joint in real-time. Fully active devices have onboard or tethered sources of power, actuators to move the joint, sensors, and a computer or electronics to control the application of torque during gait. Passive AFOs are the most common devices prescribed by clinicians to treat weakness at the ankle joint complex. However, the passive and therefore limited nature of these AFOs minimizes the functional benefits they are capable of providing. This fundamental limitation can be addressed with the use of an active AFO. Although recent technological advances have spurred the development of active AFOs, there are currently no portable powered untethered AFO systems in existence.

The development of a novel untethered active AFO system could provide significant improvements to gait assistance. Additionally, an untethered device has the potential to generate new clinical treatment strategies for rehabilitation and daily assistance. A recent review by Dollar and Herr describes work in lower extremity exoskeletons and active orthoses [2]. The purpose of this chapter is to provide a comprehensive review of the state-of-the-art in ankle-foot

orthotic technology and describe the significant technical challenges that remain for AFOs. The remainder of this chapter consists of an overview of the biomechanics of normal and pathological gait, reviews of existing passive and active AFO devices, and a discussion on the key enabling technologies required to meet this challenging human scale application.

2.3 Normal and Pathological Gait

Limb motion during steady-state constant speed locomotion involves inter-segment and inter-limb interactions for both normal and abnormal walking [4]. Each limb segment and joint undergoes a cyclic pattern of flexion, extension, rotation, abduction, and adduction during a stride. An acute injury or pathology that affects a lower limb segment disrupts the cyclic gait pattern and can result in asymmetric deviations during gait [1]. An abnormal gait cycle affects the normal energy conserving characteristics of walking, resulting in increased energy expenditure [5].

During normal gait, the ankle joint, shank, and foot play important roles in all aspects of locomotion including: motion control, shock absorption, stance stability, energy conservation, and propulsion. The gait cycle is defined from the initial contact of the heel to the following heel contact as illustrated in Fig. 2.1. At the initiation of the gait cycle, impact forces are dissipated as energy is absorbed by the soft tissues at the heel as the foot comes into contact with the ground [6]. Additionally, the muscles and tendons of the ankle joint complex dissipate energy (i.e., brake) by decelerating the foot before full contact with the ground at foot flat.

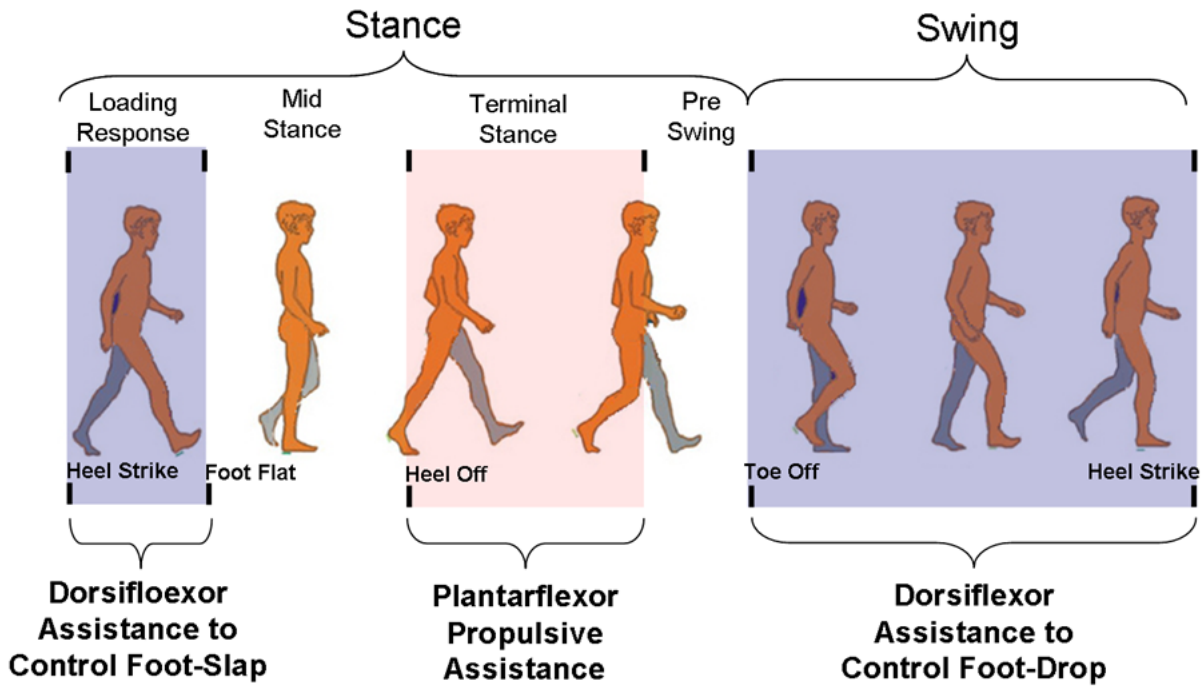

Figure 2.1 *A gait cycle is defined from heel strike to heel strike and further divided into multiple phases defined by functional tasks* ***[1]****. Ankle-foot orthoses assist gait by controlling motion during stance and swing (dorsiflexor assistance) or by providing assistive torque during stance (plantarflexor propulsive torque).*

The ankle joint complex also helps to maintain stability during stance phase. This is particularly important during single limb support in the stance phase when only one limb is supporting the body. In addition to providing stability, energy is stored through tensile loading of the tendons and muscles that traverse the ankle joint complex when the shank pivots. The ankle plantarflexor torque generated at push-off results in the highest power output for any joint during walking and is the primary source of power for forward propulsion [7]. Lower limb joint powers for a healthy walker are shown in Fig. 2.2. The significantly larger peak power at the ankle is shown just before 60% of the gait cycle. Pathology or injury that affects the ankle joint has the

potential to significantly impact quality of life by impairing some or all functional aspects of gait.

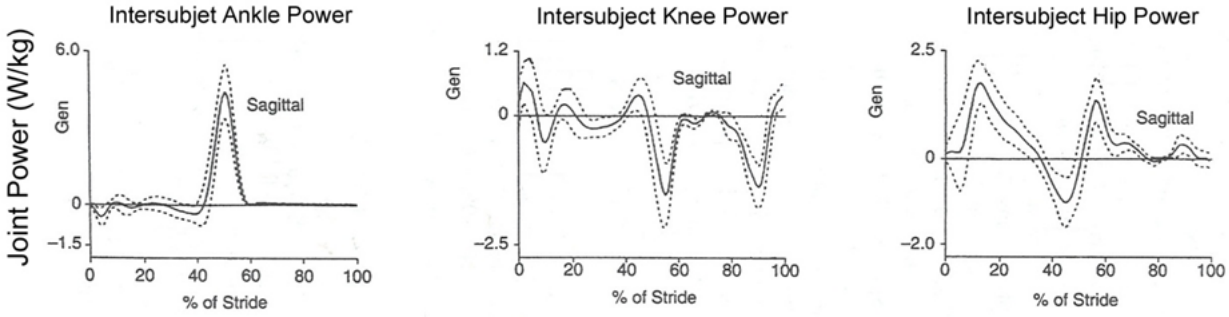

Figure 2.2 *Healthy sagittal-plane power generation (positive) and absorption (negative) at the ankle, knee, and hip joints normalized to body weight and percentage of the walking cycle. Solid lines are normalized inter-subject averages, while dotted lines show one standard deviation about the average [8].*

Weakness in the dorsiflexor and plantarflexor muscle groups is a key cause of impaired gait. Understanding muscle weakness and its effect on gait is essential to the proper design of orthotic devices that compensate for these deficiencies [9]. The dorsiflexor muscle groups are situated anterior to the ankle joint and include the tibialis anterior, extensor digitorum longus, and extensor hallucius longus [1]. Pathologies that afflict the function of the ankle dorsiflexor muscles affect gait in both swing and initial stance phases. Swing is affected by insufficient toe clearance due to weak or absent dorsiflexor muscles and results in a steppage-type gait pattern that is commonly called foot drop (Fig. 2.1). Steppage gait is a compensatory walking pattern characterized by increased knee and hip flexion during the swing phase to ensure that the toe clears the ground during walking. Weak or absent dorsiflexors may also prevent controlled

deceleration of the foot shortly after initial contact (Fig. 2.1) that often presents as an audible foot slap.

Weakness in the ankle plantarflexor muscle group primarily affects the stance phase of gait. The plantarflexor muscles situated posterior to the ankle joint are comprised of the gastrocnemius, soleus, and the peroneal and posterior tibial muscles [10]. From heel strike to middle stance, the ankle plantarflexors eccentrically contract to stabilize the knee and ankle and restrict forward rotation of the tibia [9]. At the end of stance, the plantarflexors concentrically contract to generate torque that accelerates the leg into swing and contributes to forward progression (Fig. 2.1) [11]. Weak ankle plantarflexors affect stability, particularly during single limb support. Individuals with impaired ankle plantarflexors compensate by reducing walking speed and shortening contralateral step length. Reduced walking speeds result in a corresponding reduction in torque needed for forward progression. The shortened contralateral step is thought to increase stability by limiting anterior movement of the center of pressure with respect to the ankle [9]. Impaired individuals may maintain a fast walking pace by using their hip flexors to compensate for weak plantarflexor muscles [12].

Muscle weakness can be neurological or muscular in origin and can be due to a multitude of pathologies [1, 9]. Common conditions that may result in muscle weakness include trauma, incomplete spinal cord injury, brain injury, stroke, multiple sclerosis, muscular dystrophy, and cerebral palsy. The ideal orthosis for the compensation of muscle weakness should be flexible enough to accommodate both plantar and dorsiflexor weakness. For optimal function, the orthosis would control the deceleration of the foot at the start of stance, permit free ankle plantarflexion with mild resistance while maintaining ankle and knee stability up to mid stance, generate an assistive torque at terminal stance, and block plantarflexion during swing to prevent

foot drop. All of these actions need to be accomplished using an orthosis that is compact and lightweight in order to minimize the energetic impact on the wearer. This is particularly true of an orthosis located at the ankle because the velocities at the foot are twice as fast the individual's average walking speed [13]. For example, a 2 kg load placed on each foot of a healthy adult can result in a 30% increase in the rate of oxygen uptake, whereas a 20 kg load placed on the trunk does not result in a measurable increase [5].

Currently there are no ankle-foot orthoses capable of assisting both dorsiflexor and plantarflexor function. Since maintaining toe clearance during swing has such a dramatic improvement on function, passive orthoses with their relatively simple mechanical resolution and economic viability continue to be the preferred AFO design. The subject specific nature of these designs in terms of both fit and assistance has made rigorous scientific evaluation of and comparison between novel AFO designs challenging. Instead, the effectiveness of a new AFO design tends to be demonstrated qualitatively using a small number of healthy and/or impaired subjects.

2.4 Existent Passive and Active AFO Designs

2.4.1 Passive AFO Designs

Compactness is of critical importance in daily-wear assistive devices. Consequently, AFOs used on a daily basis are generally passive. Passive AFOs can be divided into articulated or non-articulated devices. They can be further subdivided into categories based on build material such as metal and leather, thermoplastic, composite, and hybrid AFOs [14, 15]. Passive AFOs provide assistance by preventing unwanted foot motion through direct physical resistance.

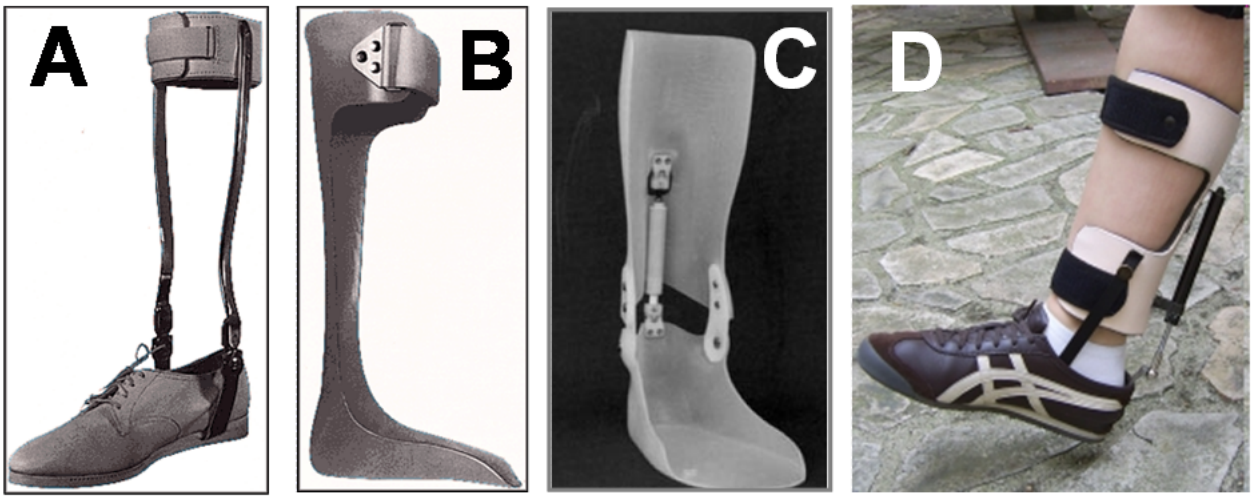

Figure 2.3 *Passive AFO designs.* ***(A)*** *Metal and leather AFO;* ***(B)*** *Posterior leaf spring AFO;* ***(C)*** *Hybrid AFO with a linear spring and thermoplastic AFO;* ***(D)*** *Pneumatically assisted Pumaflex AFO. From [3, 16-18].*

In traditional metal and leather systems, articulated hinge joints with mechanical stops are used to limit motion, while optional springs resist or assist movement. Figure 2.3 (A) shows a metal and leather AFO made by Becker Orthopedic [3]. This AFO uses metal uprights along the length of the shank for stability and an articulating joint that can be configured with various pins and/or springs to control motion in a prescribed manner by blocking, resisting, or assisting movement of the ankle joint. Metal and leather systems can accommodate fluctuations in limb volume due to swelling from inflammation or circulatory problems that would make a fixed dimension total contact fitting plastic or carbon fiber system unfeasible. Metal and leather AFOs are often less expensive than their carbon composite counterparts; however, their additional size and bulk make these systems less cosmetically attractive.

A posterior leaf spring AFO (Fig. 2.3 (B)) is a lightweight alternative to metal and leather systems and is an example of a non-articulated AFO [3]. These single piece AFOs are

constructed from both thermoformable plastics (e.g., polypropylene, copolymer) and thermosetting plastics (e.g., carbon graphite composites). The posterior leaf spring is a common strut-type AFO design where the material properties and geometry of the device determine motion control characteristics. The thermoplastic shells of these AFOs encompass the posterior and plantar aspect of the leg and foot, respectively. A one-piece thermoplastic AFO can integrate energy storage and assist elements into its structure. For example, the distal half of the shank acts as a flexible strut or leaf spring providing resistive and assistive forcing as it is deformed during loading. Motion control properties of single piece thermoplastic AFOs are controlled by the geometry of the material and the proximity of the medial and lateral trimlines with respect to the anatomical ankle rotation axis. For example, medial and lateral trimlines posterior to the ankle axis will be less stiff than trimlines anterior to the ankle [19, 20].

While both metal and leather and posterior leaf spring AFOs are commonly used to treat gait deficiencies, these devices possess motion control features (e.g., mechanical stops or material deformation) that may inhibit desirable motion. As an example, the metal and leather system shown in Fig. 2.3 (A) prevents the foot from dropping during swing with mechanical stops built into the device. Unfortunately these stops also prevent plantarflexion that would normally occur during the first half of stance, thereby altering gait. Commercial hinge joints such as the Tamarack Flexure Joint^{TM} have been used with thermoplastic AFOs to control motion in the sagittal plane. Locking these joints into stationary positions often produces conflicting gait assistance results. For example, applying assistive force at the joint in the positive direction (i.e., dorsiflexion) to control foot drop may result in a resistive force in the negative direction (i.e., plantarflexion), thereby limiting the ability to push off at the end of stance [21]. Clinical orthotic

intervention strives to provide biomechanical control necessary to improve a functional deficit without perturbing other normal movements and functions.

Several novel hybrid AFOs have been designed to more effectively control the motion of the ankle joint. A hybrid device combines lightweight thermoplastic or carbon composite shells with articulated joints and passive motion control elements. The hybrid AFOs described in this section are compared in Table 2.1. Researchers at the International University of Health and Welfare in Japan have developed the Dorsiflexion Assist Controlled by Spring (DACS) AFO for the prevention of foot drop in hemiplegic patients [17]. The 300 g DACS AFO has two thermoformable plastic pieces connected with joints on the medial and lateral sides of the ankle. An embedded spring on the dorsal side of the shank provides a peak dorsiflexor toque of 17 Nm per 10 degrees of rotation (Fig. 2.3 (C)). At heel strike, the spring resists compression and prevents an uncontrolled deceleration of the foot (i.e., foot slap). During stance, the structure of the AFO stabilizes the joint. During swing, the spring resists the foot from dropping below its neutral position perpendicular to the shank, thus resisting foot drop and providing toe clearance. To evaluate the design, joint angle data and overall walking speed from five hemiplegic subjects were recorded during trials with the DACS AFO, a plastic posterior leaf spring AFO, and a metal-leather AFO. Subjects walking with the DACS AFO had faster walking speeds and were observed to have smoother gait.

Pneumatic springs have also been used in place of mechanical springs to more easily modulate the stiffness of the passive element for patient specific tuning. The PneumaFlex is an example of this type of design (Fig. 2.3 (D)) [18]. The central component of the PneumaFlex AFO is a pneumatic spring mounted posterior to the carbon-fiber shank and footplate. The pressure in the spring's cylinder is adjustable and is selected on a patient-specific basis to

support the weight of the foot. The resulting lightweight design (130 g) is worn in a subject's shoe and is used to control the motion of the foot to prevent foot slap during stance and foot drop during swing. We could not find any published works documenting the performance of this design or comparing the benefits of the PneumaFlex AFO to other designs.

Other innovative hybrid AFO designs have focused on harvesting energy from gait in a different manner from the spring concepts described previously. In these designs, the actuators that control motion or provide assistive torque are separated from the elements used to harvest energy. Researchers at the University of Illinois in the US have designed an AFO to harvest energy during gait for use in motion control of the ankle [22]. The objective of this AFO is to achieve toe clearance during swing and free ankle motion during stance. The AFO is constructed from a two-part (tibia and foot) carbon composite structure with an articulating ankle joint and weighs 1 kg (Fig. 2.4 (A)). Ankle motion control is accomplished with a locking mechanism actuated via a pneumatic circuit connected to a pump embedded in a foam sole under the forefoot. The pump is compressed by the subject's body weight during stance. The compressed air is then used to engage the lock during swing to prevent foot drop. At heel strike, a touch valve opens to release the pressurized air and unlock the joint. Joint angle and pressure data were used to demonstrate the effectiveness of the design with a single healthy subject. The joint angle showed that the AFO restricted ankle range of motion during swing, while the pressure data indicated that proper timing of the locking mechanism was achieved.

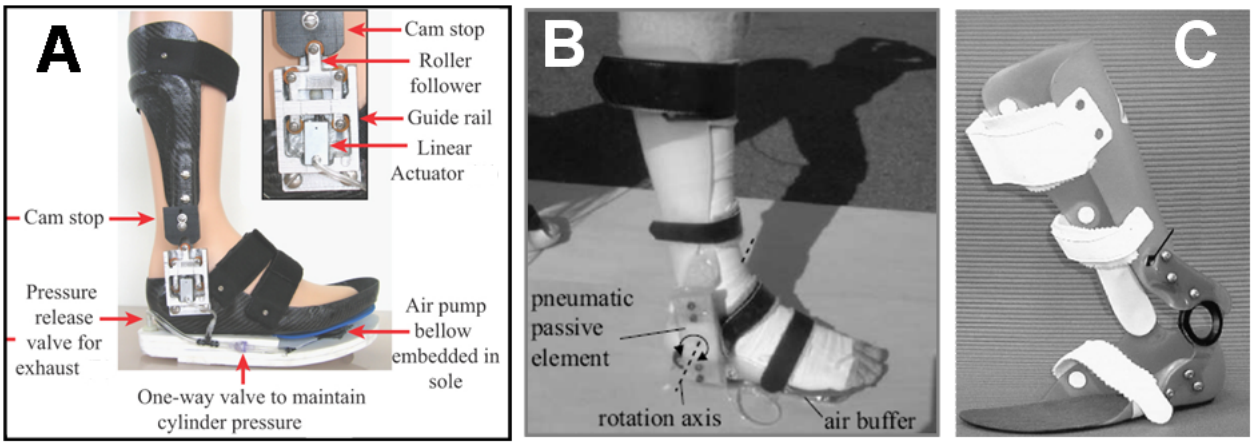

Figure 2.4 *Energy harvesting passive AFO designs.* ***(A)*** *The Illinois power-harvesting AFO;* ***(B)*** *The Osaka University AFO;* ***(C)*** *Kanagawa Rehabilitation Center AFO. From [22-24].*

Researchers at Osaka University in Japan have constructed an AFO that utilizes a passive pneumatic element actuated by the subject's bodyweight for motion control of the ankle joint [23]. The motion control element has two subassemblies: an air buffer that functions like a pump, and a passive pneumatic element that contains thin laminated sheets enclosed in an airtight plastic chamber located at the axis of rotation of the ankle joint. During stance, the buffer, located under the sole of the AFO, is compressed by the subject's weight which forces air into the passive element. This decreases the vacuum force and pushes the thin sheets of the element apart. The space between layers results in a decrease in rotational friction and allows free motion of the joint. During swing, air returns to the buffer which presses the laminated sheets together to create a maximum torsional stiffness of around 4 Nm (Fig. 2.4 (B)). The motion control provided by this AFO resists both foot drop during swing and foot slap following heel strike. The AFO design was evaluated using kinematic data from the leg with the AFO and insole pressure data from a single healthy subject. The researchers used qualitative comparisons

of the insole pressure and the kinematic marker data between trials collected with and without the AFO to conclude that the design was able to meet its functional objectives.

Oil dampers are another technique used to control ankle motion by absorbing energy from the system. Researchers from Kanagawa Rehabilitation Center in Japan have built an AFO that uses a fixed viscosity damper to control the motion of the foot by creating viscous forces to resist only plantarflexor motion [24]. The 0.4 kg AFO uses this resistive force to prevent toe drop during swing, whereas the lack of dorsiflexor resistance allows free motion during stance (Fig. 2.4 (C)). The damper provides a variable resistive torque (5-14 Nm) and can be adjusted for subject-specific need by changing the physical parameters of the damper. Gait data from two patients with hemipeliga wearing this AFO were compared to the subjects' gait data collected while wearing a conventional AFO with plantarfexion stops. The resistance provided by the oil damper was adjusted by a physical therapist. Suitable resistance was determined qualitatively based on functional need and overall patient comfort. Time and distance measures (walking velocity, cadence, step length, stride length, and cycle timing), along with kinematic parameters (peak sagittal plane joint angles), were used to evaluate and compare the performance of the AFO. The researchers concluded that there were no functionally significant differences between the two AFOs. Additionally, they found that ease of adjustability is the oil damper's biggest advantage over the traditional AFO.

Contrasting with the AFO designs that use harvested energy solely for motion control, researchers at Okayama University in Japan built a pneumatic AFO that uses harvested energy from the wearer to help power gait [25]. At heel strike, air is compressed using a bellow pump located under the heel and stored in air balloons located on the lateral side of the ankle. The compressed air is then used to actuate a custom wire-type cylinder to produce a dorsiflexor

assistive torque during swing. The device weighs 860 g and is capable of producing a peak torque of 2 Nm. The design's effectiveness was examined by qualitatively comparing EMG signals of a healthy subject walking both with and without the AFO. A decrease in EMG signal was found during the AFO trials indicating that the AFO was successfully supplementing the work done by the muscles.

The passive AFOs presented in this section provide assistance by preventing unwanted foot motion with direct physical resistance. The hybrid AFO designs, with the exception of the Okayama University AFO, have been developed to provide motion control without unnecessary restrictions to walking motion (e.g., unrestricted range of motion during stance) that are created by conventional AFOs (Table 2.1). The motion control elements used in these designs also offer greater subject-specific tuning options than comparable leaf spring or metal and leather AFOs. The stiffness of these passive AFOs range from a few Nm up to ~20 Nm of resistive torque over a 30 degree range of motion [26, 27]. In current clinical practice, there are no standard methods for identifying motion control properties that are most appropriate for improving an individual's gait. It is up to the orthotist to use his/her expertise to select and modify the stiffness of the AFO to effectively assist gait [27].

2.4.2 Active and Semi-Active AFO Designs

Despite the successful integration of passive elements in hybrid AFOs for both motion control and torque assistance, there are limitations to what can be accomplished with a purely passive device. Passive elements improve gait deficiencies by controlling motion, but generally do not provide direct assistance during the propulsive phase of gait. Further, the control of passive AFO elements relies on the activation of springs, valves, or switches in an open-loop

manner as the individual walks. This type of control has limited robustness and does not adapt to changing walking conditions or a changing functional task. Semi-active and fully active AFOs that take advantage of external power supplies and are equipped with powered actuators address both of these limitations. Semi-active and active AFOs can be divided into two groups: AFOs that have the potential to be realized as daily-wear devices, and AFOs intended strictly for in lab rehabilitation.

2.4.2.1 Daily-Wear Devices

In order for an active AFO to be used as a daily-wear device for improved function, the use of a tether for power or computing is not practical. Current development of external powered orthoses has primarily focused on tethered systems due to the engineering design challenges. Tethered sources of power and computing allow individual components (e.g., actuators) to be designed and tested as other components of the system are developed (e.g., untethered power sources). Active systems rely on sensor feedback to determine both task (e.g., walking) and the functional assistance required by the user. For example, an individual with weak dorsiflexors might require assistance to control foot motion during swing for the prevention of foot drop. In this case, AFO sensors would be used to determine boundaries for swing phase (e.g., the identification of toe off and heel strike) and potentially, in feedback control of the actuator, to track a desirable ankle joint angle to maintain toe clearance (e.g, a 90 degree angle between the foot and shank). The AFOs described in this section are untethered or the researchers have stated their intentions to continue the development of the device into a future untethered version (Table 2.2).

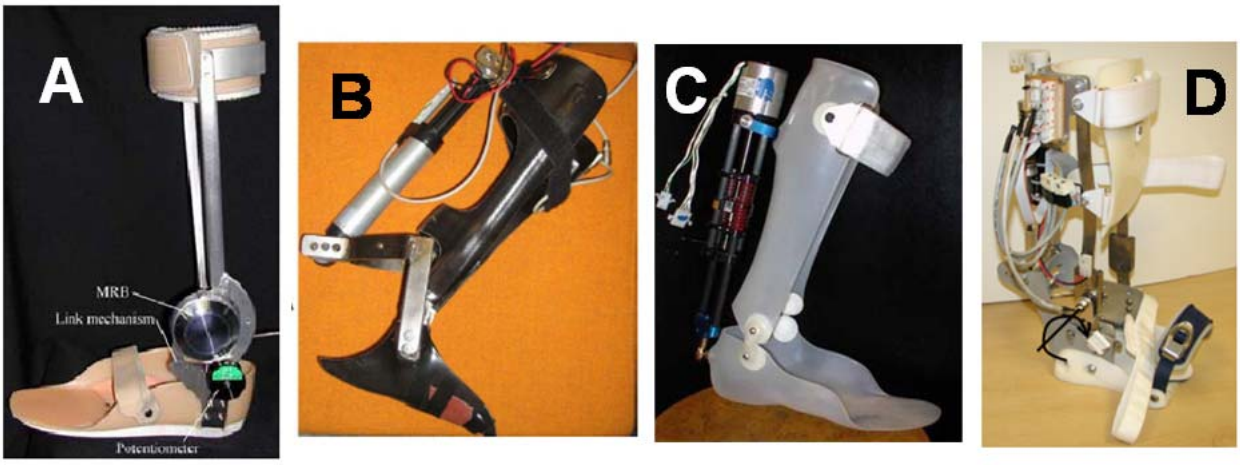

Figure 2.5 *Semi-active AFO designs.* ***(A)*** *The Oksaka magneto rheology (MR) damper AFO and torque amplifying mechanical linkage;* ***(B)*** *The Halmstad magneto rheology (MR) damper AFO;* ***(C)*** *The MIT Active AFO powered by a series elastic actuator.* ***(D)*** *The Arizona State AFO powered by a modified series elastic actuator. From [28-31].*

Active AFOs from both Osaka University in Japan and Halmstad University in Sweden utilize computer-controlled magneto rheological (MR) type dampers to modulated viscous damping for semi-active motion control [28, 29]. MR dampers use fluids with viscosities that are modulated using magnetic fields. The Osaka AFO uses an MR damper to create a resistive plantarflexor torque during swing and initial stance. The maximum resistive torque is 11.8 Nm and can be increased to 24 Nm using a mechanical linkage for torque amplification (Fig. 2.5 (A)). The amount of resistive force applied by the brake is based on the functional state of the patient during the cycle. The gait cycle is broken up into four states using information from three sensors: a potentiometer to measure the ankle joint angle, a six-axis force-torque sensor mounted in the footplate of the AFO, and a moment sensor located in the lateral AFO strut. The 1.6 kg AFO was tethered to an external power supply and computer. An experimental evaluation of the

AFO was conducted with a single subject with right ankle flaccid paralysis. Data from the AFO sensors were collected while the subject walked with and without controlled braking. The researchers used a qualitative comparison between the conditions to conclude that the subject's gait was improved by the controlled braking.

The Halstad AFO incorporates onboard position sensing, power, and electronics to create an untethered device [29]. An active control algorithm along with an MR damper allow the AFO to assist stair climbing, inclined walking, and level walking (Fig. 2.5 (B)). The AFO controller is a finite state machine with four states: damped, free, locked, and free down (limited damping to allow motion during stance and swing). The transitions between the states are determined by the position of the ankle angle and the direction of the angular motion. Maximum ankle values during the cycle are used to switch between functional tasks (walking or stair climbing). During walking, the AFO provides moderate damping to control foot slap at heel strike, free range of motion during stance, and large damping to resist foot drop during swing. During stair decent, the AFO only operates in the free down state, which allows the toes to point slightly downwards as the foot travels from one step to the next. Finally, during stair ascent, the locked state is used when the foot is raised from one step to the next and the free state is used during contact with the step. Three healthy subjects were used to evaluate the performance of the AFO. Data from the AFO sensors were used to demonstrate that foot motion was properly restricted during gait, and that their control algorithm could successful switch between functional tasks. Although MR dampers are able to control foot motion; they are not capable of generating torque at the ankle joint for use in push off.

To address the need for push off assistance, researchers have utilized a series elastic actuator (SEA) to provide both motion control of the foot and apply plantarflexor torque during

gait [30, 32]. The Biomechatronics Group at Massachusetts Institute of Technology in the US developed an active SEA AFO to assist foot drop in gait. The AFO weighs 2.6 kg and is tethered to an off-board power supply. The SEA consists of a DC motor powered ball screw mechanism in series with a helical spring (Fig. 2.5 (C)). The computer controlled motor adjusts the rotary compliance of the AFO by driving a lead screw to vary the height of the spring. The use of an elastic element with a motor offers advantages over a direct drive system including greater shock tolerance, lower reflected inertia, more accurate and stable force control, and the capacity for energy storage [33]. While the SEA actuator offers flexibility to assist patients with both plantarflexor and dorsiflexor weakness, in [33] the AFO was configured to assist individuals with weak dorsiflexors (e.g., foot drop gait) and functional plantarflexors. A finite-state controller was used to divide gait into three states each with a separate functional objective. The first control state lasted from heel strike to mid stance and prevented foot slap by using the SEA to increase the impedance at the ankle. The second control state lasted from mid stance until toe off and minimized the impedance of the AFO to allow full plantarflexor movement. The third control state occurred during swing and maintained toe clearance by lifting the foot. Ground reaction force and angular position data from onboard sensors were used to transition between states during walking, while an adaptive control algorithm was used to accommodate different walking speeds within the control states. The AFO was evaluated using kinematic and kinetic data from two foot drop and three normal subjects. The normal subjects were selected to match the impaired subject's demographics. The subjects walked with the AFO set to zero, constant, or variable impedance at slow, self-selected, and fast gait speeds. The performance of the AFO to assist foot drop gait was evaluated by counting the number of foot slaps that occurred per 5 gait cycles and measuring the angular difference between the maximum plantarflexion and

dorsiflexion angles during swing. Larger angular differences indicated free motion during plantarflexion and a reduction of foot drop during swing. These metrics were used to illustrate that the SEA AFO with a variable impedance control algorithm outperformed both the zero and constant impedance controllers. Current work is focused on developing an untethered version of this device.

Researchers at Arizona State University in the US have also built an AFO around a highly compliant actuator called a robotic tendon [31, 34, 35]. Like the SEA, the robotic tendon uses a motor/screw/spring arrangement to offer greater compliance than a direct drive system (Fig. 2.5 (D)). This AFO also uses the increased elasticity to harvest energy from the gait cycle, reducing both average and peak motor power requirements, which in turn results in a reduction in motor size and weight. Additionally, the internal compliance of the robotic tendon allows the user to deviate from a prescribed trajectory if the walking environment changes. The researchers suggest this flexibility provides added safety for the user. The AFO built around the robotic tendon allows motion in the sagittal plane and utilizes an encoder, potentiometer, and one force sensor embedded at the heel for sensor feedback. The control algorithm described in [35] accommodates gait initiation and cessation, and allows the device to accommodate different level walking speeds. An earlier version of this design used a 0.95 kg tendon that required 77 W of power to produce a torque comparable to a healthy individual during level walking [35]. An updated AFO design uses a lighter tendon (0.5 kg) and weighs 1.75 kg. [31]. This modified design uses a seven state finite-state machine to control the stiffness and the velocity of the AFO. In this design, a digital incremental encoder is used to control the position of the motor. An absolute angle encoder along with foot switches in the heel and toe of the AFO footplate are used to switch between states. The first five states occur during stance and alternate between stiffness

and velocity control. The sixth and seventh states occur during swing when the foot is raised and then supported at a constant angle until the following heel strike. The functionality of the device was verified using kinematic and kinetic data from a single able-bodied subject. The results showed that the controller switches states correctly and that the actuator generates power comparable to a healthy individual during level walking. While this AFO is still tethered to an external power source and computer, the researchers suggest that the device could be powered for 8 hours of continuous operation using a battery worn in a fanny pack.

One type of untethered semi-active AFO uses functional electrical stimulation (FES) to create ankle flexion. The BIONic WalkAide [36] and the NESS L300 [37] are commercially available FES devices that use small surface electrical stimulation signals to stimulate the peroneal nerve and activate the ankle dorsiflexors in order to provide functional toe clearance during swing. These devices are customized to an individual using trial and error methods during the initial fitting. The BIONic WalkAide uses a tilt sensor to monitor the orientation of the shank, initiating surface FES stimulation when the tilt sensor passes through a set threshold (indicating the onset of swing). The work conducted by Weber et al. used a modified WalkAide stimulator to control implantable micro stimulators (BIONS). This study compared the effectiveness of surface and implantable stimulation to correct the foot drop in a subject with nerve damage resulting from a spinal cord injury. Kinematic data and heart rate were collected during treadmill walking. These data, along with a physiological cost index (PCI), were used for the comparison. PCI was calculated by dividing the difference between quiet-state and walking heart rate by ambulatory velocity. The BION stimulation produced a more balanced ankle dorsiflexion movement and had a slightly lower PCI than the surface stimulation.

The NESS L300 uses a force sensitive resistor placed under the foot to detect swing. A study of 24 patients with chronic hemiparesis was used to show that the NESS L300 enhanced gait and improved dynamic stability. Subjects were asked to walk for 6 minutes with and without the device at 0, 4, and 8 week assessments. Gait speed, heart rate, and temporal gait parameters (stance and swing times during each gait cycle) were collected during the trials. The researchers found improved walking speed, decreased asymmetry, and decreased temporal variability when using the device. Both devices are compact because the user's own muscles and skeleton provide the actuation and support that AFOs traditionally provide. Because FES directly stimulates an individual's nerves and muscles, there is the potential to increase the fatigue resistance and strengthen muscles [36]. However, FES devices require careful positioning of the electrodes on a daily basis and have a limited suitable patent population.

2.4.2.2 Active AFOs for Use in Patient Diagnosis and Rehabilitation

Fully active AFOs are able to provide net power to the ankle, unlike passive and semi-active designs that can only dissipate or store and release available energy. To date, most active AFOs are tethered because technology capable of meeting the power requirements for full assistance cannot meet the size and weight requirements of a daily-wear device. Tethered devices are suitable for laboratory research and for clinic-based rehabilitation treatments that aid in recovery from a pathology or injury [38]. Rehabilitation and diagnostic AFOs have been used as training devices to help restore normal walking function, instruments for the measurement of motion and force at the ankle joint, and in locomotion studies to perturb gait. Accordingly, the devices described in this section are not meant to be portable.

Researchers at the University of Michigan in the US, Arizona State University in the US, and the Center for Interdisciplinary Research in Rehabilitation and Social Interaction (CIRRIS)

in Quebec, Canada have built fluid powered AFOs intended for human locomotion study and gait rehabilitation [39-43]. The Michigan AFO uses FES to control McKibben style uni-axial artificial pneumatic muscles in various arrangements to provide dorsiflexor and plantarflexor torque. The AFO has a total weight of 1.6 kg excluding the off-board computer and air compressor (Fig. 2.6 (A)). The orthosis provides a peak plantarflexor torque of 70 Nm and peak dorsiflexor torque of 38 Nm [39].

The Arizona State University rehabilitation AFO, called the Robotic Gait Trainer, utilizes pneumatic spring over muscle (SOM) actuators to create bi-directional forcing [43]. The SOM actuators enclose a cylinder-plunger containing a compression spring (K = 1.40 N/mm) within a McKibben style pneumatic muscle. The AFO is arranged in a tripod configuration with the subject's leg acting as a static link and two SOM actuation links (Fig. 2.6 (B)). Both dorsi/plantarflexor and inversion/eversion are allowed by this design. The researchers envision this system being used for home repetitive task therapy and strength building rehabilitation.

The CIRRIS AFO is powered by a water-filled hydraulic master cylinder, which is driven by an electrical motor. The master cylinder is connected to a slave cylinder mounted posterior to the shank (Fig. 2.6 (C)) [42]. This AFO produces several torque profiles: constant torque, position-dependent torque, and phase-dependent torque. Additionally, the AFO can be used to produce a high velocity displacement disturbance at the ankle joint for the study of proprioceptive reflexes during human locomotion. The motor delivers a continuous torque of 70 Nm and a peak torque of 98 Nm to the master cylinder. The weight of the AFO worn by the subject was kept to 1.7 kg by locating the electric motor away from the device. Torque cancellation was performed in order to minimize the influence of the passive torque induced from the electro-hydraulic drive system.

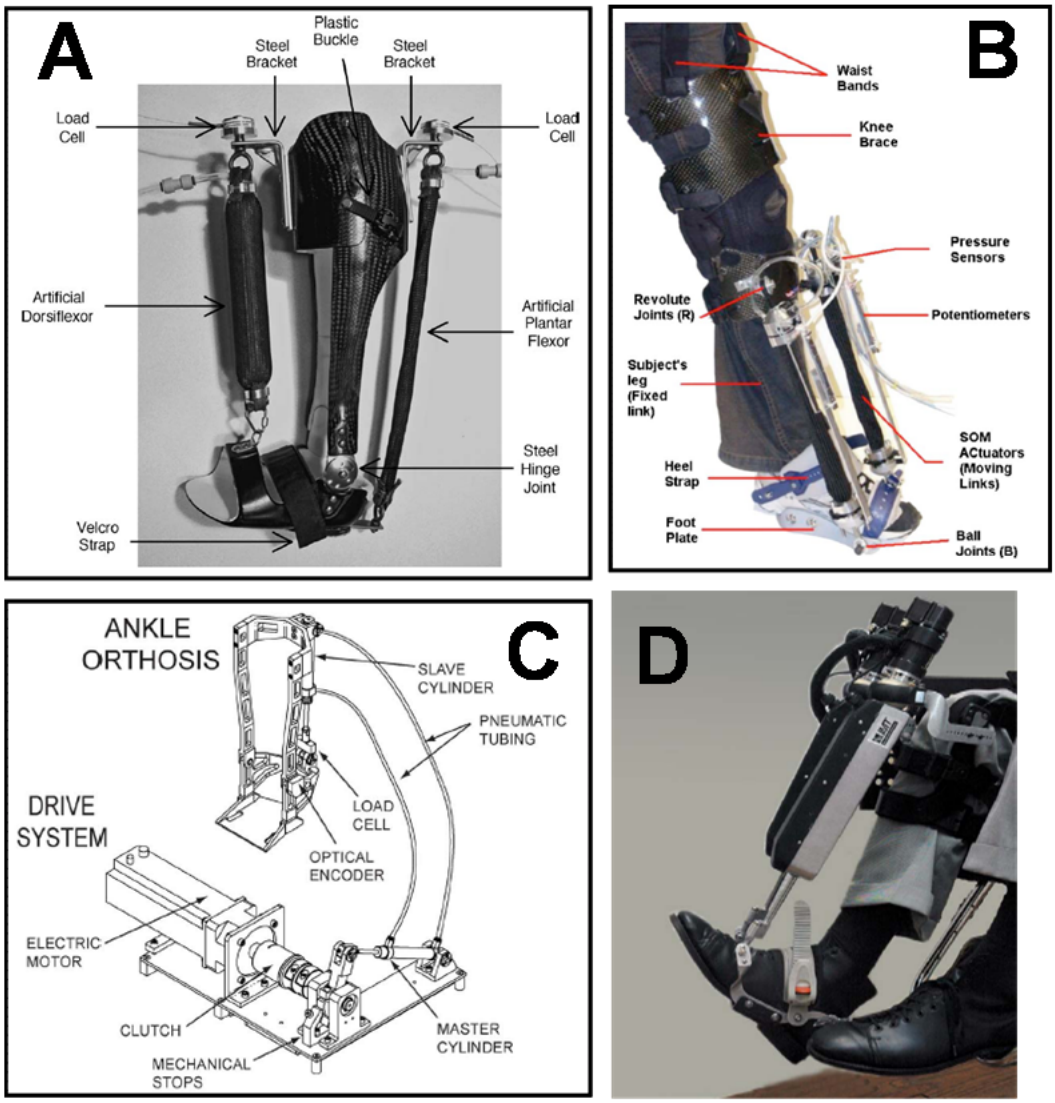

Figure 2.6 *Tethered active AFO designs.* ***(A)*** *University of Michigan AFO powered by pneumatic muscles;* ***(B)*** *Arizona State University Robotic Gait Trainer with spring over muscle pneumatic actuators;* ***(C)*** *A mechanical drawing of the hydraulically powered CIRRIS AFO;* ***(D)*** *MIT AnkleBot shown with the two front mounted DC-motor-powered linear actuators. From [41-44].*

Directly measuring the physical properties of the ankle joint complex is also an important function performed by AFOs used in a rehabilitation setting. The AnkleBot, designed by researchers in the Newman Laboratory at Massachusetts Institute of Technology, has been used for both rehabilitation and direct measurement of the passive stiffness of the ankle joint complex [44, 45]. The device is actuated by two DC-motor-powered linear actuators mounted to the front of the shank using a knee brace and footplate. The tripod arrangement of the components allows three degrees of freedom at the foot (Fig. 2.6 (D)). Dorsi/plantarflexor torque is produced when both actuators pull/push in the same direction, whereas inversion/eversion rotational torque is created when the actuators act in opposing directions.

2.5 Discussion

Current commercial daily-wear AFO systems are generally limited to passive designs that control undesirable motion of the foot, but do not provide powered assistance during the propulsive phase of gait [14, 15]. These AFOs are successfully used as daily-wear devices because of the simplicity, compactness, and durability of the designs. While motion control can improve functionality for an individual (e.g., the prevention of foot drop during swing), passive AFOs can impede gait at other points in the cycle (e.g., restrict range of motion during stance) and provide no supplemental torque assistance. Further, the motion control provided by passive systems has limited functional benefit for an impaired individual because these systems do not adapt to a changing environment and may interfere with tasks such as stair assent or decent.

Semi-active AFOs address some of the limitations of passive AFOs by utilizing sensors and controllable braking mechanisms to manage the motion of the foot. The most promising of these designs use MR dampers to modulate the resistance of the AFO based on the phase of gait

[28, 29]. Of the designs which implement MR dampers, the untethered Halstead AFO appears to be the most technologically developed [27]. This AFO provides variable motion control of the foot and makes use of embedded sensors and predefined states to switch between level walking and stair climbing. While this particular system shows promise as a daily-wear AFO, it lacks the ability to provide supplemental assistive torque.

Fully active AFOs provide net power to the ankle for use in both motion control and propulsive assistance. To date, active AFOs have not been commercialized and exist only in laboratory settings. The size and power requirements of these designs have resulted in systems that are tethered to power supplies, electronics, or both. The active AFOs that make use of Series Elastic Actuators (SEA) come the closest to the idealized AFO described in this work, but are currently tethered to computers and power supplies [30-32, 34, 35]. The other active systems described in this chapter are used in laboratory and clinical settings for rehabilitation and the direct measurement of physical properties of the ankle joint complex.

Design considerations for the ideal AFO must account for the diverse functionality required to accommodate the many aspects of gait that can be affected by injury or pathology. The AFO also must be compact and lightweight in order to minimize the energetic impact to the wearer. These requirements illustrate the great technological challenges facing the development of non-tethered, powered AFOs for daily-wear. Currently, state-of-the-art AFOs fall short of the goal of a day-scale portable powered orthosis. The core challenges that must be met to realize such a device for both daily-wear and rehabilitation are: (1) a compact power source capable of day-scale operation, (2) compact and efficient actuators and means of power transmission capable of providing forces comparable to healthy individuals, and (3) control schemes that

efficiently and effectively apply assistance during a variety of functional tasks that an individual may encounter on a daily basis.

Shape Memory Alloy (SMA), also called "muscle wire," and Electroactive Polymer Actuators (EPAs) both show potential as future actuation methods for a portable AFO [46]. The key feature of SMA is its ability to undergo large seemingly plastic strains, and then recover from these strains when a load is removed or the material is heated. SMA has high power-to-mass ratio, which is consistent with the compactness goal of a portable AFO. However, the relatively slow response rate of this kind of actuator (~0.25 Hz) and the mechanical inefficiencies that result from poor conversion of thermal energy into mechanical energy (approximately 2-3%) are significant disadvantages that limit the applicability of this kind of actuator at the present time [46]. Electroactive Polymer Actuators (EPAs) have been used in biologically inspired robotic arms, but have not been effectively incorporated into a prosthetic or orthotic device [47]. While EPAs may be used in portable AFOs in the future, the current focus for these actuators is on smaller applications that require soft and flexible actuation schemes (e.g., emulating the hovering ability of an insect) [48]. Electroactive polymers show great promise as artificial muscles. However, challenges from improving the actuator durability and life time at high levels of performance, scaling up the force and stroke capabilities in order to meet the needs of orthotic and prosthetic devices, and developing efficient and compact driving electronics must be met before this can be realized [49].

Hydraulic and pneumatic fluid power systems also show potential as enabling devices for future orthotic devices, with many current research AFOs already using fluid power [18, 23, 25, 28, 39, 42, 50, 51]. Human motion is powered by relatively high torques acting at low velocity. Electric motors, on the other hand, are low torque, high velocity actuators. As a result, orthotic

systems that make use of electric motors require co-located transmissions with the output at the joint. While the electric motor may be light, current off-the-shelf options for the transmission (planetary gear head or ball screw) are heavy. Fluid power is ideal for high-force, low-velocity applications like gait. The key advantages of fluid power are the high force-to-weight and force-to-volume ratios of the actuator, the ability to actuate a joint without a transmission, and the ability to transport pressurized fluid to the actuator through flexible hoses that can be placed in locations where a shaft from a traditional motor could not reach. This allows flexibility in the placement of system components on the assistive device or elsewhere on the body, resulting in compact packaging that does not sacrifice high force and power [52]. The ankle has a brief 200 W peak power with a 13 W average during a single gait cycle [8]. The short 200 W peak power requirement during gait is a good match for an accumulator-delivered power burst as accumulators have excellent power density. However, there are significant challenges associated with fluid power. While some aspects of a fluid power system are compact, fluid power generation requires a supply that can be large and noisy [52], e.g., a compressor powered by a combustion engine. Combination systems (electrohydraulic or electropneumatic) may also be a possible solution. Moreover, as the components and transmission lines of a fluid power system are reduced to a size suitable for an orthotic device, losses in efficiency are created by the proportionally larger friction forces that result from the smaller parts. These are among the reasons why most current applications for fluid power are large, heavy equipment.

The creation of a compact, lightweight, efficient, portable powered ankle-foot orthosis has the potential to dramatically improve both treatment and rehabilitation of injury and pathology at the ankle joint complex. In a daily-wear application, this improvement would result from an ability to accommodate a variety of functional deficits with a single device. Clinicians

generally prescribe passive motion control AFOs that only address deficiencies associated with weak dorsiflexors for daily-wear. This is due to the fact that a daily-wear assistive device capable of providing a supplemental torque at the ankle joint does not currently exist. A portable powered AFO would also be of use for in-home rehabilitation, because it would allow the clinician to prescribe an at home physical therapy routine built around the device. This application will broaden the impact of a portable powered device from those with a permanent deficit to any individual recovering from an acute ankle injury. While there are significant technological challenges that must be met in order to realize the enabling technologies that will result in a portable powered AFO, the successful development of this device will significantly advance the field of orthotics and benefit numerous individuals with lower limb neuromuscular deficiencies.

Chapter 3 will introduce a novel portable powered AFO capable of providing torque at the ankle joint for motion control and propulsive assistance during gait. The untethered nature of this system addresses the key limitation of existing powered AFOs.

Table 2.1 *A comparison of weight, torque, advantages, disadvantages, performance metrics, and effectiveness of the novel passive AFO designs described in Section 2.4.*

	Type	Weight	Resistive or Assistive	Active Element	Maximum Applied Torque	Advantages	Disadvantages	Performance Metrics	Experimental Evaluation	Results	Control
Passive Hybrid AFOs	DACS AFO (18)	0.3 kg	Resistive	Mechanical Spring	17 Nm (per 10 deg of rotation)	Compact, lightweight, untethered. Interchangeable springs for patient specific assistance	Constant resistive force impedes motion	Gait speed and qualitative visual inspection of gait	Five Hemiplegic subjects walked with DACS, posterior leaf spring, and metal-leather AFO	DACS AFO users had faster and smoother gait	NA
	PneumaFlex AFO (19)	0.13 kg	Resistive	Air Spring	**?**	Compact, lightweight, untethered. Adjustability of pneumatic springs allows for patient specific assistance	Constant resistive force impedes motion	**?**	**?**	**?**	NA
	University of Illinois AFO (20)	1 kg	Resistive	Locking CAM	**?**	Variable motion control, untethered, energy needed to actuate the locking mechanism harvested during gait	Bulky AFO structure, complicated locking system	Joint angle kinematics, pneumatic line pressure	Single healthy subject	Joint angle data demonstrated proper foot motion; pneumatic pressure data showed correct locking sequence during gait	NA
	Osaka University Hybrid AFO (21)	**?**	Resistive	Friction Break	4 Nm	Variable motion control, untethered, compact resistive element, energy harvested during gait	The resistance provided by the break not easily adjustable	Kinematic data from the assisted leg and insole pressure sensor data	Single healthy subject	Kinematic data were used to verify the correct restriction of joint range of motion during swing	NA
	Kanagawa Rehabilitation Center AFO (22)	0.4 kg	Resistive	Oil damper	5-14 Nm (at 10 degrees of plantar flexion)	Variable motion control, untethered, lightweight, resistive force is easily adjustable	Resistive force is the same during initial stance and swing	Time, distance, and kinematic parameters	Two hemiplegic patients walked with oil damper and conventional AFO	No significant functional difference between the AFOs. Oil damper's largest advantage was ease of adjustability	NA
	Okayama University AFO (23)	0.86 kg	Assistive	Pneumatic Actuator	2 Nm	Variable motion control, untethered, energy to actuate the active element harvested during gait	Bulky AFO structure, only generates small assistive torques	EMG	Single healthy individual	Decrease in EMG signal during trials indicates supplemental assistance	NA

Table 2.2 *A comparison of weight, torque, advantages, disadvantages, performance metrics, and effectiveness of the novel Active and Semi-Active AFOs designs described in Section 2.4.*

	Type	Weight	Resistive or Assistive	Active Element	Max Applied Torque	Advantages	Disadvantages	Performance Metrics	Experimental Evaluation	Results	Controller
Active and Semi-Active AFOs	Osaka University AFO (24)	1.6 kg	Resistive	Magneto Rheological (MR) Damper	24 Nm	Variable motion control, large peak breaking torques	Tethered, only resists motion	Qualitative comparison of AFO sensor data	Single subject with right ankle flaccid paralysis	Qualitatively observed an improvement in gait with the controlled braking AFO	Finite State Control
	Halstead University AFO (25)	**?**	Resistive	Magneto Rheological (MR) Damper	**?**	Variable motion control, untethered	Only resists motion	Qualitative comparison of AFO sensor data	Three healthy subjects	Foot range of motion was properly restricted during gait and stair climbing. Control algorithm successfully switched between functional tasks.	Finite State Control
	MIT Active AFO (26-27)	2.6 kg	Assistive	Series Elastic Actuator (SEA)	**?**	Provides both dorsi- and plantarflexor assistance	Tethered	Kinematic and kinetic data	Two foot drop subjects and three matched healthy subjects	Foot slaps per five gait cycles were reduced and foot drop during swing was prevented	Finite State Control
	Arizona State Robotic Tendon AFO (29-31)	1.75 kg	Assistive	Robotic Tendon (modified SEA)	~ 60 Nm	Provides both dorsi- and plantarflexor assistance	Tethered	Kinematic and kinetic data	Single healthy individual	Control states were triggered correctly during gait. AFO generated power comparable to a healthy individual during level walking	Finite State Control
	BIONic WalkAide (32)	**?**	Assistive	Function Electric Stimulation (FES)	**?**	Compact, lightweight	Limited patient population	Kinematic data and physiological cost index (PCI)	Single subject with nerve damage	Implantable micro stimulators produced balanced ankle flexion with a low PCI score	Finite State Control
	NESS L300 (33)	**?**	Assistive	Function Electric Stimulation (FES)	**?**	Compact, lightweight	Limited patient population	Gait speed, heart rate, and temporal gait parameters (stance and swing times)	24 subjects with chronic hemiparsis	Improved walking speed, decreased asymmetry, and decreased temporal variability when using the AFO	Finite State Control

Chapter 3

A PORTABLE POWERED ANKLE-FOOT ORTHOSIS FOR REHABILITATION*

3.1 Introduction

The ability for an orthosis to apply an assistive torque (e.g., dorsiflexor or plantarflexor) at the ankle joint could play a significant role in how patients are rehabilitated with ankle-foot orthotic systems. Conceptually, users may benefit from a daily use portable powered ankle-foot orthosis (PPAFO) through enhanced walking function, gait training in physical therapy, and/or the ability to provide prescribed external power assist modalities for strength and range of motion improvement. Impaired veterans are a motivating potential subject pool for these devices because of the high number of lower extremity battle injuries seen in recent years [53].

Between October 2001 to May 2006, approximately 7,018 US soldiers from the Iraq and Afghanistan conflicts have suffered a severe lower-limb injury that did not result in a major lower-limb amputation [53]. This figure represents 43.7% of all soldiers wounded in action that did not return to duty within 72 hrs [53]. Thus, the lower extremity is one of the most common regions harmed in wartime conflicts, often leading to major functional deficits that can affect

*This chapter is based on reference [61].

joint motion and mobility. Since the impact of combat injuries to the lower limbs is so devastating, the therapeutic treatment interventions used to rehabilitate veterans are of significant importance to insure that the rehabilitation outcome of these individuals is maximized.

As was discussed in the previous chapter and [54], current clinically prescribed ankle-foot orthoses (AFOs) utilize mechanical elements such as springs, dampers, or the AFO itself to provide functional assistance during gait by restricting unwanted motion of the foot [14, 15]. While these passive devices enable improved gait, they are unable to provide active assistance for plantarflexor deficiencies that may be present in the user. As a result, current clinical orthotic management strategies for the loss of volitional plantarflexion are limited.

Novel active devices have been developed to address the inherent limitations of passive AFOs by providing net power to the ankle joint for motion control and torque assistance. These powered systems are currently tethered to off-board sources of power and electronics and take two forms: (1) devices undergoing continued development for future untethered daily-wear applications, or (2) devices intended for laboratory research and/or clinic-based rehabilitation treatments that aid in recovery from a pathology or injury [38].

One of the critical design elements in these active devices is the actuator. Researchers have used a variety of components including series elastic actuators that consist of a DC motor powered ball screw in series with a helical spring [30, 31], electric motors for direct drive and series elements [43, 44], and fluid powered (pneumatic or hydraulic) actuators [39-42, 55].

To date, active AFOs have not been commercialized and only exist as custom devices constructed mainly from off-the-shelf components. While they are capable of providing power to the ankle for both motion control and propulsive assistance, the size and power requirements of the current designs have resulted in systems that are tethered to power supplies, electronics, or

both. As a result, state-of-the-art powered AFOs cannot be used outside of the laboratory, which greatly restricts their potential to improve gait. The creation of a portable powered orthotic system would offer a new treatment modality outside of the lab or clinic with the potential to greatly improve the functional outcome of the rehabilitation process.

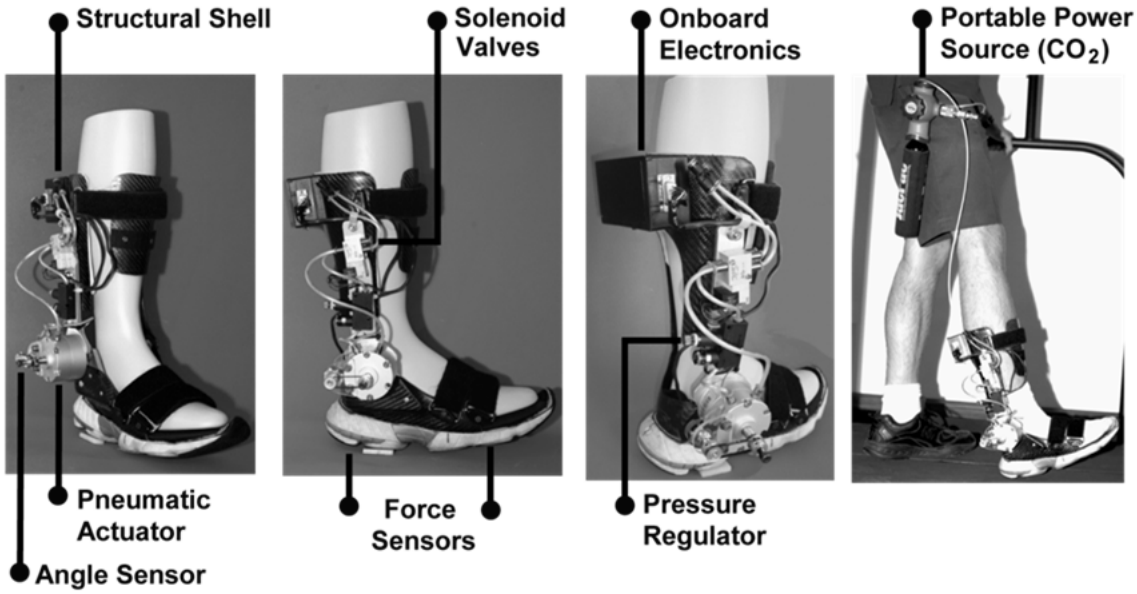

Figure 3.1 *First prototype of the PPAFO. The rotary actuator is powered using a compressed CO_2 bottle (far right) worn by the subject on the waist.*

In this chapter, we present a novel portable powered AFO (PPAFO) to provide untethered assistance for daily in-home rehabilitation treatment (Fig. 3.1). Fluid power is used to actuate the PPAFO. The key advantages of fluid power for this application are the high force-to-weight and force-to-volume ratios of the actuator, the ability to actuate a joint without a transmission, and the ability to transport pressurized fluid to the actuator through flexible hoses that can be placed in locations where a shaft from a traditional motor would not reach. The use of high force-to-weight fluid power actuators that do not require transmissions, combined with flexibility in the

placement of system components, allows the weight of the device at the shank and foot to be reduced. The remainder of this chapter will introduce the novel PPAFO, characterize the performance of the system, and present results from healthy and impaired subjects walking with the PPAFO to demonstrate device functionality.

3.2 Methods

The PPAFO was designed to assist impaired gait by: (1) controlling forefoot velocity at heel strike to prevent foot slap, i.e., eccentric dorsiflexor assistance, (2) providing modest assistive torque for propulsion and stability at the end of stance, i.e., concentric plantarflexor assistance, (3) supporting the foot in the neutral position during swing to prevent foot drop, i.e., concentric dorsiflexor assistance, and (4) allowing free range of motion for the remainder of the gait cycle (Fig. 3.2). This section is divided into three parts: a detailed description of the PPAFO system hardware and control scheme, empirical characterization of the system performance, and empirical testing with both healthy and impaired subjects to evaluate PPAFO functional performance during assistance.

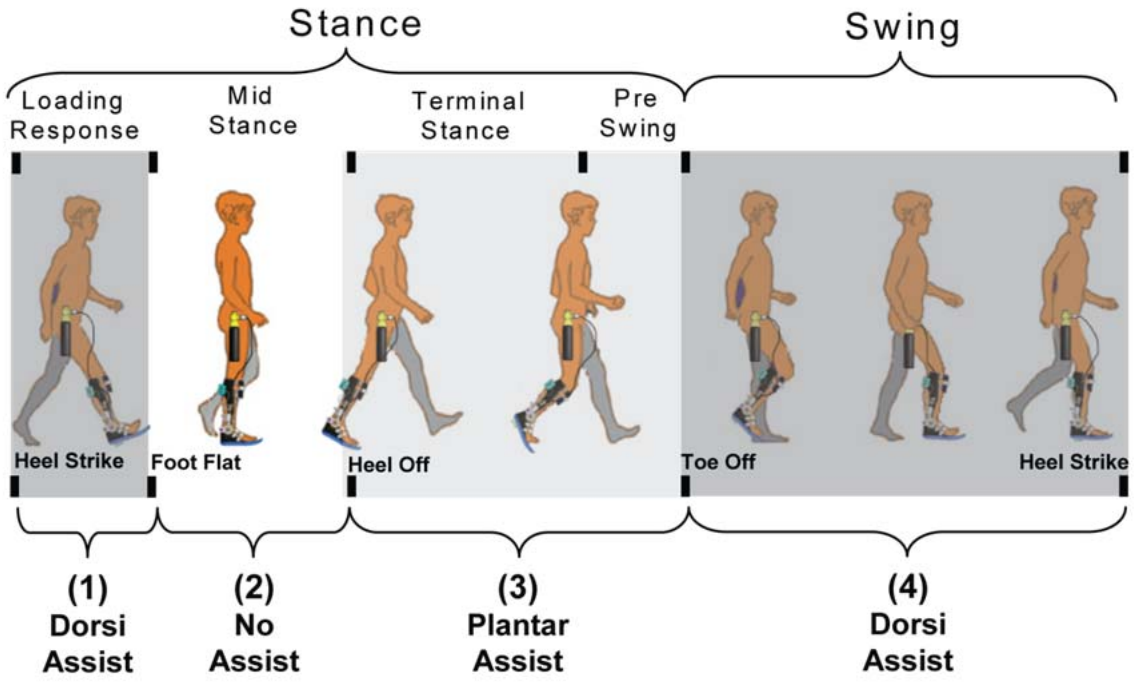

Figure 3.2 *The cycle is divided into multiple phases defined by functional gait tasks [1]. The Portable Powered Ankle-Foot Orthosis (PPAFO) assists gait by providing assistive dorsiflexor torque at heel strike to prevent foot slap (**1.** darker grey shading), plantarflexor torque during stance to assist propulsion (**3.** Lighter grey shading), and dorsiflexor torque during swing to control foot motion (**4.** Darker grey shading). No assistance from the PPAFO is provided during mid stance (**2.** White shading).*

3.2.1 PPAFO System Description

3.2.1.1 PPAFO Hardware

The PPAFO system consisted of subsystems that addressed power, actuation, structure, and sensing (Fig. 3.1). A commercially-available portable compressed liquid CO_2 bottle and pressure regulator (JacPac J-6901-91, 9 oz capacity; Pipeline Inc., Waterloo, ON, Canada) were

used to power a dual-vane bidirectional rotary actuator at the ankle joint with a maximum pressure rating of 150 psig (Fig. 3.1) (CRB2BW40-90D-DIM00653; SMC Corp of America, Noblesville, IN, USA). The pressure regulator on the bottle modulated plantarflexor torque for propulsion assistance. Compressed gas can be used safely near the human body in a number of common applications (e.g., scuba tanks, paintball guns, pneumatic hand tools). The same type of power source used in the PPAFO has also been used to power pneumatic hand tools. To ensure user safety during operation, the equipment was used within the manufacturer's published specifications. A second pressure regulator was mounted on the PPAFO (LRMA-QS-4; Festo Corp-US, Hauppauge, NY) and used to modulate dorsiflexor torque for foot support during swing. The orthotic tibial and foot piece components were custom fabricated from pre-impregnated carbon-composite laminate materials over a positive model of a leg and serve as the structural elements of the system. The foot shell (US men's size 11) incorporated a shoe-last profile that placed the heel 1.0 cm higher with respect to the metatarsal heads. The toe section of the footplate was oriented at a five degree angle (pitch) relative to the ground to emulate late stance rollover since the foot section was rigid. A standard running shoe sole provided the interface between the foot piece and the ground. A conventional free motion ankle hinge joint connected the foot piece to the tibial section on the medial aspect. Velcro straps secured the PPAFO to the leg and foot.

The direction of the torque could be switched from dorsiflexor to plantarflexor via two solenoid valves (VOVG 5V; Festo Corp-US, Hauppauge, NY). Switching of the valves was selected based on specific events during the gait cycle. Event boundaries for these states were determined using two force sensors (402, 0.5" circle; Interlink Electronics Inc., Camarillo, CA, USA) placed on the interface of the foot section under the heel and metatarsal heads. Onboard

electronics (eZ430-F2013 microcontroller; Texas Instruments, Dallas, TX, USA) and the portable power source allowed the PPAFO to provide untethered powered assistance.

The power source and regulator (regulator = 0.57 kg, CO_2 bottle = 0.63 kg) were worn on a belt attached to the waist, physically separate from the structural elements of the PPAFO (AFO = 1.9 kg), to distribute the weight of the prototype (3.1 kg total). Working to minimize additional weight to the lower limbs is particularly important for AFOs, because velocities at the foot are twice as fast as an individual's average walking speed [13]. Even with moving weight to the torso, the ~2 kg PPAFO could be expected to result in an ~30% increase in the rate of oxygen uptake when worn by a healthy adult [5] if no torque assistance were generated by the PPAFO.

3.2.1.2 PPAFO Control

The magnitude and timing of the PPAFO applied torque needed to be controlled in order to provide appropriate assistance during gait. Magnitudes of both the plantarflexor and dorsiflexor assistive torques were modulated by the pressure regulators. Plantarflexor assistance was set with the regulator attached to the CO_2 bottle, while dorsiflexor assistance was set by a regulator fixed to the PPAFO (Fig. 3.1). The dorsiflexor assist could be tuned to a subject's individual needs by adjusting the PPAFO regulator such that the weight of the subject's relaxed foot was supported in a neutral (90 degree) position.

Timing of the PPAFO assistance was dictated by four regions with different functional gait requirements: (1) loading response, (2) mid stance, (3) terminal stance through pre swing, and (4) swing (Fig. 3.2). During loading response, the PPAFO provided dorsiflexor assist to prevent foot slap. In mid stance, the PPAFO provided no torque and allowed free range of motion at the ankle joint. The structure of the device provided stability to the wearer during mid stance. From the beginning of terminal stance through pre swing, plantarflexor torque was

generated to provide assistance with propulsion. During swing, dorsiflexor torque was generated to prevent foot drop by maintaining toe clearance.

The force sensors in the PPAFO foot piece were used to detect the event boundaries of the four regions (Fig. 3.2). Events were detected when sensor magnitudes exceeded tuned user-specific thresholds for the heel and metatarsal sensors. Loading response began when the heel sensor threshold was exceeded at heel strike and lasted until the metatarsal sensor threshold was exceeded at foot flat. Mid stance began at foot flat and continued until the heel sensor reading dropped below the threshold at heel off. Terminal stance began at heel off and continued until the metatarsal sensor dropped below threshold at the end of pre swing. Swing then lasted until the following heel strike detection. These specific events were used to direct switching control of the solenoid valves for proper assistance. The block diagram in Fig. 3.3 illustrates the event based control scheme used with the PPAFO.

A heuristic tuning scheme was used to determine the timing and magnitude of the PPAFO assistance for each subject. Force sensor thresholds were adjusted for each subject to determine event boundaries during the gait cycle. Adjusting sensor thresholds modifies the event boundaries that are determined by the force sensors. With the PPAFO tethered to a computer interface, the subject walked at a comfortable self-selected pace. Threshold values for both heel and metatarsal force sensors were systematically adjusted using feedback from the subject to maximize user comfort. Redundant triggers were avoided by maintaining a threshold large enough to exceed the noise level of the unloaded sensors. Once the sensor thresholds were determined, the values were then downloaded to the embedded microcontroller on the PPAFO, which allowed untethered operation of the device. In these trials, the subject specific sensor

thresholds did not have to be robust to changes in the subject's gait pattern because only level walking at a self-selected pace was examined.

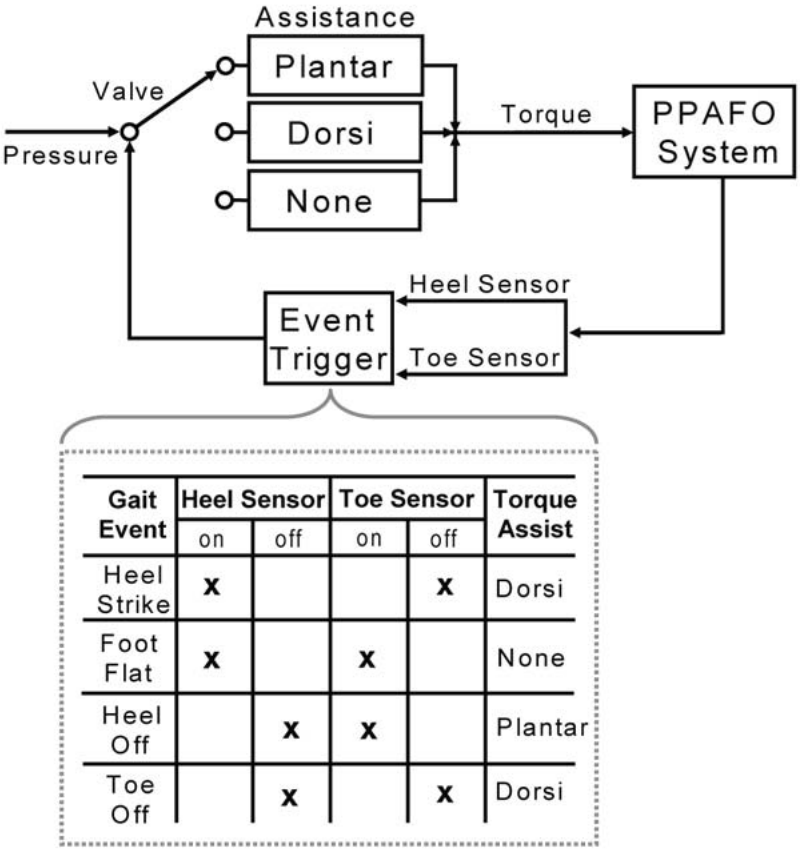

Gait Event	Heel Sensor		Toe Sensor		Torque Assist
	on	off	on	off	
Heel Strike	x			x	Dorsi
Foot Flat	x		x		None
Heel Off		x	x		Plantar
Toe Off		x		x	Dorsi

Figure 3.3 *PPAFO force sensor data are used to identify the current gait event. The initiation of the event determines the corresponding valve configuration, which dictates the type and direction of torque assistance.*

3.2.1.3 Empirical Characterization of PPAFO System Performance

Performance characteristics of the PPAFO system were determined experimentally. These performance metrics were: torque generation as a function of input pressure, positional

response rate of the system, energy consumption per actuation cycle, initial stored energy of the CO_2 bottle, and continuous use duration.

The off-the-shelf PPAFO actuator was rated to a working pressure of 150 psig, a range within which a linear relationship between torque and pressure existed as stated in the manufacturer's documentation (CRB2BW40-90D-DIM00653; SMC Corp of America, Noblesville, IN, USA). The goal of the initial characterization was to validate this linear relationship once the actuator had been integrated into the system. Torque was estimated indirectly as a function of input pressure. Two tethered pressure transducers were used to directly measure the pressure, P, in the actuator chambers in order to calculate assistive torque (4100 series; American Sensor Technology, Mt. Olive, NJ, USA). Output PPAFO torque, τ, was calculated by measuring the force generated at a fixed distance from the PPAFO axis of rotation. Direct force measurements were made using a digital scale (Berkley, IA, USA) over a 95 psig input range. The scale was secured to the unloaded foot piece 15 cm away from the axis of rotation. Three repetitions of measurements were made at increasing 5 psig increments and then repeated for decreasing increments. The averages of each repetition were then used to determine a best-fit straight line between output torque and input pressure, such that $\tau = K_{actuator} P$. The coefficient $K_{actuator}$ represented the linear relationship between pressure and torque.

To evaluate the response rate of the PPAFO, a step response analysis was conducted for both a loaded and unloaded system. The loaded weight (0.96 kg) was selected based on the anthropometric foot weight of a healthy subject with body mass of 73 kg [8]. During the experiment a 90 psig pressure was used to power the actuator. The foot piece was allowed to rotate through the full 90 degree range of motion capacity of the rotary actuator. The 90 psig

activation level was selected because it was the largest assistive pressure used during the empirical subject testing and would result in the fastest system response. Position of the PPAFO foot piece was measured with an angle sensor (53 Series; Honeywell, Golden Valley) (Fig. 3.1). Five repetitions of measurements were used to calculate the average initiation and completion of the 90 degree range of motion for both the unloaded and loaded PPAFO foot piece. The time required to fully disable the system was determined by pressurizing the actuator to 90 psig and then timing the discharge of CO_2 from the system after valve activation. Ten repetitions of the discharge were conducted while the PPAFO shank and footplate were maintained at a neutral position.

The energy consumption of the PPAFO for an actuation cycle was determined by measuring the CO_2 consumed by the system during steady-state walking of a healthy individual (1.0 m/s). Trials at both high and low levels of assistance were examined to span the range of energy consumption. Plantarflexor assistance at 90 psig (0.62 MPa) and dorsiflexor assistance at 30 psig (0.21 MPa) were chosen for the high level trial. The low level trial was conducted with both plantar and dorsiflexor assistance at 30 psig (0.21 MPa), respectively.

In order to analyze the energy consumption of the PPAFO, the exhausted CO_2 for each actuation cycle was first collected. It was assumed that the temperature of the CO_2 after the regulator was the same as the actuator CO_2 exhaust to make use of the ideal gas law, $P_1V_1 = P_{atm}V_2$. Here P_1 was the pressure at the regulator, V_1 was the volume of the unexpanded CO_2 in the actuator, P_{atm} was atmospheric pressure (1.01 MPa), and V_2 was the measured volume of the exhausted gas. The mass of the CO_2 was then calculated for 20 actuation cycles during both the high and low levels of assistance, $m = P_{atm}V_2\frac{\mu}{RT}$. Here R is the universal gas

constant (8.314 J/(mol·K)), T is the gas temperature (298 K), and μ is the molecular weight of CO_2 (0.044 kg/mol). The energy consumed per cycle was calculated from, $E_{cycle} = P_1 V_1 \ln \frac{P_1}{P_{atm}}$ [56]. Additionally, the initial stored energy of the bottle was calculated using the equation, $E_{bottle} = \frac{m}{\mu} RT \ln \frac{P_1}{P_{atm}}$, where m is the mass of CO_2 in the bottle (0.255 kg).

To examine the longevity of the system, a duration of use test was conducted. During this test, a healthy individual walked at the low assistance level with the portable CO_2 bottle (filled with 0.255 kg of CO_2) until the final charge pressure dropped below 20 psig. The low level of assistance was selected to minimize the energy consumption and maximize the duration of use for the system.

3.2.2 Empirical Testing of PPAFO Functional Performance during Gait

3.2.2.1 Healthy Subjects

Three healthy male volunteer subjects (mean age 26 ± 4 yrs; height 187 ± 7 cm; weight 79 ± 6 kg) walked with the PPAFO on a treadmill to evaluate device functionality. Subjects had no gait impairments, no history of significant trauma to the lower extremities or joints, and were experienced treadmill walkers.

3.2.2.2 Impaired Subject

One male volunteer subject (51 yrs; height 175 cm; weight 86 kg) was recruited for the study. The subject presented with a diagnosis of cauda equina syndrome (CES) caused by spinal disc rupture that occurred during a physical therapy session. At the time of the study, the subject was five years post-surgery to decompress the site of injury. The primary functional motor

deficit was an almost complete loss of functional plantarflexion and partial loss of sensation in the lower legs and feet with bilateral involvement. The general muscle group strength values for the impaired subject's lower limbs using a 0-5 muscle grade scale (0 = no contraction; 5 = normal strength against gravity and with resistance) was as follows: Gluteal - 5, Quadricep - 5, Hamstring - 4.5, Dorsiflexor - 4.5, Plantarflexor - 0.5. The subject could walk without the use of orthoses and walking aids (e.g., cane or walker), but used two bilateral off-the-shelf canvas lace-up AFOs designed to restrict movement for community ambulation. In addition to these orthoses, the subject had a pair of pre-fabricated carbon composite AFOs (Blue Rocker™, Allard, NJ, USA) that were used for bicycling activities and occasionally for community ambulation. The subject stated that he rarely used the carbon composite AFOs for walking.

3.2.2.3 Subject Data Collection and Analysis (Functional Walking Analysis)

Functionality of the device was demonstrated during treadmill walking trials. Five footwear conditions were tested: walking or running shoes, and the PPAFO with [0, 30, 50, 90] psig assistance. Each subject initially walked in his shoes, followed by randomized order of the four PPAFO assistance conditions. For the healthy subject, each trial length was 90 s. For the impaired subject, each trial length was 60 s and shoe walking trials included no orthotic support.

Before the start of testing, self-selected walking speed was determined. For the healthy subjects, comfortable treadmill walking speed was determined by averaging three self-selected comfortable speeds chosen while wearing the PPAFO with no torque assist. Because the unassisted PPAFO walking was anticipated to impose the greatest walking difficulty, it was selected to define comfortable walking speed. Average walking speed for the three healthy subjects was 1.1 m/s, with a range of 0.91 – 1.3 m/s. The impaired subject’s comfortable walking speed was determined while wearing his running shoes on the treadmill with no assistive devices

on either leg. This walking condition was used because it was the impaired subject's most difficult condition. Walking speed for the impaired subject was 0.7 m/s.

During the walking trials, kinematic and kinetic gait data were collected. To aid in data collection, subjects wore a sleeveless top and snug-fitting shorts. Forty-five reflective markers were attached to the head, torso, arms, legs, and AFO. Data from healthy subjects were collected at the University of Illinois. Kinematic data were collected using a 6 camera motion analysis system sampled at 150 Hz (Model460; Vicon, Oxford, UK). Ground reaction force and center of pressure data for each foot were collected with a split belt treadmill with embedded force plates sampled at 1500 Hz (Bertec, Columbus, OH, USA). Data from the impaired subject were collected at Georgia Institute of Technology. Kinematic data were collected using a similar 6 camera system (Model 460; Vicon, Oxford, UK) sampled at 120 Hz, and kinetic data were collected with a split belt custom-built treadmill with custom AMTI force plates sampled at 1080 Hz [57]. During the walking trials, the impaired subject was allowed to use a forward handrail placed at chest height for stabilization if necessary. Motion and force data for all subjects were filtered using low-pass, fourth-order, zero-lag, Butterworth filters with cut-off frequencies of 8 Hz and 15 Hz, respectively. During all trials, data were also collected from the two pressure transducers and the PPAFO force sensors sampled at 30 Hz. Surface electromyography data (Bagnoli-16 Desktop EMG System; Delsys, Boston, MA, USA) were collected from the healthy subject's right tibialis anterior (TA) at 1500 Hz. The EMG data were rectified and low-pass filtered using a fourth-order, zero-lag, Butterworth filter with a cut-off frequency of 6 Hz.

Following the application of the markers and EMG sensor, all subjects completed their shoe walking trial. The randomized PPAFO trials were then conducted. Because all subjects in this study had similarly sized feet and no dorsiflexor deficits, a consistent 30 psig of dorsiflexor

assistance was used with all subjects during their assisted walking trials. For the healthy subjects, sensor thresholds for the identification of event boundaries were determined for the 30, 50, and 90 psig plantarflexor propulsive assistance after the subject's shoe walking trial. The PPAFO was not removed once the sensor thresholds had been determined to reduce variability in the force sensor readings due to the strapping of the device. The impaired subject used a heel walking pattern due to his impairment; as a consequence, he was not able to apply enough force on the metatarsal force sensor to activate the plantarflexor torque assistance. Plantarflexor torque was therefore triggered remotely for each cycle by an investigator based on visual observation of the foot placement and verbal commentary by the subject.

3.3 Results

3.3.1 PPAFO System Performance Characteristics

Several parameters were used to evaluate PPAFO system performance including torque generation, positional system response, energy consumption per actuation cycle, initial stored energy of the CO_2 bottle, continuous duration of use, and sensor performance. The relationship between input pressure and output torque generation was found to be represented by the slope of a best-fit straight line between the data points shown in Fig. 3.4 (A) such that $K_{actuator} = 1.451 \times 10^{-5}$ m^3. The best-fit line fell between the data points because of the frictional torque in the actuator. As pressure increased during the evaluation (x), static friction opposed the vane motion thereby reducing force measurements at the scale. The opposite effect occurred as pressure was decreased from 95 to 0 psig (o) resulting in higher force measurements. Therefore, the torque difference between data points at equivalent pressures was estimated to be twice the static frictional torque of the actuator, yielding $\tau_{static} = 0.45$ Nm.

To evaluate the response rate of the PPAFO, a step response test was performed on both the loaded and unloaded system (Fig. 3.4 (B)). Initiation of rotation (t_1) occurred for both the loaded and unloaded footplate 0.017 s after the activation signal was sent. The completion of the full 90 degrees of rotation (t_2) of the unloaded system was faster (t_2 = 0.1 s) than the loaded system (t_2 = 0.15 s). The response rates of the unloaded and loaded system were thus determined to be 900 deg/s and 600 deg/s, respectively. The time required to disable the system from a fully activated state was found to be 0.23 s.

The energetic cost for the high and low actuation levels was determined by measuring exhausted CO_2 over 20 consecutive cycles. During the evaluation of the high actuation, the PPAFO exhausted an average of 0.166 L/cycle of gas. This resulted in an average energy consumption of 33.0 J/cycle. In comparison, the system at the low actuation level exhausted an average of 0.085 L/cycle of gas and had an average energy consumption of 9.6 J/cycle.

The duration of use test was conducted with 30 psig (0.21 MPa) plantar and dorsiflexor assistance. The test lasted for 37.5 min, during which the subject took 1914 steps. Initial stored energy of the bottle was calculated to be 16 kJ. Therefore, based on continuous usage, these results translated to an energy consumption of 8.4 J/cycle, a comparable rate to the energetic cost at the same level of assistance determined from the 20 cycle CO_2 exhaust experiment (9.6 J/cycle).

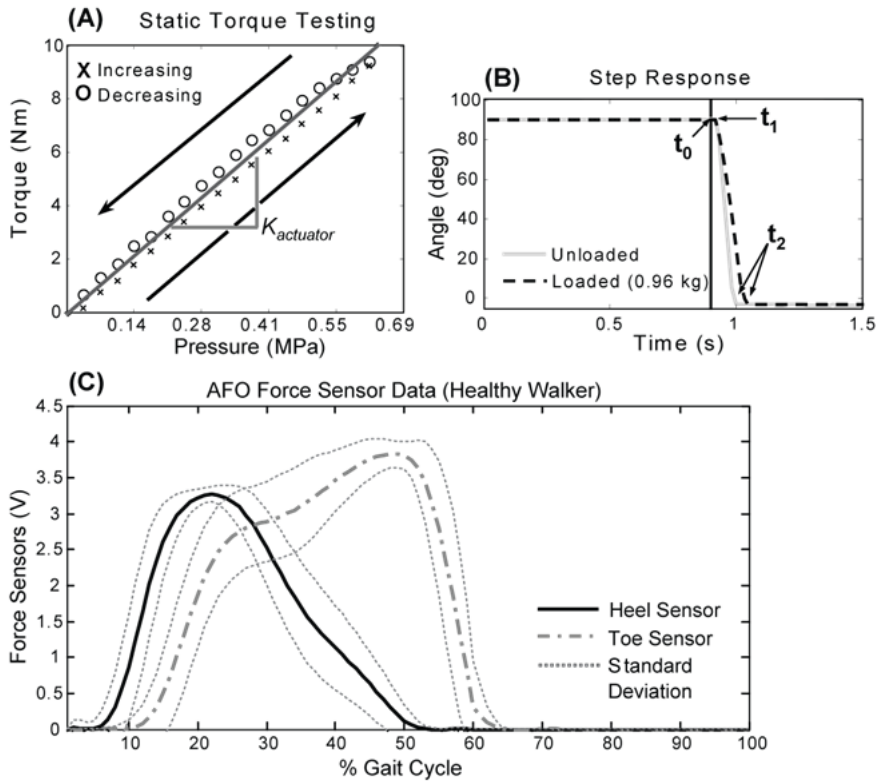

Figure 3.4 ***(A)****: Experimental determination of output torque generation of the PPAFO system as a function of input pressure. Pressure was increased in 5 psig (0.034 MPa) increments (denoted as* X*) to 90 psig (0.621 MPa) and then decreased in 5 psig increments from 95 psig (0.655 MPa) (denoted as* O*). The torque increased linearly with pressure as noted by slope* $K_{actuator}$ *.* ***(B)****: Positional step response of the PPAFO system. Valve activation (*t_0*), initiation of rotation (*t_1*), and the cessation of rotation (*t_2*) are shown in the plot. Average response of the unloaded (solid) and load (dashed) system.* ***(C)****: Average footplate force sensor data (78 cycles) from a healthy subject. Data were normalized to percent gait cycle with toe off occurring at 60% of the cycle.*

The ability of the PPAFO footplate force sensors to detect gait events (e.g., heel strike and toe off) was also examined. Figure 3.4 (C) shows the average of 78 cycles from a healthy walker normalized to percent gait cycle with toe off occurring at 60% of the cycle. The gait

events used to ground truth the sensors were found using ground reaction force data from force plates in the split-belt treadmill. The force sensors detected toe off accurately, but there was a delay of ~5% in the detection of heel strike. This delay has the potential to disrupt the timing of the assistance from the PPAFO, and could be due to the placement of the sensors between the carbon fiber footplate and the foot of the subject instead of on the sole of the AFO.

3.3.2 Functional Walking Results

3.3.2.1 Healthy Walkers

Results from the healthy walking trials demonstrated that the PPAFO provided functional torque assistance during the targeted phases of the gait cycle (Fig. 3.5 (A)): (1) dorsiflexor torque to resist foot motion during loading response, (2) free range of motion early in stance, (3) modest plantarflexor assistive torque late in stance, and (4) dorsiflexor torque during swing. Sensor data were successfully used for event detection during the healthy walking trials (Fig. 3.5 (B)). At the highest level of plantarflexor assistance (90 psig), the ankle kinematics were affected during both stance and swing. Dorsiflexion was reduced throughout stance, while peak plantarflexion of the joint was delayed into swing (Fig. 3.5 (C)). Neither the timing nor the magnitude of the vertical ground reaction force was significantly affected by the PPAFO assistance (Fig. 3.5 (D)).

EMG data collected from the healthy walkers indicated reduced muscle activation during assistance (Fig. 3.6). This reduction in activation level was most apparent in the tibialis anterior. Muscle activation was reduced during both loading response for motion control of the foot and during swing to maintain toe clearance.

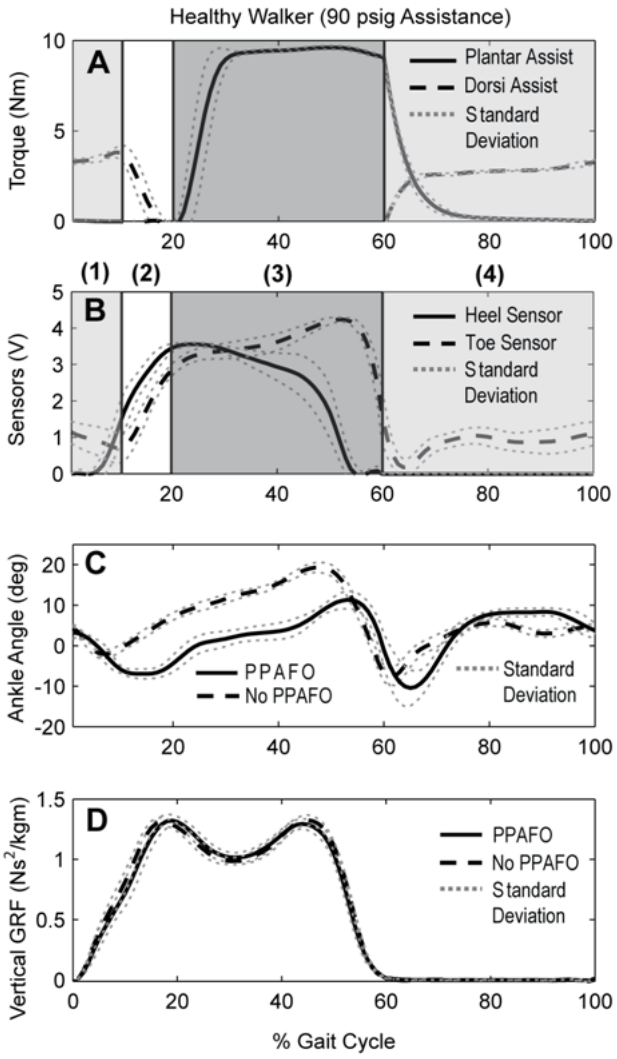

Figure 3.5 *Averaged data (25 gait cycles) from a healthy walker at self-selected walking speed with a peak assistive torque of 9.2 Nm from an operating pressure of 90 psig. The data were normalized to stance and swing with toe off occurring at 60%.*

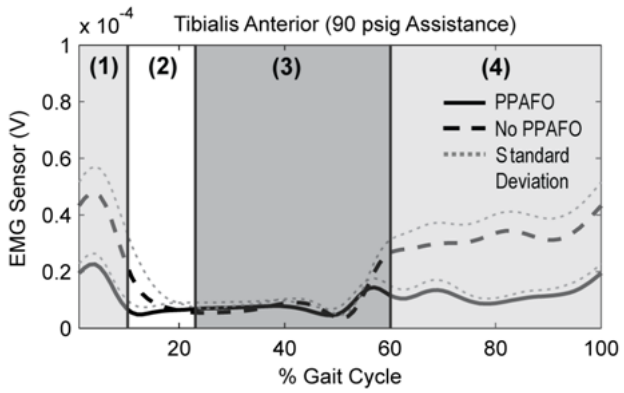

Figure 3.6 *Averaged data (25 gait cycles) for the tibialis anterior from a healthy walker at self-selected walking speed with and without assistance. The subject walked with 90 psig plantarflexor assistance and 30 psig dorsiflexor assistance. A visible decrease in activation level is present in the EMG data from the sensor placed on the tibialis anterior. The data were normalized to stance and swing with toe off occurring at 60%.*

3.3.2.2 Impaired Walker

The impaired walker had retained dorsiflexor functionality, but required assistance for an almost complete loss of functional plantarflexion. The subject's assisted walking trials demonstrated that the PPAFO was capable of providing functional plantarflexor assistance. However, the device was not able to apply the plantarflexor assistance correctly during the cycle due to the impact of the subject's heel walking pattern (Fig. 3.7 (B)). The heel walking pattern was characterized by excessive dorsiflexion throughout the cycle, and reduced loading of the forefoot during stance. This reduced loading resulted in a significantly reduced loading of the forefoot force sensor, preventing correct PPAFO event detection. As a result, the plantarflexor torque was triggered remotely for each cycle by an investigator, with the timing dependent on investigator observation and subject comment (Fig. 3.7 (A): region 2). Dorsiflexor assist was applied in the other regions of the cycle (Fig. 3.7 (A): regions 1 and 3). The kinematics of the

ankle joint were minimally affected by the PPAFO assistance. A small increase in dorsiflexion (black line) at heel strike is visible in the cycle shown in Fig. 3.7 (C). The assistive capabilities of the PPAFO are most clearly illustrated in the vertical GRF data (Fig. 3.7 (D)). The second peak in the assisted vertical GRF data (black line) indicated the presence of a push off force during late stance, which was not present in the unassisted data (grey dotted). Additionally, during PPAFO assistance the subject spent a greater percentage of the cycle (70%) in stance than during the shoe trial (64%).

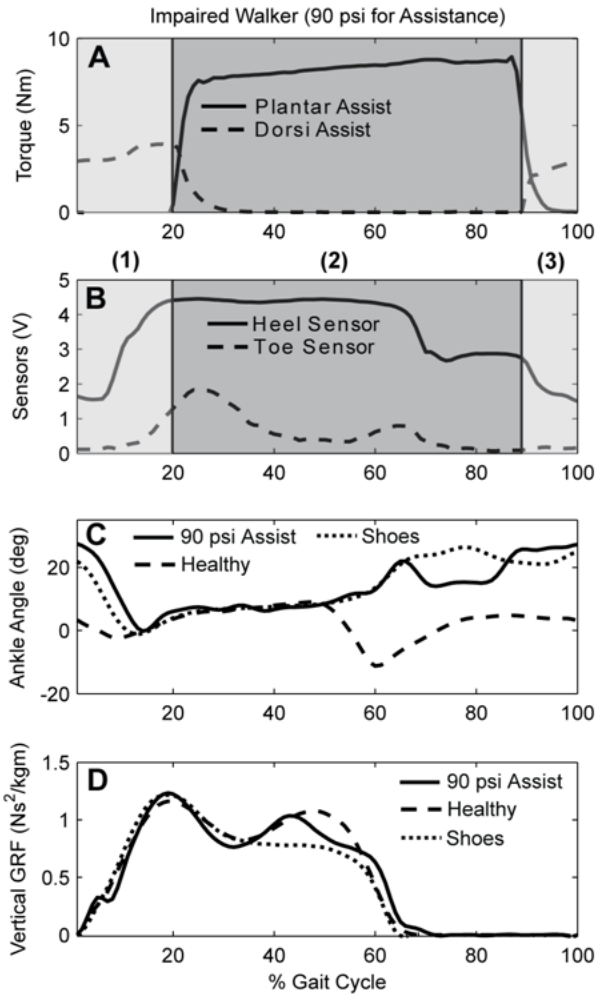

Figure 3.7 *One gait cycle from the impaired subject with a peak assistive torque of 9 Nm from an operating pressure of 90 psig. The data were normalized to percent gait cycle.*

3.4 Discussion

Ankle-foot orthoses are often an integral part of the rehabilitation process for lower limb injuries and impairments. Current clinically available AFO technology is passive and is limited by its inability to actively modulate the assistance provided by the AFO during gait. Powered orthoses have been developed in several university laboratories to provide net power to the ankle joint for motion control and torque assistance, but these systems are tethered and must remain in the lab.

In this chapter, we presented a novel portable powered AFO (PPAFO) with potential applications for daily in-home rehabilitation treatment and demonstrated its functionality with healthy and impaired walkers. The torque generation of the system, up to 9 Nm at 90 psig, resulted in a device that was capable of supplying significant dorsiflexor assistance and modest plantarflexor assistance during gait. The loaded positional system response speed (600 deg/s) was fast enough to actuate the PPAFO during individual phases of gait (where cycle times are on the order of 1 s with ankle range of motion on the order of 30 deg).

In addition to presenting and characterizing a novel untethered fluid powered assist device, pilot data from healthy and impaired subjects were used to demonstrate the potential of the PPAFO to provide both plantarflexor and dorsiflexor assistance during gait. Plantarflexor assistance was demonstrated directly using the data collected from an impaired subject. A suitable individual with impaired dorsiflexors for direct demonstration of dorsiflexor assistance was not available at the time. As a substitute, EMG data from the tibialis anterior (TA) of a healthy individual walking with PPAFO assistance were included in this chapter to demonstrate the effect of the device on dorsiflexor activation. The potential of this device for dorsiflexor assistance could be inferred from the reduction of TA activation observed in the data (Fig. 3.6).

The slow walking pace during the trials (0.8 m/s) may have been responsible for the lack of a distinct TA peak at toe off [58]. The literature indicates that, during slower walking speeds, muscle activation patterns may be more individualized. In a side study, this particular subject was reexamined at the original self-selected walking speed of 0.8 m/s and at 1.5 and 2 times the self-selected walking pace. The data from these trials show TA activation without a distinct peak at toe off during the 0.8 m/s trial (similar to the data presented in Fig. 3.6). As the walking speed was increased, the peaks in TA activation became apparent at both toe off and heel strike.

The results from the healthy walking trials also verified that the PPAFO was capable of providing appropriately timed powered assistance during gait (Fig. 3.5 (A)). PPAFO assistance did perturb ankle joint kinematics of the healthy subject shown in Fig. 3.5 (C). This perturbation resulted in reduced dorsiflexion during stance and greater, but delayed, plantarflexion during the start of swing. The reduced dorsiflexion could have been due to the PPAFO assistance resisting motion, and/or to the structure and strapping of the device reducing dorsiflexor range of motion. The increased plantarflexion seen in swing could also be due to the plantarflexor assist. The valve was closed at toe off, but due to the non-instantaneous release of fluid pressure in the actuator, the magnitude of the plantarflexor assistance did not drop below the level of dorsiflexor assistance until ~65% of the cycle (the approximate location of the peak assisted plantarflexion).

The results from the impaired subject pilot data clearly exhibited the ability of the PPAFO to provide plantarflexor assistance. The impaired subject had bilateral impairment of the lower legs due to CAS, but was able to walk without external aids. The subject's ability to walk without assistance permitted the direct comparison between unassisted and PPAFO-assisted walking. The subject did not use the handrail rail during unassisted walking, but did use the rail during the assisted trial. During the assisted trial, the subject used a single hand as a guide and

did not lean heavily on the rail for support. The use of the light grasp on the handrail allowed the subject an additional sensory cue to aid balance during the trial [59]. While posture may be affected by handrail walking, it has been demonstrated that this may have little effect on sagittal plane kinematics [60]. Grasping the rail will affect the kinetics during walking. In our case, we believe that this affect was minimized by the subject's light grasp and the location of the rail at chest height. The subject employed a heel walking compensation strategy due to his inability to plantarflex and invoke push-off. Unfortunately, the tendency to bear a greater portion of stance phase loading with the heel prevented the correct triggering of the metatarsal force sensor, which was an important control element (Fig. 3.7 (B)). To compensate for this, the plantarflexor assist was manually operated during the walking trials.

The pilot data shown in Fig. 3.7, along with feedback from the subject that the PPAFO provided substantive assistance, demonstrated that this device was capable of providing plantarflexor assistance sufficient for gait modification. Subject feedback during the PPAFO assisted walking trials was positive, reporting that he could sense an improvement in his gait with the power assist on and could markedly distinguish the difference. We speculate that the power assist, activated at foot contact, provides resistive dorsiflexion control throughout stance. During unassisted walking the absence of plantar flexors did not permit a heel rise during late stance resulting in dorsiflexion throughout stance phase. With the loss of plantarflexion and push-off, the third rocker of gait is compromised. This was demonstrated by the single peak ground reaction force data during unassisted walking (Fig 3.7 (D): dotted line). During assisted walking, a second peak in the ground reaction force, indicative of push off in healthy gait, was present in the data (Fig. 3.7 (D): solid line). We theorize that the additional plantarflexor torque from the PPAFO acted as a dorsiflexor resist that may serve as a type of alternative rocker that

transmits forces at terminal stance creating push off. Essentially the second rocker, which is the forward advancement of the tibia over the foot, was modified by a controlled forward progression via the power assisted plantarflexion. Additionally, based on the subject's perception of improved performance during gait, we speculate that the subject actively worked to maximize the efficiency of this load transmission via the controlled advancement of the tibia over the foot during stance.

Although results from the study presented in this chapter are encouraging, several important limitations must be discussed. First, we were able to demonstrate untethered assistance with healthy walkers, but device control issues that resulted from the impaired subject's heel walking strategy and the fit of the device to the user prevented a full demonstration of untethered functional assistance for the impaired subject. We believe that the placement of the force sensors between the carbon fiber shell of the PPAFO and foot was partially to blame for our inability to reliably detect gait events during the testing of the impaired subject. The sensors became saturated when the PPAFO was secured to the impaired subject. As a result, the sensors did not reliably detect gait events. This problem could be addressed by relocating the sensors between the carbon fiber footplate and the sole of the PPAFO. A change in sensor location may result in readings that are not impacted by the subject specific fitting issues associated with assistive devices. The experimental data collection for the study in Chapter 4 was conducted with improved sensor position.

Second, the binary control strategy used during the healthy walking trails created a perturbation to the ankle joint kinematics. Control strategies that result in assistance with improved timing could resolve this issue and will be discussed in Chapter 6.

Third, the ability to assist a functional plantarflexor deficit was demonstrated, but we were not able to demonstrate functional dorsiflexor assistance since all subjects had functional dorsiflexors. We were able to infer that the PPAFO provided dorsiflexor assist with the tibialis anterior EMG data from the subjects, but experimental confirmation with an impaired subject with dorsiflexor weakness needs to be done. Chapter 4 presents results from a subject with a dorsiflexor impairment.

3.5 Conclusion

In this chapter we introduced the design of a novel portable pneumatically powered ankle-foot orthosis. Pilot data from both healthy walkers and an impaired individual demonstrated device functionality and laid the ground work for future studies with larger subject populations. While direct comparisons between the healthy and impaired subjects are not possible, taken as a whole, data from the two groups can be used to make a strong case for the potential benefits of this device. Unlike other powered orthoses, the untethered nature of the PPAFO would allow for in-home rehabilitation use. This would provide the user with increased autonomy by increasing the extent of the rehabilitation process that could take place outside of a clinical setting. The PPAFO provides portability combined with the flexibility to modulate the direction (dorsal or plantar), timing, and magnitude of assistance. Such diversity allows the orthosis to meet an individual's changing functional requirements, and offers promise as a clinical tool in many arenas of the rehabilitation process. While the pilot data presented in this chapter demonstrated functional plantarflexor assistance, the quantification of the PPAFO's ability to provide assistance requires further examination. To this end, data from a subject with a dorsiflexor impairment and two additional healthy subjects were added to the data set presented

in this chapter. The data from this enlarged set were then examined using an expanded set of gait analysis metrics to quantify the biomechanical effect that the PPAFO had on gait. These results are presented in Chapter 4.

Chapter 4
EXPERIMENTAL EVALUATION OF THE PPAFO

4.1 Introduction

Chapter 3 introduced a novel PPAFO and demonstrated the functionality of this device with experimental data collected from healthy walkers as well as an impaired walker. These preliminary results confirmed the PPAFO's ability to provide functional plantarflexor assistance, while inferring dorsiflexor assistance through the healthy subject data [61]. The current chapter seeks to further quantify the functional performance of the PPAFO.

Functional performance of both passive and powered PPAFOs has been quantified in a number of ways. Time and distance measures such as walking velocity, cadence, step length, stride length, and cycle timing have provided simple metrics for comparison [17, 24]. Kinematic marker data have been used for both direct performance comparisons and to calculate other parameters such as joint angles for quantitative and qualitative assessment of an PPAFO's effect on movement patterns during gait [17, 22, 23]. Kinetic data collected from both force plates and sensors on an PPAFO have also provided information about device performance. In addition to direct evaluation of performance, the kinetic data have been used, in conjunction with kinematic data, to calculate joint moments and powers during assisted gait [30, 31]. Finally, embedded PPAFO angle sensors and foot switches have been used to quantify the functionality of the

device [29, 30, 61]. In this chapter, time and distance measures along with ankle joint moments and powers will be used to evaluate the functional performance of the PPAFO.

As a compliment to traditional analysis metrics, two recently developed gait analysis techniques were used to quantify PPAFO performance here. Diberardino et al. introduced a new approach to assess changes to complexity and variability during gait [62]. These changes, illustrated through segment angular phase portraits of the thigh, shank, and foot, were used to provide insight into how the dynamics of gait were modified by the PPAFO. Additionally, recent work by the authors includes the development of a regions of deviation (ROD) analysis technique to improve the quantification of asymmetry in gait [63]. In that study, ROD analysis was used to quantify bilateral lower limb joint angle asymmetries and to examine individual deviations between an impaired subject's joint angles and healthy group reference angles. A more detailed examination of changes in symmetry is warranted because asymmetries are symptomatic of pathological gait, and changes in symmetry can be used to identify and track the resolution of gait impairments [64]. These additional metrics will offer increased insight into both kinematic and kinetic changes created by PPAFO assistance.

The proposed combination of traditional and new analysis metrics was used to evaluate the functional performance of the PPAFO in two different scenarios. Specifically, PPAFO performance was evaluated during treadmill walking with 1) five healthy subjects at variable walking speeds, and 2) two impaired subjects (one subject with only plantarflexor impairment and one subject with only dorsiflexor impairment) at their comfortable walking speed. These particular scenarios provided insight into the sensitivity of the PPAFO assistance to varying walking conditions, and demonstrated the PPAFO's ability to provide a range of functional

assistance. Additionally, the impairments highlighted the ability of the PPAFO to provide appropriately timed motion control and torque assistance during gait.

Along with quantifying the PPAFO's ability to provide functional assistance, this chapter also addressed two PPAFO system limitations identified in Chapter 3. First, device control issues that resulted from the location of the PPAFO foot sensors have been resolved through improved sensor placement. Second, the PPAFO's ability to provide both functional dorsiflexor and plantarflexor assistance was confirmed through experimental testing of two impaired subjects.

The remainder of this chapter is structured in the following manner. Section 4.2 includes a description of system hardware, detailed subject demographics, a further description of the gait analysis techniques used in this study, and the experimental testing protocol for the subjects. Section 4.3 contains the results from the experimental trials. Section 4.4 provides a discussion of the results, with concluding remarks presented in Section 4.5.

4.2 Methods

4.2.1 System Description Hardware and Control

As in Chapter 3, functional assistance at the ankle joint during gait is created by the PPAFO worn on the right shank and foot. The PPAFO uses a rotary actuator at the PPAFO ankle joint powered by a portable pneumatic power supply for motion control and propulsion assistance [61].The magnitudes of the assistive torques are modulated with two separate pressure regulators. The assistance levels can be adjusted separately to allow the dorsiflexor assistance to be reduced below plantarflexor levels to ensure that this muscle group is not overpowered. The dorsiflexor assist is tuned to a subject's individual needs by adjusting the regulator until the PPAFO supports the relaxed weight of the subject's foot in a neutral (90 degree) position. The

structure of the device provides support and stability throughout the cycle. The PPAFO is controlled using sensor feedback from two force sensors (0.5 in circle, Interlink Electronics, Camarillo, CA, USA). These sensors are mounted underneath the heel and toe between the carbon fiber shell and the sole of the PPAFO.

Feedback from the PPAFO sensors are used to trigger assistance in three regions determined by functional gait requirements: (1) dorsiflexor assist to prevent foot slap during loading response by controlling the motion of the foot, (2) plantarflexor torque to provide assistance for propulsion during stance, and (3) dorsiflexor torque to prevent foot drop by maintaining toe clearance during swing [1]. The force sensors in the PPAFO foot plate are used to detect the event boundaries of the three regions. Events are detected when sensor magnitudes exceed tuned thresholds for the heel and metatarsal sensors. A more detailed explanation of both the PPAFO hardware and control scheme can be found in Chapter 3.

4.2.2 Subject Information

All procedures were approved by the institutional review boards of the University of Illinois and Georgia Institute of Technology, and all participants gave informed consent.

4.2.2.1 Healthy Subjects:

Five healthy male subjects (28 ± 4 yrs; height 186 ± 5 cm; mass 72 ± 8 kg) were used to evaluate the robustness of the PPAFO control scheme during level walking. The subjects had no gait impairments and no history of significant trauma to the lower extremities or joints.

4.2.2.2 Impaired Subjects:

The subject with the plantarflexor impairment (male; 51 yrs; height 175 cm; mass 86 kg) has a diagnosis of cauda equine syndrome (CES) caused by a spinal disc rupture and will be

referred to as ISubPF. This bilateral impairment rendered the subject unable to generate a plantarflexor torque to push his toes down. However, the subject was able to generate and control a dorsiflexor torque to lift the toes up. ISubPF could walk without walking aids (e.g., cane or walker), but wore pre-fabricated carbon composite PPAFOs for daily use (Blue Rocker TM, Allard, NJ, USA).

The subject with the dorsiflexor impairment (female; 37 yrs; height 157 cm; mass 62 kg) has a diagnosis of muscular dystrophy and will be referred to as ISubDF. This condition has resulted in bilateral muscle weakness to the lower limbs that affected the subject's ability to dorsiflex properly, but this subject was able to plantarflex. ISubDF wore soft ankle braces in place of rigid AFOs for extra support during gait. This subject was also able to walk without walking aids, but used the treadmill handrails for increased stability during the walking trials.

4.2.3 Experimental Procedure and Data Collection

For all subjects, a comfortable treadmill walking speed was determined at the start of the testing session by averaging three self-selected speeds. For the healthy subjects, comfortable treadmill walking speeds were identified while wearing the PPAFO with no torque assist. This walking condition was assumed to impose the greatest walking difficulty on the healthy subjects. The average self-selected walking speed for the five subjects was 1.2 ± 0.1 m/s. The comfortable walking speeds for the two impaired subjects were determined while wearing running or walking shoes without their individual daily-wear PPAFOs. The self-selected speed was determined without the support of a PPAFO to ensure that the subjects could walk comfortably in their most difficult walking condition. The self-selected walking speed for ISubPF was found to be 0.6 m/s, while the self-selected walking speed for ISubDF was found to be 0.2 m/s.

Kinematic and kinetic data were collected from the subjects during the experimental walking trials. To aid in the data collection, the subjects wore sleeveless tops and snug-fitting shorts. For the kinematic data collection, thirty-two reflective markers were attached to the body, including the torso, thighs, shanks, feet, and the PPAFO. Data from the healthy subjects were collected at the University of Illinois. Kinematic data were collected using a 6-camera motion capture system sampled at 150 Hz (Model 460; Vicon, Oxford, UK). Ground reaction force data for each foot were collected on an instrumented split-belt treadmill with embedded force plates sampled at 1500 Hz (Bertec, Columbus, OH, USA). Data from the impaired subjects were collected at Georgia Institute of Technology. Kinematic data were collected using a 6-camera system sampled at 120 Hz (Model 460; Vicon, Oxford, UK). The kinetic data were collected on a custom force-sensing instrumented split-belt treadmill sampled at 1080 Hz [57].

Experimental trials with the healthy subjects were conducted to examine the sensitivity of the PPAFO system to a speed perturbation. Data were collected continuously during 30 second walking trials with three footwear conditions and at three speeds during each condition. The healthy subjects first walked in running shoes, then with the unpowered PPAFO on their right leg and a running shoe on the left, and finally with the powered PPAFO on their right leg and a running shoe on the left. For each footwear condition the healthy subjects first walked at their self-selected walking speed as described above (normal condition), 25% faster than normal (fast), and 25% slower than normal (slow). For the assisted walking trials, the PPAFO provided the maximum propulsive (plantarflexor) assist during stance and a predetermined amount of dorsiflexor assist during swing. The maximum assist, provided during stance, that the PPAFO is capable of generating is ~12 Nm (110 psig). The magnitude of the dorsiflexor assistance for each

subject was determined a priori by selecting a torque capable of supporting the relaxed foot at neutral (30 ± 10 psig, ~3 Nm).

The experimental trials with the impaired subjects were conducted to demonstrate the PPAFO's ability to provide plantarflexor and dorsiflexor assistance during level walking. Data from the two subjects were collected during 30 second walking trials at the self-selected speeds for three different conditions. First, both subjects walked with running shoes on the right and left feet. During the shoe walking trials the subjects wore their own daily-wear carbon fiber PPAFO on their left leg and no PPAFO on the right leg. Second, the subjects walked with the unpowered PPAFO on the right leg and a running shoe with their daily-wear carbon fiber PPAFO on their left leg. Third, the previous footwear condition was modified by powering the PPAFO to provide functional assistance. For ISubPF, the PPAFO provided a ~12 Nm (110 psig) propulsive assist during stance beginning at foot flat and continuing to heel off. For ISubDF, the PPAFO provided a ~6 Nm (60 psig) assist during swing beginning at toe off and continuing to the following heel strike. Additionally, data were collected from ISubPF for a fourth trial with his daily-wear carbon fiber PPAFO and running shoes on both legs.

4.2.4 Data Analysis

4.2.4.1 Traditional Metrics

Time and distance measures along with ankle joint moments and powers were calculated from the experimentally collected kinetic and kinematic data. Kinetic data were used to identify gait events and divide the data into individual gait cycles for each side of the body. A gait cycle was defined from consecutive ground contacts (heel strikes) of the same limb. Data for each cycle were normalized to a percentage (1-100%) of the cycle. Within a cycle the data were also

normalized to align at the average toe off time for each trial. Kinematic and kinetic data were also used to calculate the following bilateral univariate parameters: ankle, knee, and hip maximum joint angle ranges of motion (ROM), step length (SL), step width (SW), cycle time (CT), and stance time (ST) time. Flexion-extension joint angles were computed using the procedure proposed by [65]. Joint angles were calculated from kinematic data, which were filtered by a low-pass, fourth-order, zero-lag, Butterworth filter with cut-off frequency of 6 Hz. Maximum range of motion was defined as the absolute value of the difference between the largest and smallest angles for a given cycle. Step lengths for each side were defined as the anterior-posterior (AP) distance between the consecutive heel strikes. Single-leg support time was defined as the time spent between toe off and heel strike of the contralateral foot, as determined from the treadmill data. Step width was defined as the medial-lateral distance between heel markers of subsequent heel strikes [65]. A symmetry index was also calculated for the bilateral parameters:

$$SI = \frac{P_R - P_L}{0.5 \cdot (P_R + P_L)} 100\%, \qquad (4.1)$$

where P_R is the value of the parameter on the right side of the body, and P_L is the value of the parameter on the left side of the body [66]. Inverse dynamics analysis was used to calculate the sagittal plane joint moments and powers for the healthy subjects and for ISubPF [8]. Moments and powers were not calculated for ISubDF because she grasped the treadmill handrail throughout the trial leading to an unmeasured contact force during the walking trials.

4.2.4.2 Regions of Deviation Analysis

Both symmetry (SROD) and individual (IROD) regions of deviation analysis were used to examine bilateral sagittal plane joint angles for the healthy and impaired subjects [63].

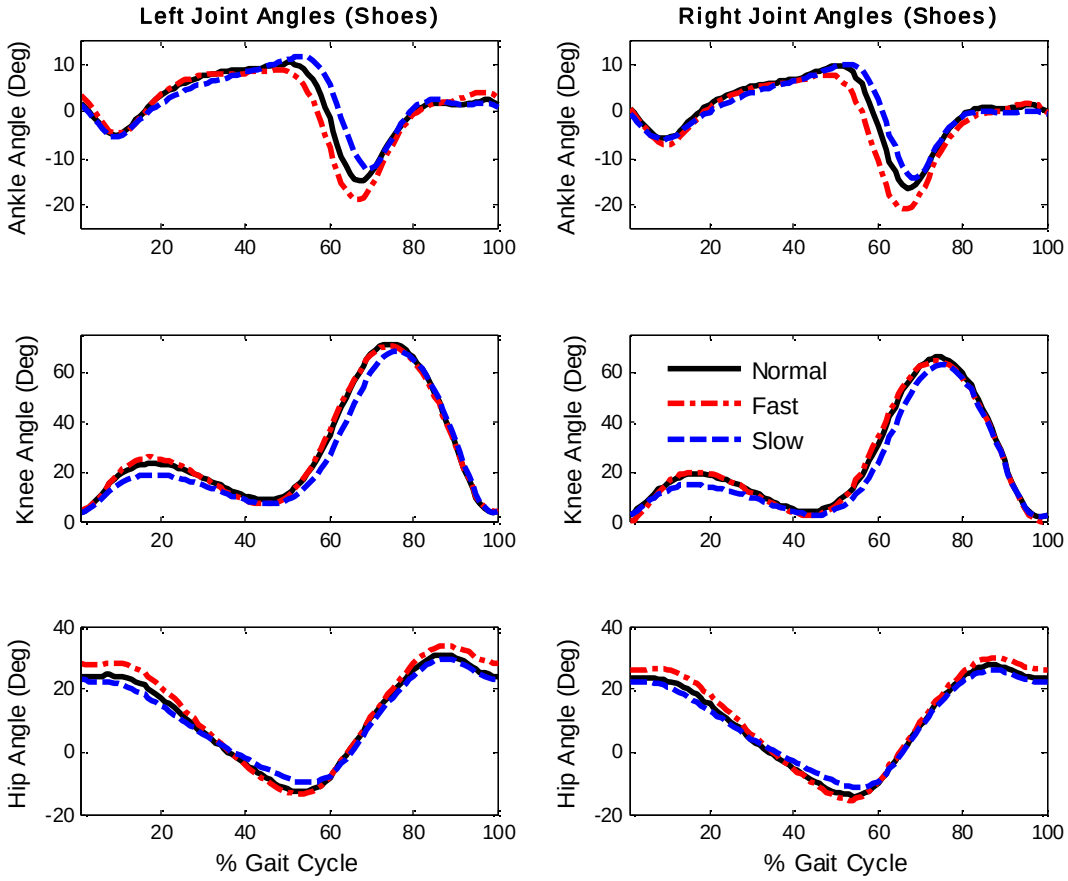

Figure 4.1 *Mean sagittal plane joint angle data for the ankle, knee, and hip. Data were collected from the healthy subjects at their normal, fast, and slow walking speeds. Data from the 30 second walking trials from each subject for each condition were first normalized and then averaged over the five subjects. For the normal trial, right and left toe off occur at 65% of the cycle. For the fast trial, right toe off occurs at 63% and left toe off at 64% of the cycle. For the slow trials, right toe off occurs at 67% and left occurs at 68% of the cycle.*

SROD analysis was used to quantify the magnitude and timing of asymmetric behavior in the ankle, knee, and hip joint angle pairs. IROD analysis quantified deviations of individual joint behavior. Both SROD and IROD analysis use normative models of joint behavior

constructed from reference data. For this work, the healthy shoe walking data from the five healthy subjects were used to construct normative models, against which all subjects were compared. Joint angle data from each healthy subject were first normalized to percent gait cycle as described in Section 4.2.4.1. The normalized data from the five subjects were then averaged together to create the reference models at each gait speed. At least 137 cycles were used to create the normative data for the healthy joint angles at the normal walking speed, 138 cycles for the fast walking speed, and 90 cycles for the slow walking speed. Figure 4.1 shows the representative mean data from the normal, fast, and slow trials.

4.2.4.3 Complexity and Variability Analysis

PPAFO related changes to the complexity and variability of gait over multiple gait cycles were examined using phase portraits and the methodology described in [62]. The phase portraits were constructed from bilateral sagittal plane foot, shank, and thigh segment angles. In these phase portraits, the segment angular position was plotted against its velocity. Representative phase portraits from a healthy subject for one speed and three footwear conditions are shown in Fig. 4.2. Metrics were used to describe the complexity and inter-cycle variability of 20 consecutive gait cycles.

Inter-cycle variability was quantified by the area and drift (the cartesian distance the centroid travels) created by the portrait centroid over multiple cycles. Complexity was quantified by the number of harmonics required to describe the portrait with an Elliptical Fourier Analysis approximation. The complexity and variability analyses were performed on 20 consecutive gait cycles for each limb segment in each trial. Health Subject 04 and ISubDF were excluded from this analysis because their data did not contain 20 consecutive cycles of data. The reduction in

cycles was due to missing marker data (Healthy Subject 04) and a slow self-selected walking speed (ISubDF), respectively.

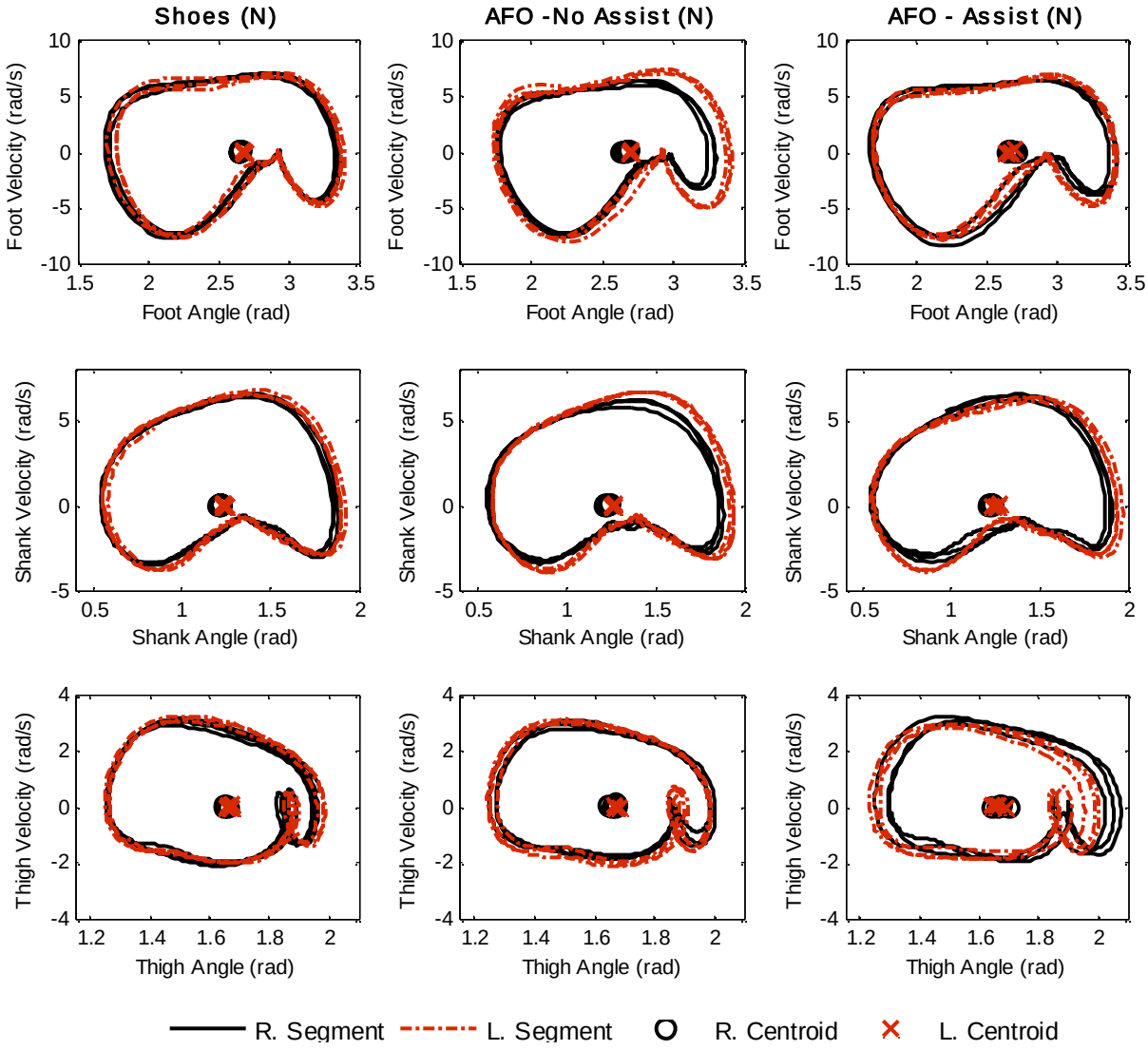

Figure 4.2 *Representative phase portraits from Healthy Subject 05. Sagittal plane foot, shank, and thigh segment angles and velocities from the three footwear conditions at normal walking speeds are shown. Only five of the 20 consecutive cycles are shown for clarity.*

4.3 Results

4.3.1 Results from the Healthy Walkers

4.3.1.1 Traditional Parameters

During the experimental trials, the gait of the healthy walkers was perturbed by the PPAFO (with and without assistance) and by increasing and decreasing treadmill speed. The range of motion (ROM) for all the sagittal plane joint angles increased slightly at the fast walking speed and decreased slightly at the slow speed, with the exception of the left knee joint angle, Table 4.1 and Fig. 4.1. The different footwear conditions resulted in asymmetries between joint angle pairs, particularly at the ankle joint during the unassisted PPAFO walking trials. The average ROM symmetry index (SI) during the unassisted PPAFO walking at the normal speed decreased by 23 at the ankle, 4.6 at the knee, and 6.6 at the hip from the recorded values during shoe walking. A decrease in the ROM SI index indicates that the ROM on the right side of the body was smaller than the left. On the other hand, the ROM SI values during the trials with the PPAFO assistance were similar to the values observed during the trials with shoe walking. For a given footwear condition, the ROM SI values were only minimally affected by a change in speed. For example, the ankle joint ROM SI values for the unassisted PPAFO walking condition were -20.1 at normal, -23.1 at fast, and -23.7 at slow walking speeds.

The effect of speed was more noticeable in the calculated step length and cycle times of the walkers, Table 4.2. For all footwear conditions, the fast walking speed resulted in increased step length and decreased cycle time, while the slow speed perturbation resulted in decreased step length and increased cycle times. The unassisted PPAFO footwear condition had the greatest effect on the length and time parameters. During this footwear condition, the step length SI

decreased at all speeds as compared to the shoe walking footwear condition with differences of 3.2 at normal, 3 at fast, and 2.7 at slow walking. The step length SI increased during the assisted walking trial when compared to the unassisted trials, but still exhibited a decrease as compared to shoe walking SI values. The SI values for the cycle times were small and not greatly affected by the PPAFO (either assisted or unassisted).

Table 4.1 *Healthy subject joint range of motion, mean (and standard deviation), for each speed and footwear condition. N unitless ROM symmetry index (SI) between the bilateral joint pairs was calculated for each joint pair. A negative SI indicates that the parameter value for the left side was greater than the right.*

	Ankle ROM (Deg)			Knee ROM (Deg)			Hip ROM (Deg)		
Trial	Right	Left	SI	Right	Left	SI	Right	Left	SI
Shoes N	26.7 (2.7)	25.9 (2.8)	3.1	66.3 (2.4)	69.9 (4.0)	-5.1	42.7 (3.5)	44.2 (3.5)	-3.5
Shoes F	28.8 (3.2)	28.7 (3.9)	0.4	66.8 (2.0)	68.4 (2.9)	-2.3	45.6 (3.3)	47.1 (2.5)	-3.3
Shoes S	24.9 (1.9)	25.3 (1.3)	-1.6	64.3 (3.1)	67.9 (3.7)	-5.3	38.1 (3.3)	39.4 (1.6)	-3.5
AFO No Assist (N)	21.5 (2.8)	26.2 (3.0)	-20.1	63.4 (4.7)	69.8 (3.6)	-9.7	45.0 (3.4)	43.3 (3.2)	3.8
AFO No Assist (F)	22.7 (2.5)	28.7 (4.8)	-23.1	63.8 (6.3)	68.4 (2.5)	-7.2	49.2 (4.6)	47.5 (5.0)	3.7
AFO No Assist (S)	19.5 (2.8)	24.5 (1.2)	-23.7	62.4 (8.7)	68.0 (3.1)	-8.8	39.7 (3.5)	39.2 (2.1)	1.0
AFO Assist (N)	26.2 (6.2)	25.1 (3.0)	2.4	65.9 (5.4)	68.8 (4.4)	-4.4	44.7 (3.5)	43.7 (2.8)	2.2
AFO Assist (F)	28.7 (6.7)	28.1 (4.1)	1.0	65.1 (4.1)	68.6 (3.6)	-5.4	48.6 (3.1)	48.0 (5.3)	1.7
AFO Assist (S)	24.5 (5.5)	23.3 (0.8)	3.1	62.0 (5.2)	66.0 (5.6)	-6.2	41.1 (3.7)	39.4 (1.9)	4.0

Stance time (ST) time was not greatly affected by either the speed or PPAFO perturbations. The ST values indicate that healthy walkers were spending more time in stance on the PPAFO side of the body during the unassisted PPAFO walking trials. Following the application of assistance, the ST SI values dropped below those present during the shoe walking. Finally, step width was only minimally affected by either speed or the PPAFO perturbations.

Table 4.2 *Healthy subject, mean (and standard deviation), values for step length, cycle time, stance time, and step width for all speed and footwear conditions. A unitless symmetry index (SI) was also calculated for the bilateral parameters. A negative SI indicates that the parameter value for the left side was greater than the right.*

	Step Length (mm)			Cycle Time (s)			Stance Time (s)			Step Width (mm)
Trials	Right	Left	SI	Right	Left	SI	Right	Left	SI	
Shoes (N)	720.3 (31.1)	723.1 (25.7)	-0.4	1.15 (0.07)	1.15 (0.07)	-0.02	0.74 (0.05)	0.75 (0.05)	-1.35	159.7 (25.6)
Shoes (F)	790.4 (28.8)	793.1 (23.5)	-0.4	1.03 (0.05)	1.03 (0.05)	0.06	0.65 (0.04)	0.66 (0.03)	-0.48	158.7 (23.8)
Shoes (S)	644.0 (49.1)	644.2 (40.5)	-0.1	1.28 (0.09)	1.29 (0.09)	0.12	0.86 (0.07)	0.88 (0.07)	-1.80	166.9 (42.3)
AFO No Assist (N)	702.4 (29.0)	728.1 (22.8)	-3.6	1.16 (0.09)	1.16 (0.09)	0.01	0.74 (0.06)	0.77 (0.06)	-3.25	169.5 (21.5)
AFO No Assist (F)	783.8 (29.7)	810.9 (19.7)	-3.4	1.06 (0.07)	1.05 (0.07)	0.82	0.66 (0.05)	0.68 (0.05)	-2.37	173.6 (25.4)
AFO No Assist (S)	625.3 (40.4)	642.6 (30.9)	-2.8	1.30 (0.09)	1.30 (0.09)	0.1	0.88 (0.06)	0.89 (0.06)	-2.15	172.9 (23.3)
AFO Assist (N)	713.3 (52.0)	731.7 (44.1)	-2.6	1.18 (0.04)	1.18 (0.04)	-0.01	0.77 (0.04)	0.77 (0.04)	-0.70	166.7 (25.4)
AFO Assist (F)	794.0 (27.6)	812.4 (24)	-2.3	1.05 (0.03)	1.05 (0.02)	-0.02	0.67 (0.04)	0.67 (0.03)	-0.03	163.1 (24.1
AFO Assist (S)	655.4 (64.3)	661.7 (46.6)	-1.1	1.39 (0.08)	1.38 (0.08)	0.82	0.93 (0.05)	0.92 (0.06)	0.77	164.3 (27.9)

The moment and power generated at the ankle joint were affected by the speed and assistance perturbations, Figs. 4.3 and 4.4. For all footwear conditions, faster walking speeds resulted in higher joint powers and slower walking speeds resulted in lower joint powers, Tables 4.3 and 4.4. Peak power shifted slightly earlier in the cycle for the fast trials and later for the slow trials. During the shoe and unassisted walking conditions the right and left peak ankle moments increased slightly during the fast trial and decreased slightly during the slow walking. This trend was not seen in the data from the assisted walking trials. The average peak moment at the unassisted (no PPAFO assist) left ankle joint during the normal speed was larger than both the fast and slow trials, Fig. 4.3 bottom left panel.

Table 4.3 *Peak moment and powers and associated % gait cycle timing for the left ankle joint.*

	Left Peak Ankle Moment (Nm/kg)		Left Peak Ankle Power (W/kg)	
Trials	Magnitude	% Gait Cycle	Magnitude	% Gait Cycle
Shoes (N)	0.87	49	1.57	56
Shoes (F)	0.93	49	2.10	55
Shoes (S)	0.79	50	1.05	59
AFO No Assist (N)	0.97	50	1.82	57
AFO No Assist (F)	1.07	49	2.55	55
AFO No Assist (S)	0.91	50	1.29	59
AFO Assist (N)	1.12	49	1.77	56
AFO Assist (F)	1.06	49	2.79	55
AFO Assist (S)	0.93	49	1.32	57

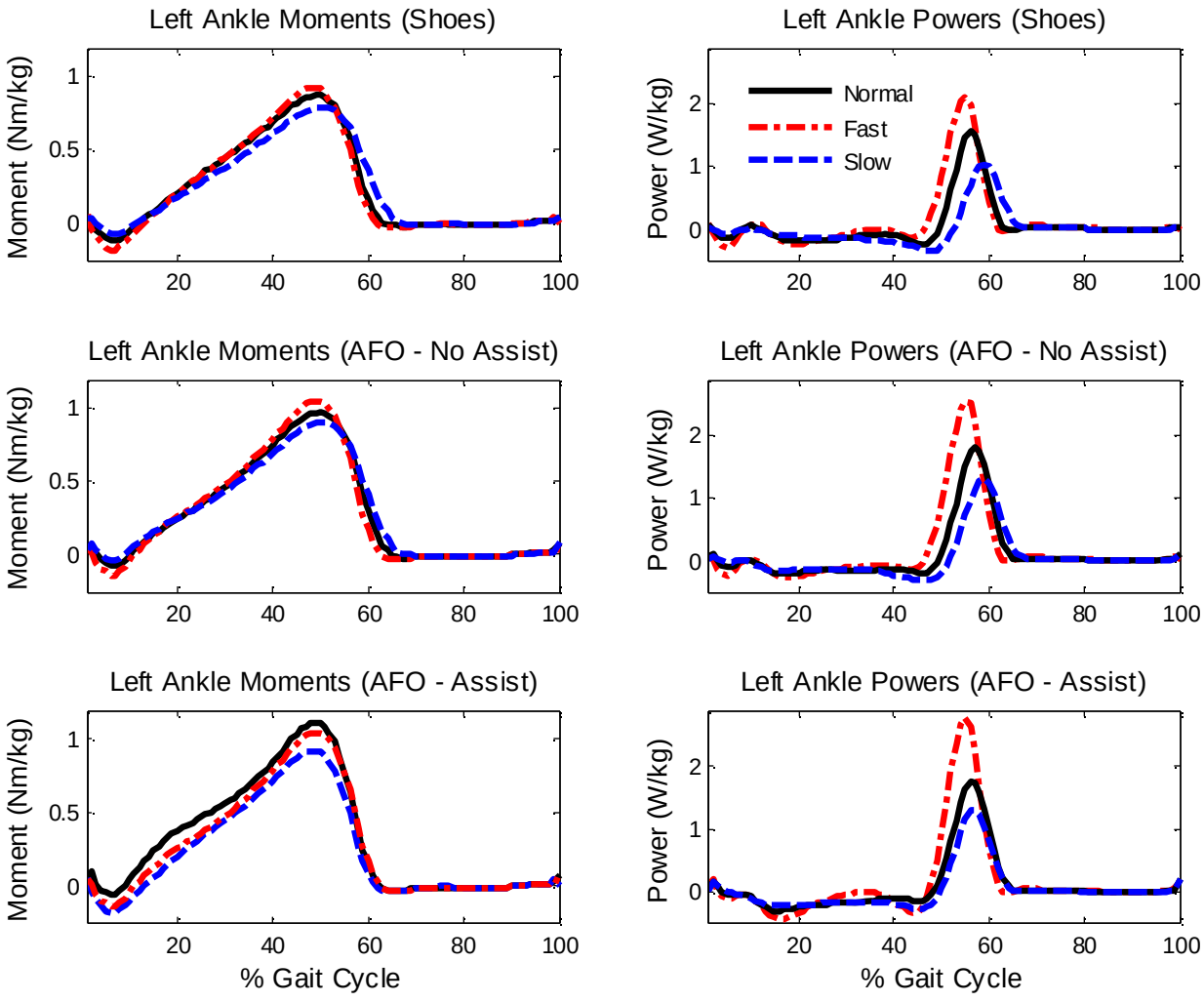

Figure 4.3 *Healthy walker average left ankle moments and powers for the three footwear conditions and three walking speeds.*

Table 4.4 *Peak moment and powers and associated % gait cycle timing for the right ankle joint.*

	Right Peak Ankle Moment (Nm/kg)		Right Peak Ankle Power (W/kg)	
Trials	Magnitude	% Gait Cycle	Magnitude	% Gait Cycle
Shoes (N)	0.85	50	1.55	56
Shoes (F)	0.91	49	2.08	54
Shoes (S)	0.76	51	1.04	58
AFO No Assist (N)	0.97	50	1.49	55
AFO No Assist (F)	1.06	49	1.92	53
AFO No Assist (S)	0.91	50	1.05	58
AFO Assist (N)	0.89	50	1.51	56
AFO Assist (F)	0.89	49	2.07	54
AFO Assist (S)	0.91	49	1.12	58

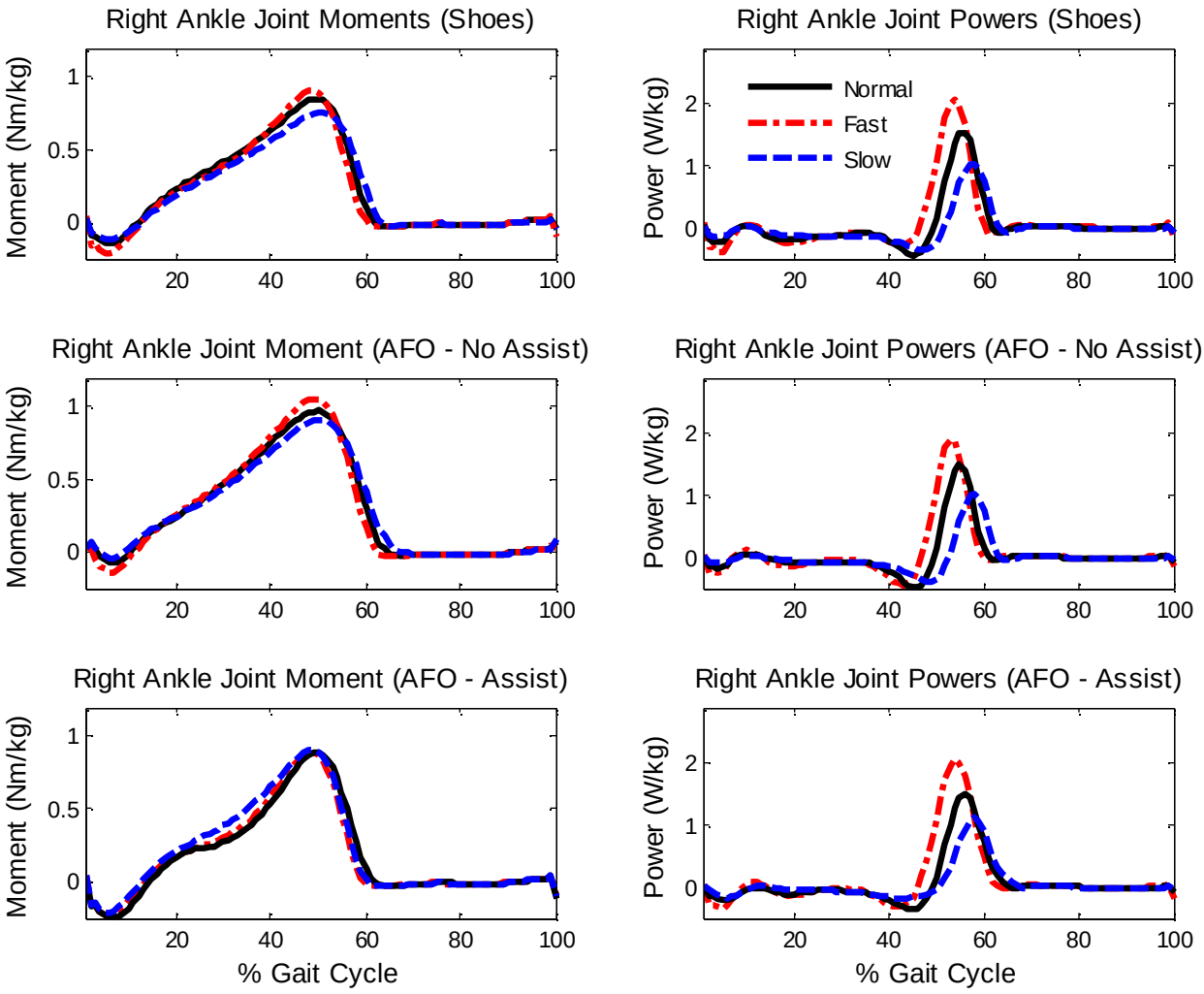

Figure 4.4 *Healthy walker average right ankle moments and powers for the three footwear conditions and three walking speeds.*

At the assisted (PPAFO) right ankle joint, the peak moments for all three walking speeds were approximately equal, Fig. 4.4 bottom left panel. Interestingly, there is a visible dip in the right ankle moment during mid stance (~20-40% Gait Cycle) for all three speeds. Overall, the average peak moments and powers for the left ankle were larger during assisted walking trials then during the shoe trials. However, the average peak moment and power values for the assisted right ankle were comparable at the normal and fast walking speeds.

4.3.1.2 ROD Analysis

ROD analysis was used to quantify joint angle asymmetries and individual deviations from normative data that were created as result of speed and footwear perturbations. Symmetry ROD (SROD) values calculated during shoe walking at the three speeds were small for all joint pairs, Fig. 4.5 left panels. For all speeds, the joint asymmetries at the ankle and hip were less than one degree, while asymmetries at the knee were less than two degrees. SROD results for the PPAFO assisted walking trials showed increased asymmetry in the joint pairs, Fig. 4.5 right panels. The largest asymmetries were at the ankle during loading response (~0-10% Gait Cycle) and swing (~60-100% Gait Cycle). The peak SROD value at the ankle during stance was 5.5 deg during the slow walking trial and 7.5 deg during swing for the normal walking trial. For both shoe and PPAFO assisted walking, changing the speed did not seem to greatly affect the trends in the data: increased asymmetry at the ankle during early stance and swing, a small positive increase in asymmetry at the knee that gradually increased throughout the cycle, and a small positive increase in asymmetry at the hip, Fig. 4.5 right panels.

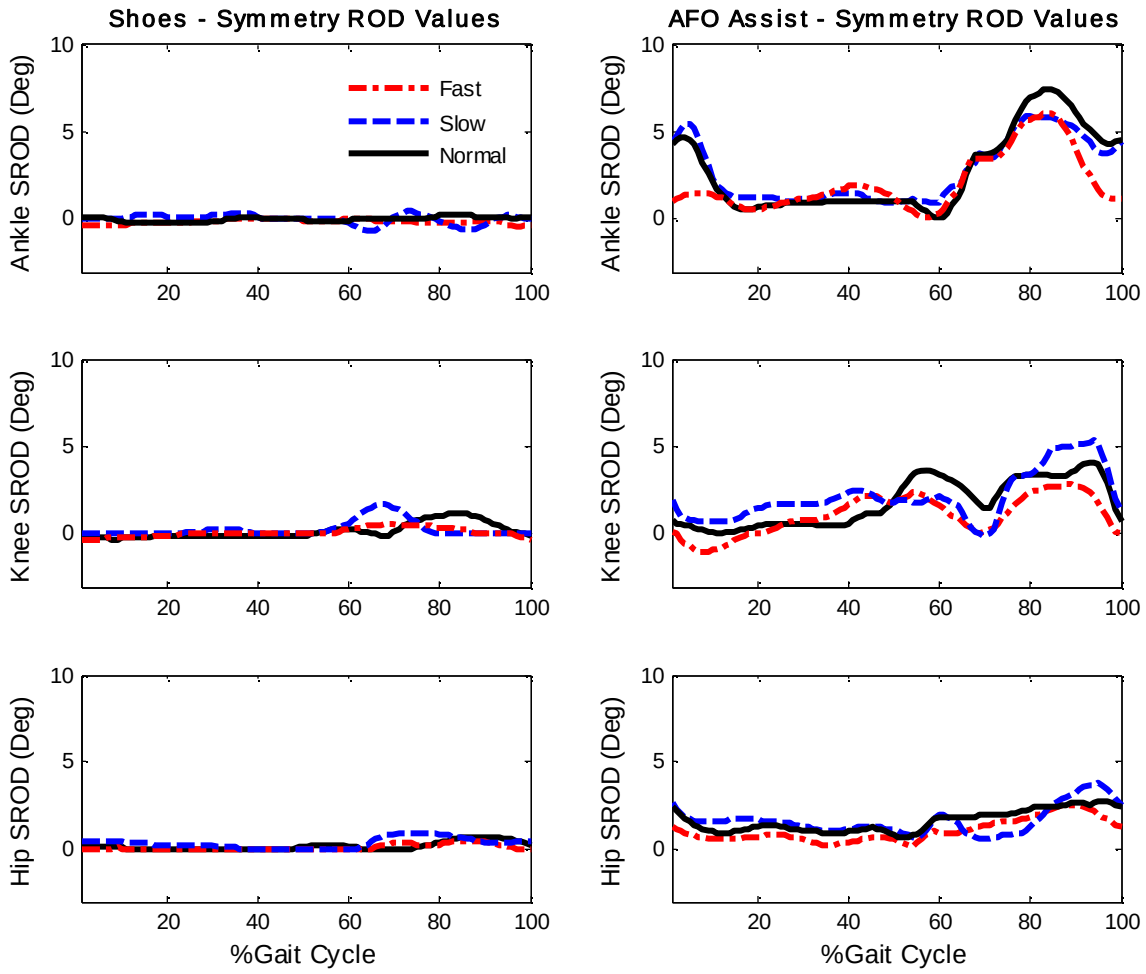

Figure 4.5 ***Left Panels:*** *SROD values for the healthy subjects' during the shoe walking trials that illustrate normative levels of asymmetry in the joint angle data.* ***Right Panels:*** *SROD values during the PPAFO assisted walking trials. These plots illustrate the asymmetries in the joint angle data of the healthy subjects during PPAFO assisted walking.*

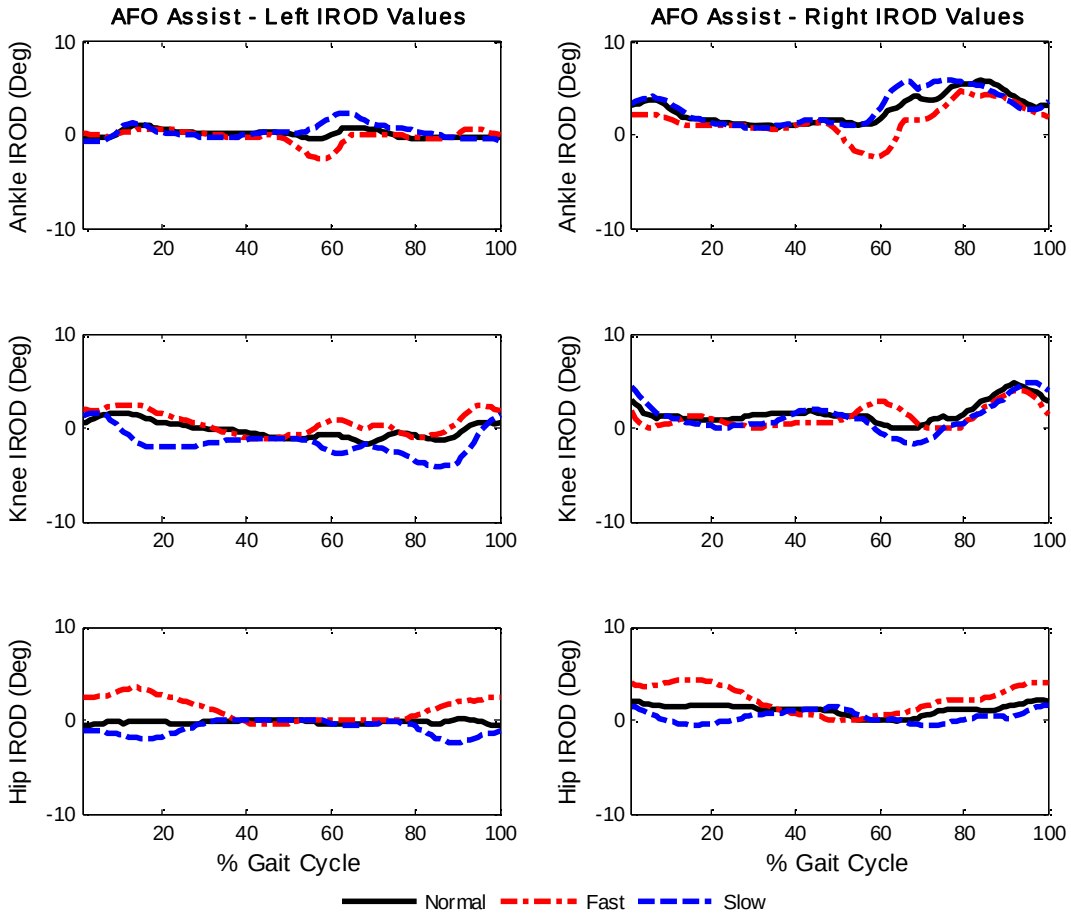

Figure 4.6 *Left and right IROD values for the normal, fast, and slow PPAFO assisted trials.*

To identify which joints were contributing to the increased asymmetries seen in Fig. 4.5 right panels, the individual ROD (IROD) values for the PPAFO assisted condition were examined. IROD values indicated deviations from normative behavior at all joints, Fig. 4.6. At the ankle, joint behavior deviated further from the norm on the assisted side during loading response and swing accounting for the larger asymmetries present at the ankle during these phases. IROD data also showed speed affects for the left knee, left hip, and right hip that were not present in the SROD data. IROD values increased during the fast trials, remained near zero

during the normal walking trials, and decreased during the slow trials. Even though the IROD data for the left and right hip deviated from the normative joint behavior, the symmetric trends present in the data resulted in lower SROD values.

4.3.1.3 Complexity and Variability

The complexity and variability of the thigh, shank, and foot were affected by both the speed and PPAFO perturbations, Tables 4.5- 4.7. Table 4.5 presents data that demonstrated how the PPAFO affected the complexity and variability of the segment phase portraits. For the normal speed trials, segment complexity was found to be the highest during shoe walking. Complexity decreased during both the assisted and unassisted PPAFO walking conditions, with the assisted trials having the lowest complexity scores at every segment except the thigh. On the other hand, variability tended to increase during the PPAFO trials. Variability in the segments, in terms of both drift and area, tended to be highest during the assisted PPAFO walking trials.

Table 4.5 *Mean (and standard deviation) values of complexity and variability separated by body segment, side of the body, and footwear condition at the normal walking speed.*

	Normal Walking Speed		**Left**			**Right**	
Segment	Measure	Shoes	AFO - No Assist	AFO - Assist	Shoes	AFO - No Assist	AFO - Assist
Thigh	Complexity (# of harmonics)	249 (62)	215 (32)	217 (29)	244 (69)	206 (25)	215 (28)
	Drift (Cartesian dist.)	0.63 (0.22)	0.77 (0.20)	0.91 (0.23)	1.11 (1.10)	1.44 (1.48)	1.54 (1.56)
	Area (rad^2/s)	0.0046 (0.0018)	0.0069 (0.0014)	0.0097 (0.0035)	0.0104 (0.0140)	0.0156 (0.0189)	0.0160 (0.0189)
Shank	Complexity (# of harmonics)	200 (71)	175 (17)	162 (11)	205 (73)	190 (25)	170 (8)
	Drift (Cartesian dist.)	1.08 (0.52)	0.71 (0.23)	1.26 (0.45)	0.79 (0.27)	1.74 (1.13)	1.37 (1.04)
	Area (rad^2/s)	0.0095 (0.0035)	0.0074 (0.0039)	0.0139 (0.0066)	0.0085 (0.0095)	0.0166 (0.0118)	0.0183 (0.0102)
Foot	Complexity (# of harmonics)	226 (81)	211 (29)	203 (28)	225 (82)	191 (16)	187 (13)
	Drift (Cartesian dist.)	1.45 (0.97)	0.85 (0.45)	1.62 (0.94)	1.08 (0.95)	2.65 (1.60)	2.87 (3.79)
	Area (rad^2/s)	0.0145 (0.0091)	0.0107 (0.0081)	0.0201 (0.0147)	0.0180 (0.0262)	0.0306 (0.0223)	0.0600 (0.0837)

The speed perturbations resulted in changes to complexity and variability to gait during both shoe and PPAFO perturbed gait. During shoe walking, modifying gait speed resulted in changes to the complexity and variability of all six segments, Table 4.6. Increasing the speed

resulted in phase portraits with increased complexity at all segments and increased variability at every segment except the right thigh. Slowing the subject's walking speed had the opposite effect on the complexity, decreasing the value for all segments. However, the slow walking speed did increase the variability of every segment except the left foot.

Table 4.6 *Mean (and standard deviation) values of complexity and variability separated by body segment, side of the body, and walking speed for shoe walking.*

	Shoes	Left			Right		
	Measure	Shoes (N)	Shoes (F)	Shoes (S)	Shoes (N)	Shoes (F)	Shoes (S)
Thigh	Complexity (# of harmonics)	249 (62)	256 (83)	224 (69)	244 (69)	266 (81)	212 (64)
	Drift (Cartesian dist.)	0.63 (0.22)	0.84 (0.23)	0.82 (0.33)	1.11 (1.10)	1.07 (0.67)	1.39 (0.82)
	Area (rad^2/s)	0.0046 (0.0018)	0.0073 (0.0050)	0.0089 (0.0048)	0.0104 (0.0140)	0.0091 (0.0058)	0.0138 (0.0116)
Shank	Complexity (# of harmonics)	200 (71)	220 (75)	184 (66)	205 (73)	218 (76)	190 (76)
	Drift (Cartesian dist.)	1.08 (0.52)	1.97 (1.46)	0.96 (0.38)	0.79 (0.27)	1.43 (0.51)	1.60 (0.74
	Area (rad^2/s)	0.0095 (0.0035)	0.0201 (0.225)	0.0116 (0.0086)	0.0085 (0.0095)	0.0142 (0.0048)	0.0179 (0.110)
Foot	Complexity (# of harmonics)	226 (81)	260 (84)	200 (62)	225 (82)	246 (88)	200 (66)
	Drift (Cartesian dist.)	1.45 (0.97)	2.24 (1.94)	0.94 (0.84)	1.08 (0.95)	1.47 (1.06)	2.85 (1.54)
	Area (rad^2/s)	0.0145 (0.0091)	0.0342 (0.0439)	0.0101 (0.0103)	0.0180 (0.0262)	0.0180 (0.0110)	0.0399 (0.0243

AFO assisted walking resulted in lower complexity values, Table 4.7, for all segments when compared to the data from the shoe walking, Table 4.6. This trend held true for the normal, fast, and slow speed conditions. As with the data from the shoe walking, (Table 4.6), the complexity of the segments for the PPAFO assistance trials increased during fast walking and decreased during slow walking. The drift decreased at all segments for both speeds except the left thigh and right shank during fast walking. On the other hand, the area decreased at all segments for both speeds except the left and right shank and the right foot during the slow walking condition.

Table 4.7 *Mean (and standard deviation) values of complexity and variability separated by body segment, side of the body, and walking speed for PPAFO assisted walking.*

	AFO Assist	Left			Right		
	Measure	AFO Assist (N)	AFO Assist (F)	AFO Assist (S)	AFO Assist (N)	AFO Assist (F)	AFO Assist (S)
Thigh	Complexity (# of harmonics)	217 (29)	232 (9)	187 (29)	215 (28)	230 (10)	171 (22)
	Drift (Cartesian dist.)	0.91 (0.23)	1.03 (0.66)	0.59 (0.11)	1.54 (1.56)	0.83 (0.45)	1.14 (0.57)
	Area (rad^2/s)	0.0097 (0.0035)	0.0096 (0.0040)	0.0075 (0.0044)	0.0160 (0.0189)	0.0096 (0.0090)	0.0153 (0.0107)
Shank	Complexity (# of harmonics)	162 (11)	186 (17)	145 (9)	170 (8)	190 (11)	150 (11)
	Drift (Cartesian dist.)	1.26 (0.45)	1.04 (0.19)	1.10 (0.44)	1.37 (1.04)	1.54 (1.51)	1.19 (0.65)
	Area (rad^2/s)	0.0139 (0.0066)	0.0113 (0.0022)	0.0150 (0.0129)	0.0183 (0.0102)	0.0172 (0.0140)	0.0262 (0.0233)
Foot	Complexity (# of harmonics)	203 (28)	225 (25)	176 (19)	187 (13)	205 (13)	159 (10)
	Drift (Cartesian dist.)	1.62 (0.94)	1.35 (0.59)	0.89 (0.57)	2.87 (3.79)	2.05 (1.61)	2.03 (1.49)
	Area (rad^2/s)	0.0201 (0.0147)	0.0170 (0.0078)	0.01456 (0.0134)	0.0600 (0.0837)	0.0354 (0.0416	0.0690 (0.0865)

4.3.2 Results from ISubPF

4.3.2.1 Traditional Parameters

For ISubPF, assistive torque was applied at the subject's right ankle during stance to assist propulsion. The joint range of motion on the right side of the body decreased between the assisted and shoe walking trials at the ankle, but increased at the knee and hip, Table 4.8. The decrease in the ankle joint ROM was created by reduced dorsiflexion during late stance and early swing (Fig. 4.10 top panel, 60-80 % of the Gait Cycle, solid and dot-dashed lines). The joint ROM on the left side of the body did not change appreciable between the trials. The changing ROM resulted in decreased SI values at the ankle but large increases at the knee and hip. The PPAFO assistance did not change the step length on the right side, although cycle time, stance time, and step width were all increased, Table 4.9. The step length on the left side increased during the PPAFO assistance, creating a corresponding increase in cycle time and stance time, Table 4.9.

Table 4.8 *ISubPF joint range of motion, mean (and standard deviation), for shoe and PPAFO footwear conditions. A symmetry index (SI) between the bilateral joint pairs was calculated for each joint. A negative SI indicates that the parameter value for the left side was greater than the right.*

ISubPF	Ankle ROM			Knee ROM			Hip ROM		
Trials	Right	Left	SI	Right	Left	SI	Right	Left	SI
Shoes	26.3 (2.3)	18.0 (1.7)	37.3	63.7 (6.2)	58.4 (6.7)	8.7	43.3 (2.8)	42.2 (2.1)	2.7
AFO - No Assist	21.9 (3.0)	17.7 (1.4)	21.4	65.2 (5.2)	59.9 (5.2)	8.5	49.0 (2.7)	41.7 (1.8)	16.1
AFO - Assist	21.2 (3.0)	19.1 (1.4)	10.6	75.5 (4.4)	56.8 (10.1)	28.3	51.4 (2.4)	42.3 (3.2)	19.4

Table 4.9 *ISubPF mean (and standard deviation), values for step length, cycle time, stance time, and step width for shoe and PPAFO footwear conditions. A symmetry index (SI) was also calculated for the bilateral parameters. A negative SI indicates that the parameter value for the left side was greater than the right.*

ISubPF	Step Length			Cycle Time			Stance Time			Step Width
Trials	Right	Left	SI	Right	Left	SI	Right	Left	SI	
Shoes	492.7 (26.7)	483.4 (28.5)	1.9	1.09 (0.03)	1.09 (0.04)	0.07	0.76 (0.06)	0.79 (0.04)	-4.26	202.6 (21.4)
AFO - No Assist	479.2 (27.9)	488.8 (21.4)	-2.0	1.09 (0.04)	1.09 (0.04)	-0.06	0.75 (0.05)	0.78 (0.03)	-4.91	213.5 (14.5)
AFO - Assist	490.0 (20.1)	512.3 (22.1)	-4.4	1.13 (0.03)	1.13 (0.03)	0.03	0.84 (0.04)	0.81 (0.04)	3.15	216.4 (16.8)

The right side peak ground reaction forces in all three directions increased during the PPAFO assisted walking trial, Fig. 4.7. During the propulsive phase of gait, forward propulsive force (denoted by negative AP-GRF values) increased by 25 N (at 57% of the gait cycle) and vertical force (Z-GRF) increased by 112 N (at 55% of the gait cycle). Figure 4.7 illustrates that stance time increased during the assisted trials. The assistance-driven increase in the forces and the changes in timing contributed directly to changes observed in the moment and power generated at the assisted ankle joint, Fig. 4.8. The right ankle moment for the assisted case is similar to the moment from the shoe walking data; however, the peak power at the joint has increased significantly. Without assistance, the subject did not generate significant power at the

end of stance for propulsion. With the addition of PPAFO assistance, the subject was able to generate a peak power of 0.31 W/kg at 68% of the cycle.

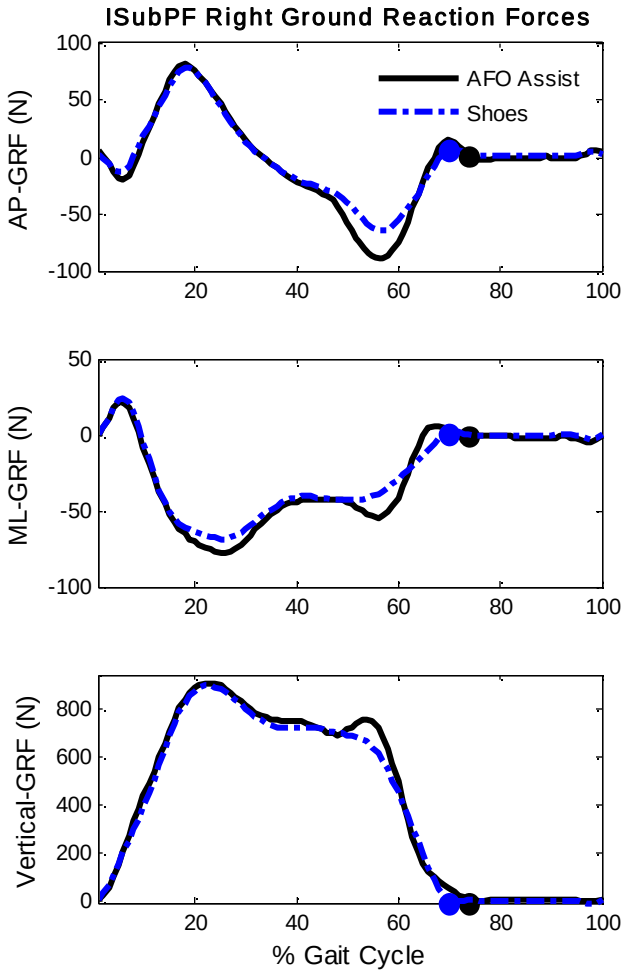

Figure 4.7 *Average anterior-posterior (AP), medial-lateral (ML), and vertical ground reaction force (GRF) data for ISubPF during PPAFO assisted and shoe walking trials. Positive AP-GRF data indicates forces directed towards the anterior direction, while negative ML-GRF data indicates forces directed towards the right side of the subject. Average toe off for each condition is indicated by a circle.*

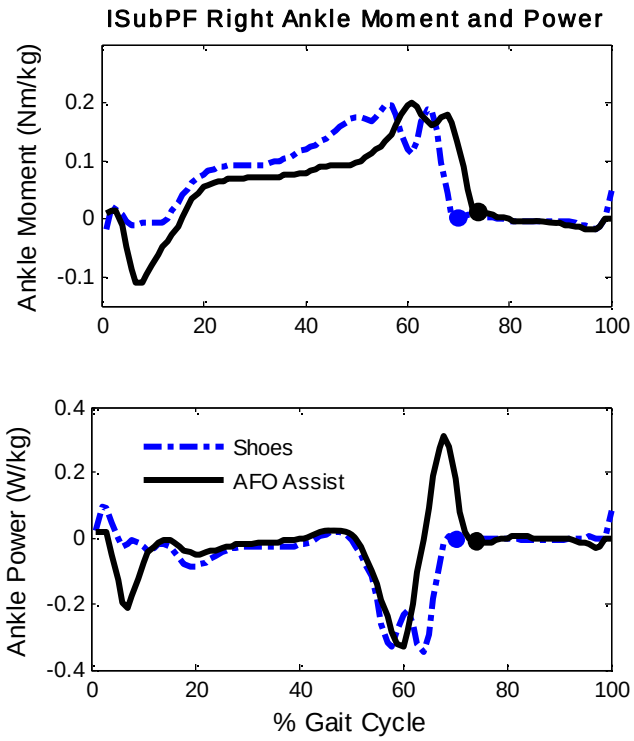

Figure 4.8 *Average right ankle moments (Top) and powers (Bottom) for the assisted and shoe walking trials for ISubPF. Positive moment values are in the plantarflexion direction. Average toe off for each condition is indicated by a circle.*

4.3.3 Regions of Deviation Analysis

For ISubPF, SROD values at the ankle joint decreased during loading response and mid stance with PPAFO assistance, Fig. 4.9. SROD values were present starting at 64% of the gait cycle (late stance), but opposite in sign as compared to the shoe walking trial. The ankle joint angles, Fig. 4.10 top panels, illustrated that while the left joint angle was not greatly affected by the PPAFO assistance, the right joint angle was (60-100% of the gait cycle). This difference indicates that the negative SROD values are the result of modified behavior at the right ankle. IROD values for the unassisted (left) ankle were only modified slightly at the beginning and end

of the cycle as a result of the assistance, Fig. 4.10 bottom left panel. For the right ankle, IROD values decreased on the whole, although large IROD values were still present in the data.

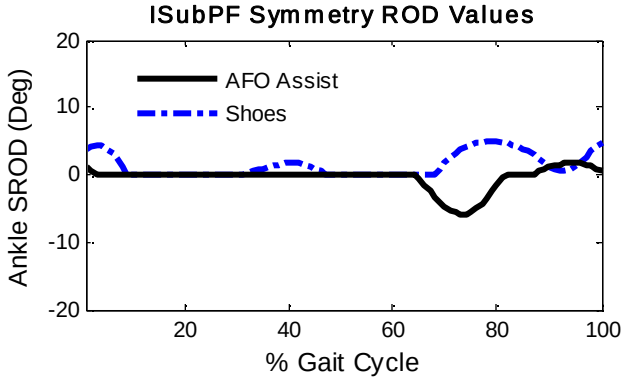

Figure 4.9 *ISubPF Symmetry ROD values calculated for the ankle joint during shoe and PPAFO assisted walking.*

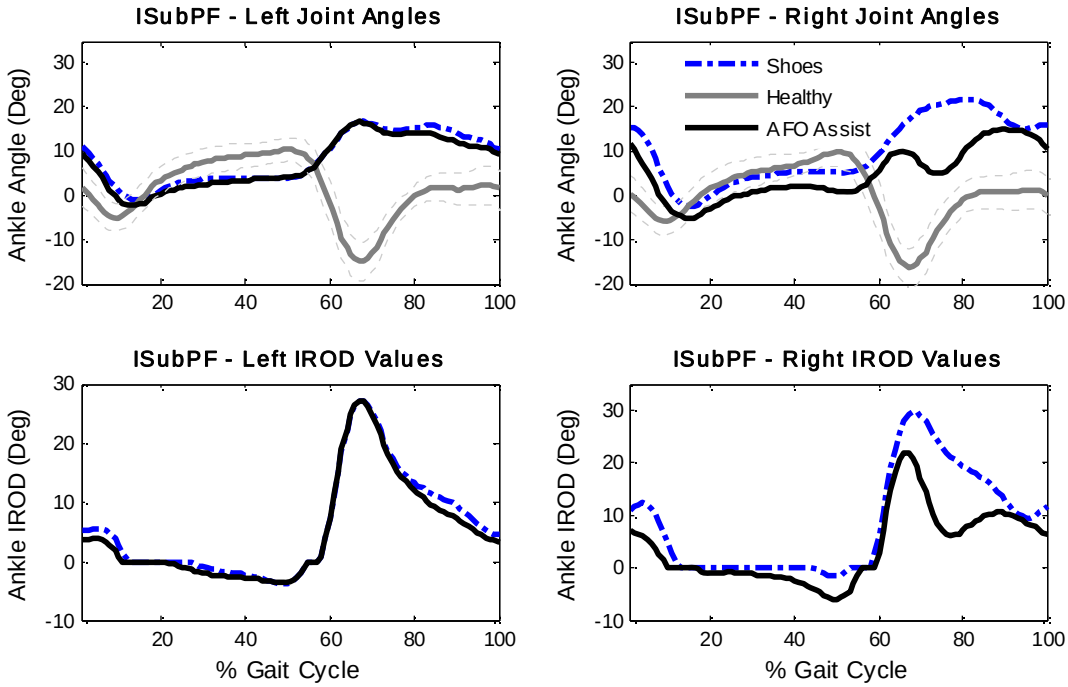

Figure 4.10 *Average left and right ankle IROD values for the shoe walking and PPAFO assisted trials for the subject with the impaired plantarflexors (ISubPF), bottom left and bottom right respectively. The subject's average left and right ankle joint angles are plotted against normative data for comparison in the top left and right plots.*

4.3.3.1 Complexity and Variability Analysis

Complexity and variability analysis was conducted for the shoe and PPAFO assisted walking conditions. For ISubPF, the complexity of all segments decreased during the assisted walking trial on both the left and right side, Table 4.10. The variability of the left side increased from the shoe to the PPAFO assisted condition at all segments. On the right side, the drift values increased from the shoe to the PPAFO assisted condition, while the area decreased for all segments, Table 4.10.

Table 4.10 *Mean (and standard deviation) values of complexity and variability separated by body segment, body side, and footwear condition for the plantarflexor impaired subject (ISubPF).*

	ISubPF	Left			Right		
	Measure	Shoes	No Assist	Assist	Shoes	No Assist	Assist
Thigh	Complexity (# of harmonics)	215	201	164	222	217	192
	Drift (Cartesian dist.)	0.8922	1.3641	1.0229	1.9918	0.6533	1.9197
	Area (rad^2/s)	0.016	0.0231	0.0205	0.0251	0.0087	0.0304
Shank	Complexity (# of harmonics)	226	209	177	226	213	180
	Drift (Cartesian dist.)	0.8779	1.1142	3.1236	4.4637	0.8343	1.0813
	Area (rad^2/s)	0.0165	0.0261	0.0848	0.1354	0.023	0.014
Foot	Complexity (# of harmonics)	252	238	208	274	248	201
	Drift (Cartesian dist.)	0.8562	0.5773	3.0325	4.7028	1.8176	1.2903
	Area (rad^2/s)	0.0137	0.0073	0.0549	0.1231	0.0475	0.0208

4.3.4 Results from ISubDF

4.3.4.1 Traditional Parameters

As with the previous results, traditional parameters were used to help evaluate the effect of the PPAFO on the gait of ISubDF. Joint angle ROM for ISubDF on the assisted side decreased at the ankle and the knee during the assisted trial, Table 4.11. Joint angle ROM from the hip was not available because of missing marker data during the assisted walking trial for ISubDF. As

with ISubPF, the reduced ROM resulted in a smaller ROM SI at the ankle and an increased ROM SI at the knee. Step length (SL), cycle time, stance time (ST), and step width (SW) all decreased during the assisted trial, Table 4.12. The SI for ST time increased by 9, but the SIs for SL and cycle time did not vary greatly between the shoe and PPAFO assisted trials.

Table 4.11 *ISubDF joint range of motion, mean (and standard deviation), for shoe and PPAFO footwear conditions. A symmetry index (SI) between bilateral joint pairs was calculated. A negative SI indicates that the parameter value for the left side was greater than the right.*

ISubDF	Ankle ROM (Deg)			Knee ROM (Deg)			Hip ROM (Deg)		
Trial	Right	Left	SI	Right	Left	SI	Right	Left	SI
Shoes	27.4 (2.4)	14.4 (0.6)	62.5	60.0 (3.6)	60.8 (2.8)	-1.2	48.1 (4.1)	41.6 (2.9)	14.4
AFO No Assist	29.0 (2.3)	14.1 (0.7)	69.3	56.7 (6.9)	45.5 (3.8)	21.9	42.8 (5.4)	33.0 (2.5)	25.8
AFO Assist	18.1 (1.7)	12.7 (0.8)	35.2	49.8 (7.8)	61.5 (9.4)	-20.9	NA	NA	NA

Table 4.12 *ISubDF mean (and standard deviation), values for step length, cycle time, stance time, and step width for shoe and PPAFO footwear conditions. A symmetry index (SI) was also calculated for the bilateral parameters. A negative SI indicates that the parameter value for the left side was greater than the right.*

ISubDF	Step Length (mm)			Cycle Time (s)			Stance Time (s)			Step Width (mm)
Trials	Right	Left	SI	Right	Left	SI	Right	Left	SI	
Shoes	364.2 (22.7)	362.9 (26)	0.3	2.48 (0.12)	2.49 (.17	-0.14	1.82 (0.13)	1.91 (0.15)	-4.66	175.4 (21.2)
AFO - No Assist	275.3 (20.7)	287.2 (25.6)	-4.3	2.21 (0.13)	2.23 (0.15)	-0.64	1.71 (0.11)	1.72 (0.12)	-0.56	193.1 (17.4)
AFO - Assist	276.9 (16.4)	282.0 (27.5)	-1.8	2.16 (0.09)	2.16 (0.13)	0.11	1.67 (0.06)	1.58 (0.09)	5.34	165.9 (10.2)

4.3.4.2 ROD Analysis

The ankle joint angle plots for ISubDF showed that the PPAFO assistance was able to restrict the ROM of the foot during swing, Fig. 4.11 top panel. Without PPAFO assistance the joint angle dropped to ~10 deg below neutral during swing. However, with PPAFO assistance

the joint angle was held at ~8 deg above neutral. The dorsiflexor assist resulted in better positioning of the foot for initial contact at heel strike.

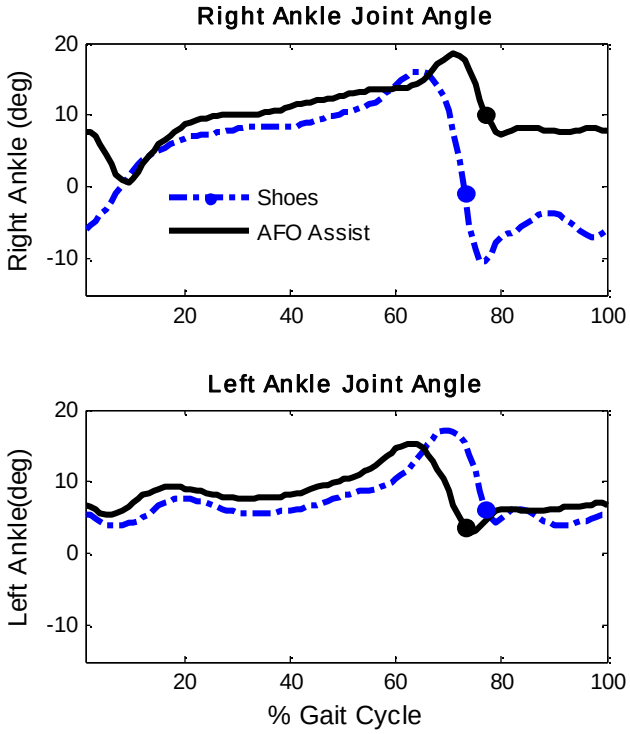

Figure 4.11 *Average right and left ankle joint angles for the shoe walking and PPAFO assisted trials for subject ISubDF, top and bottom respectively.*

Although the results illustrated functional assistance, the PPAFO was unable to completely eliminate asymmetries as evident by the presence of non-zero SROD and IROD values for ISubDF in the data during the assisted trials, Figs. 4.12-4.13. SROD values were reduced at initial stance (0-10% of the gait cycle) and during swing (80-100% of the gait cycle), but were still present during terminal stance (30-50% of the gait cycle). IROD values decreased slightly for the left ankle and increased slightly for the right ankle.

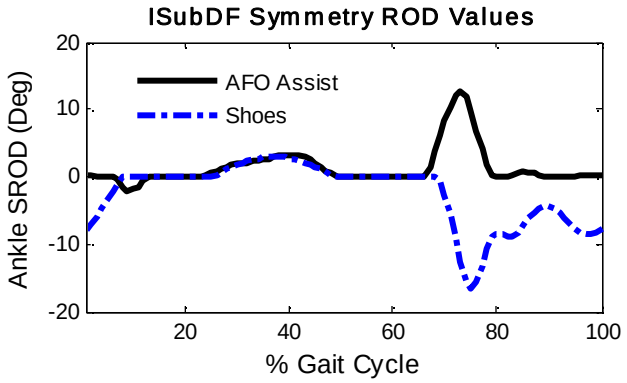

Figure 4.12 *ISubDF Symmetry ROD values calculated for the ankle joint during shoe and PPAFO assisted walking.*

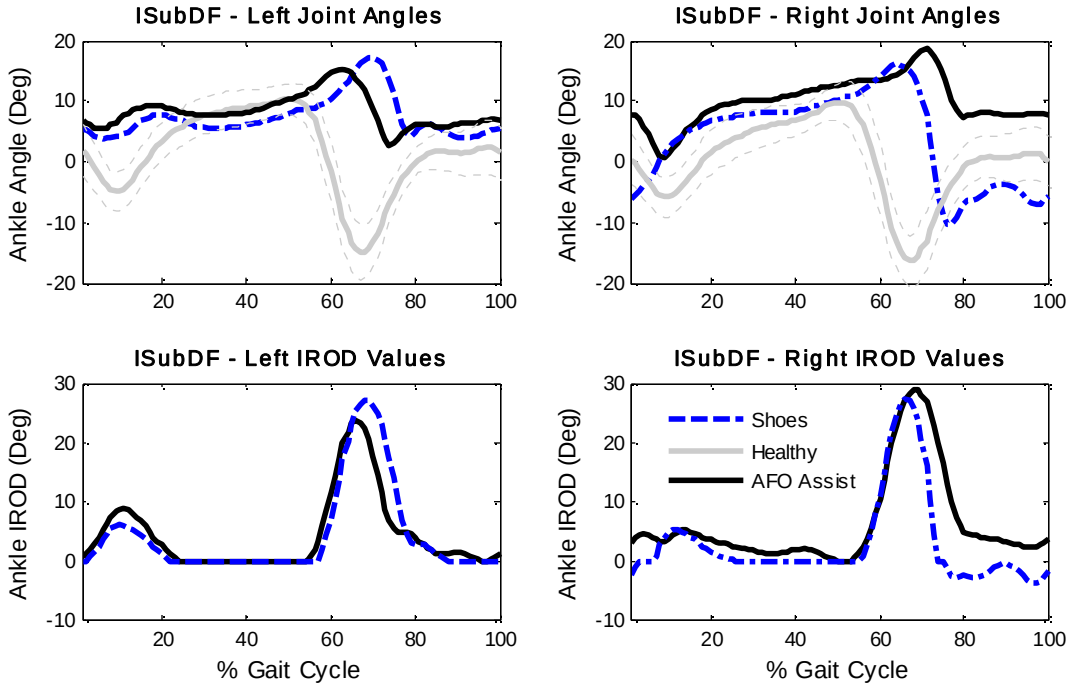

Figure 4.13 *Average left and right ankle IROD values for the shoe walking and PPAFO assisted trials for subject ISubDF, bottom left and bottom right respectively. The subject's average left and right ankle joint angles are plotted against normative data for comparison in the top left and right plots.*

4.4 Discussion

The results from the impaired subject walking trials in this chapter provide evidence of the PPAFO's ability to provide functional assistance during gait. For ISubPF, this functional assistance was observed in the increased power (Fig. 4.8), the increased ground reaction forces (GRF, Fig. 4.7), and the increased cycle and stance times (Table 4.13) during the assisted walking. PPAFO assistance resulted in a peak power increase from ~0 W/kg, during shoe walking, to 0.31 W/kg with assistance. This is a clear indication of functional assistance from the PPAFO. While the peak power generated during the assisted walking was 36% of that generated by a healthy walker (1.55 W/kg, shoes, normal walking speed), it was a significant increase from the subject's unassisted levels. The functional benefit provided by the PPAFO was also illustrated by the increased ground reaction forces in the vertical and anterior-posterior directions during the assisted trial. Without the assistance, ISubPF's vertical GRF data had only a single peak present in early stance, a symptom of weak plantarflexors (Fig. 4.7 bottom panel, dot-dashed line). When the assistance was turned on, a second peak in the vertical reaction force was present at 54% of the gait cycle (Fig. 4.7 bottom panel, solid line), and the magnitude of the propulsive force in the anterior-posterior GRF grew more negative in late stance (Fig. 4.7 top panel, solid line, 57% of the cycle). The second peak in the vertical GRF data was indicative of push off during healthy gait, while increased anterior-posterior GRF indicated more force for forward propulsion. Both changes demonstrated appropriately timed functional assistance from the PPAFO.

Functional dorsiflexor assistance was demonstrated during ISubDF's assisted walking trial. When the PPAFO dorsiflexor assistance was applied, the ankle joint angle was held above neutral throughout swing (Fig. 4.14 top panel, solid line). This functional assistance prevented

the foot drop present during the unassisted trial (Fig. 4.15 top panel, dot-dashed line) and effectively maintained toe clearance during swing. In addition to maintaining clearance, the PPAFO assistance prevented excessive dorsiflexion of the joint at heel strike. This result was comparable to normative data during loading response (Fig. 4.16 top panel, solid line, 0-20% of the cycle).

Although symmetry and individual ROD values demonstrated improvements during the assisted walking trials, these changes were not dramatic. The impaired subjects had bilateral impairments and walked with a passive carbon fiber device on their left leg to improve stability and reduce fatigue. This asymmetric assistance could have contributed to the modest changes in the ROD results for the two subjects. In the future, testing with individuals with bilateral deficits could be conducted with powered PPAFOs on each leg to address this limitation.

Feedback from both subjects about the performance of the PPAFO during the assisted trials was positive. ISubPF made the comment that as soon as the PPAFO assistance was turned on he stopped thinking about his right leg (with the PPAFO) and instead focused on the leg with the carbon fiber PPAFO. ISubDF was also aware of the dorsiflexor assistance as soon as it was turned on. She was initially apprehensive about the size of the device. However, after walking with the assistance, ISubDF made the comment that she did not have to work as hard when the PPAFO was turned on. She went on to say that she thought that this device (even in its current form) could be a useful tool to assist impaired individuals during special tasks, such as distance walking.

One important aspect of characterizing the PPAFO was evaluating how the performance of the system was affected by perturbations during gait, such as a change in speed. In this chapter, the sensitivity of the PPAFO system to a speed perturbation was evaluated using data

collected from 5 healthy subjects. To provide baseline understanding of how a change in walking speed affects gait, speed perturbations were initially analyzed for the healthy subjects during the shoe walking condition. The subjects walked at their self-selected walking speed as described above (normal condition), 25% faster than normal (fast), and 25% slower than normal (slow). The observed changes in the gait analysis parameters resulting from the speed perturbation were used as points of comparison for the data collected during the PPAFO assisted walking with the same perturbations. Differences in the trends and magnitudes between the baseline and assisted walking conditions were attributed to changes introduced by the PPAFO.

The sensor thresholds that determine the timing of the PPAFO assistance were tuned for an individual's normal walking speed. The normal walking speed threshold values were used for all of the assisted trials, regardless of the speed. In this manner the PPAFO's sensitivity to changes in speed could be evaluated. After initializing the sensor thresholds, data were collected at the same three walking speeds during both assisted and unassisted PPAFO walking conditions. Traditional gait analysis parameters as well as ROD and complexity and variability analysis were then used to quantify the affect the perturbations had on the system.

The traditional parameters indicated that gait was affected by speed changes within a given walking condition (e.g., increased joint ROM during the fast trials and decreased ROM during the slow trials). However, when different walking conditions were compared across a given speed, the traditional parameters were comparable, Tables 4.1 and 4.2. The speed perturbation affected the moments and powers at the ankle joints in a similar manner. For the unassisted walking trials (e.g., shoes and the PPAFO with no assistance), the fast walking speed resulted in higher peak moments and powers, while the slower speed resulted in smaller peak values. During the assisted walking trial, the right and left ankle joint powers continued this

trend, but the joint moments did not, Tables 4.3 and 4.4. At the left ankle joint, the peak ankle moment at the normal speed was larger than either the fast or slow speeds for the assisted trial. This value was also the largest moment calculated for any condition. At the right ankle joint, the peak moments were nearly the same for all three speeds. Additionally, the magnitude and timing of the right joint powers during the assisted walking were comparable to the values calculated for the subject's shoe walking trials.

Like the traditional univariate parameters, the SROD data at the ankle knee and hip were not greatly affected by the speed perturbation. SROD data indicated that the speed perturbation did not have a large effect on symmetry during shoe walking, Fig. 4.5left panels. Asymmetries at all of the joints increased during the PPAFO assisted walking trials. The largest asymmetries were present during swing when the assistance resulted in a dorsiflexed right foot with respect to the normative data, Figs. 4.5 and 4.6. Despite the increased asymmetry due to the PPAFO assistance, the speed perturbation did not result in significant changes to the asymmetries as illustrated in Fig. 4.5 right panels.

The complexity trends due to speed perturbations showed similar behavior for the shoe and PPAFO assisted walking trials, Tables 4.6 and 4.7. For both cases, the complexity of the segments increased during fast walking and decreased during slow walking. On the other hand, the variability of the segments did not follow a consistent trend. For example, for the shoe walking condition, the variability tended to increase due to a speed perturbation. For the PPAFO assisted condition, the variability tended to decrease due to a speed perturbation. The similar trends seen in the traditional parameters and the complexity data, along with the consistent SROD values during the speed perturbations, indicate a reasonable level of robustness to this

type of gait perturbation. However, the differences in the trends for the moments and the variability suggest some affects due to speed. Therefore, additional analysis would be warranted.

Finally, the device control issues present during the impaired subject testing in Chapter 3 were addressed here by relocating the force sensors between the carbon fiber footplate and the sole of the PPAFO. This change enabled the PPAFO to provide fully untethered assistance for the impaired subjects. A second limitation from Chapter 3, lack of a demonstration of functional dorsiflexor assistance, was also addressed in this chapter with the data from ISubDF.

4.5 Conclusion

The results from this study demonstrated that the current PPAFO threshold based control scheme was capable of providing untethered functional assistance for impaired walkers. Additionally, robustness to a specific disturbance was examined. Although the majority of the parameter trends indicated minimal changes in the performance of the PPAFO due to speed perturbations, there were parameters that indicated an affect due to speed. These results may indicate a limitation of the current design. While the results in this chapter are promising, there are potential performance and efficiency gains that could be achieved through improved system control. Chapter 5 will focus on laying the groundwork for improved control design for the PPAFO system.

Chapter 5

MODELING, ANALYSIS AND CONTROL OF A POWERED ANKLE-FOOT ORTHOSIS

5.1 Introduction

Control algorithms for powered AFOs are essential to efficient and effective functional assistance. The control problem can be divided into two main parts: (1) the detection of events during the cycle that determine AFO control objectives, and (2) the implementation of the control schemes, based on these objectives, in order to assist the users in meeting their functional requirements. The control scheme depends on both the hardware in a system, as well as the control architecture. For many systems, the potential control methods are limited by individual parts of the system. Modeling provides a useful tool for analysis and design of both hardware and software components. Currently, the PPAFO's ability to efficiently meet its functional requirements is limited by the use of solenoid valves.

A portable powered ankle-foot orthosis (PPAFO) capable of operation outside of the laboratory or clinic was introduced in Chapter 3. The original configuration of the PPAFO (Fig. 5.1) [61] was capable of assisting gait with appropriately timed constant magnitude torque as

demonstrated through experimental testing results from several subjects presented in Chapters 3 and 4. The torque was used to provide both motion control and external torque assistance at the ankle via solenoid valves with a bang-bang, event-based control scheme (Fig. 5.2). Events are defined by the configuration of the body during the gait cycle and are used to determine the timing of PPAFO control objectives during gait. These objectives are to control the motion of the foot to prevent foot slap during loading response, provide supplemental torque during stance to assist propulsion, and control the motion of the foot to maintain foot clearance during limb advancement. Objectives were based on the functional tasks necessary required for gait [1, 7, 8].

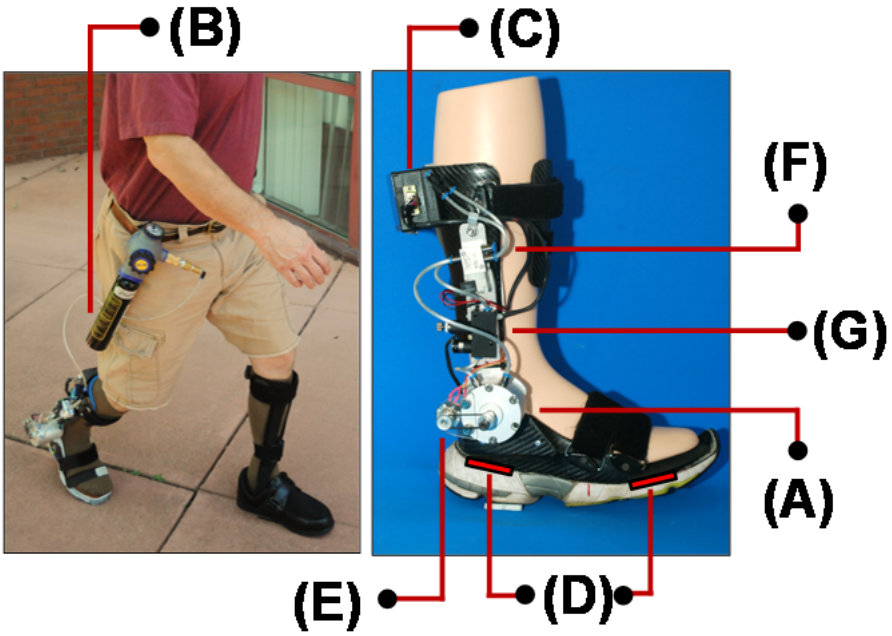

Figure 5.1 *The portable powered ankle-foot orthosis (PPAFO). The rotary actuator* ***(A)*** *is powered using a compressed* CO_2 *bottle* ***(B)*** *worn by the subject on the waist. Onboard electronics* ***(C)****, force sensors* ***(D)****, and an angle sensor* ***(E)*** *are used to control the solenoid valves* ***(F)****. A second pressure regulator* ***(G)*** *is used to modulate the magnitude of the dorsiflexor assistance.*

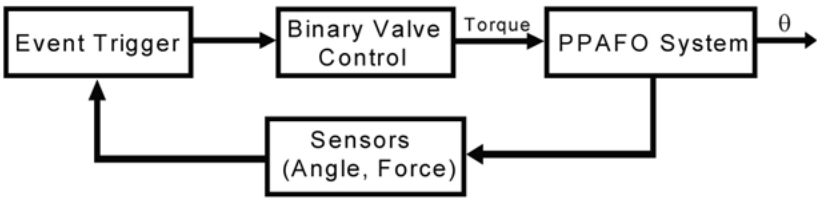

Figure 5.2 *Current binary control scheme used with the solenoid valves. PPAFO sensor data are used to identify the current gait event and open/close the corresponding valve.*

Although the current PPAFO is stable and provides some performance improvements, this particular design restricts the control objectives to those achievable with constant magnitude torque and limits the efficiency of the system due to the bang-bang switching scheme utilized with the solenoid valves. This chapter seeks to address the performance and efficiency limitations introduced by the solenoid valves through a model-based system analysis of a new hardware configuration and improved control design.

Specifically, this chapter will begin with the derivation of a model of the current system, the combined system of the PPAFO with rigid-body human foot and shank segments with solenoid valves. Section 5.2 will also introduce a second model incorporating a proportional valve for comparison with the current system. Parameters for the models will be identified using a system identification approach and will be followed by model validation. In Section 5.3, a strategy for evaluating the PPAFO hardware and control algorithms will be presented. The performance of the two different PPAFO valve configurations will be examined during three tasks designed to emulate the functional requirements of a user during gait. Simulated and experimental results are used to demonstrate strengths and weaknesses of the different hardware

configurations. Section 5.4 will provide a discussion of the results, followed by concluding remarks and future directions in Section 5.5.

5.2 Modeling, System Identification, and Model Validation

5.2.1 PPAFO System Hardware

The PPAFO is shown in Fig. 5.1 [61]. The system is pneumatically powered via a portable compressed liquid CO_2 bottle and pressure regulator (JacPac J-6901-91; Pipeline Inc., Waterloo, Canada) that can be worn at the waist. The pressure regulator at the bottle modulates the CO_2 supply pressure to the dual-vane bidirectional rotary actuator (CRB2BW40-90D-DIM00653; SMC Corp of America, Noblesville, IN, USA) at the ankle joint.

The torque generated by the actuator was used to provide both torque assistance and motion control of the foot during gait. The timing of the torque assistance was determined by gait events detected using the PPAFO sensors. Two force sensors, and an angle sensor (force sensor: 402, 0.5" circle; Interlink Electronics Inc., Camarillo, CA, USA; angle senor: 53 Series; Honeywell, Golden Valley, MN, USA) provided the sensor feedback to identify gait events. During testing, two pressure transducers were used to measure actuator chamber pressure (4100 series; American Sensor Technology, Mt.Olive, NJ, USA). The data from PPAFO sensors and the additional pressure transducers were collected with a multifunction data acquisition (DAQ) module (NI-USB-6211, National Instruments and LabVIEW 2009).

5.2.1.1 Original Hardware Configuration: PPAFO with Solenoid Valves

The PPAFO in its original configuration [61] is operated with two solenoid valves (VOVG 5V; Festo Corp, Hauppauge, NY) as shown in Fig. 5.1 [61]. One valve is used to pressurize the rotary actuator to generate dorsiflexor (toes-up) torque, and the other is used to

generate the oppositely directed plantarflexor (toes-down) torque. Since the magnitude of the dorsiflexor torque is less than the plantarflexor torque, an additional pressure regulator (LRMA-QS-4; Festo Corp - US, Hauppauge, NY) is used to modulate the dorsiflexor magnitude (Fig. 5.1).

While this configuration was successful at providing dorsi and plantarflexor torque assistance during gait, the hardware and control architecture have shortcomings. System performance was limited by how the solenoid valves were used to provide functional assistance. Pressure regulators were first used to fix the magnitude of both the dorsiflexor and plantarflexor torque inputs. The solenoid valves were then used to control the timing of the assistance. As a result, the current control scheme was incapable of providing intermediate levels of torque assistance during gait. The efficiency of the system was reduced by the high pneumatic power consumption that resulted from the all-on or all-off nature of the assistance.

5.2.1.2 Modified Hardware Configuration and Control Architecture: Proportional Valve

Performance and efficiency limitations associated with the PPAFO solenoid valves were considered in this work. To address these issues, a second PPAFO hardware configuration incorporating a single high-speed proportional valve (LS-V05s; Enfield Technologies, Trumbull, CT, USA) in place of the two solenoid valves was considered. A proportional valve enables incremental levels of torque assistance, which allow a wider range of potential control objectives that are not limited to constant torque magnitudes.

In addition to changing the hardware, a modified control architecture was implemented. Proportional valves are not restricted to the bang-bang control method utilized by solenoid valves. To improve the tracking performance and efficiency of the system, a proportional-integral-derivative (PID) control scheme was integrated into the system. A PID control scheme

was initially selected based on its ease in implementation, prevalence in industry, and heuristic tuning methodology which enables online subject-specific tuning of the PPAFO if necessary. Performance results of the modified PPAFO are presented in Section 5.3. Additional control designs will be discussed in Chapter 6.

5.2.2 Modeling of the PPAFO-Leg System

System modeling is a valuable tool for analysis and design. Accurate models provide a means for simulating and comparing the performances of varying hardware designs, analyzing different control architectures, and obtaining a realistic expectation of system performance given a set of conditions. Effective use of a model can lead to a significant reduction in hardware and control design effort by enabling the designer to evaluate system performance in a safe yet relatively accurate virtual environment.

5.2.2.1 Modeling the PPAFO

Separate PPAFO system models including either solenoid or proportional valves were derived. To simplify the modeling, the solenoid valves were represented as fully open proportional valves with modified model parameters. The models consisted of the valve (solenoid or proportional), dual-vane rotary actuator, tubing between the valve and the actuator, and the added inertia of the actuator vane and PPAFO footplate (Fig. 5.3). The moment of inertia and damping of the vane of the rotary actuator and PPAFO footplate were modeled as a single rigid body because they are physically coupled at all times.

As an additional means of simplifying the modeling process, the following assumptions were made:

A1) constant pressure at the power supply

A2) no leakage within the system (except for leakage across the actuator vane)

A3) homogeneous pressure inside each chamber

A4) negligible gas inertia

A5) isothermal processes in the chamber during expansion

A6) negligible line volume compared to the chamber

A7) negligible line loss between the power supply and actuator

These assumptions were considered reasonable for the controlled experimental environment, the low working pressures, and the short activation times used during the experimental validation. Although many of these assumptions may need to be relaxed in an uncontrolled testing environment outside of a lab or clinic, they simplified the initial development of a model of the PPAFO-Leg system. Further analysis of these assumptions and their validity with respect to actual running conditions should be considered in future work.

To solve for the position of the PPAFO, the dynamics of the system were expressed by the following relationship,

$$I_{zz}\ddot{\theta} + \beta\dot{\theta} + T_{gravity} + T_f + T_{ex} = T_{actuator} \ , \qquad (5.1)$$

where θ is the angle of the vane (which also corresponds to the ankle joint angle of the coupled PPAFO-Leg system), I_{zz} is the moment of inertia of the footplate and actuator vane relative to the axis of rotation of the ankle joint, β is the rotary damping ratio, $T_{gravity}$ is the gravitational torque due to the weight of the PPAFO, T_{ex} represents the coupling torque between the PPAFO and the wearer (when modeling and identifying the PPAFO-Leg system it was set to zero), T_f is

the friction torque opposing the motion of the vane, and $T_{actuator}$ is the output torque from the actuator (Fig. 5.3). The following sections explain how model parameters were determined.

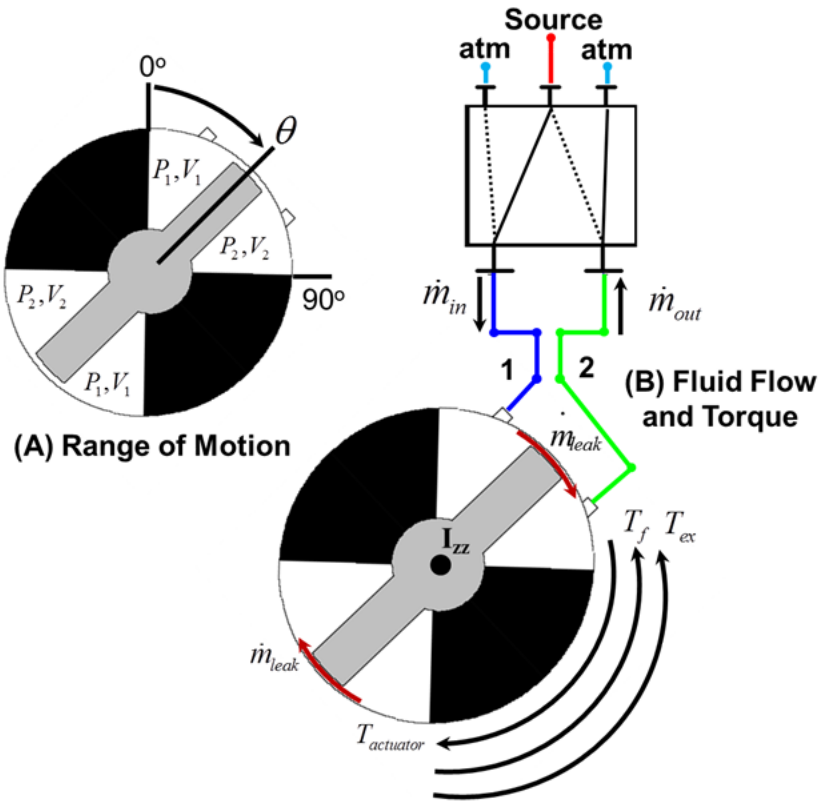

Figure 5.3 *The PPAFO pneumatic actuation system included a dual-vane rotary actuator, a solenoid or proportional valve, pneumatic lines, and the AFO footplate (not shown). The solid lines in the valve indicate the connected configuration. Port 1 is connected to the source (regulated CO_2 bottle) Port 2 is connected to atmosphere. Pneumatic pressure builds in chamber 1, while chamber 2 remains at atmospheric pressure. The resulting pressure differential creates rotational actuator torque (clockwise). Hard stops prevent the vane from rotating more than 90 degrees. Leakage occurs between chambers ($\dot{m}_{leak}$). Additional symbols are defined in the text.*

The actuator torque was approximated by the following equation [67],

$$T_{actuator} = (P_1 - P_2)K_{actuator} \ , \qquad (5.2)$$

where $K_{actuator}$ is the experimentally determined torque-to-pressure ratio for the rotary actuator, and P_1 and P_2 are the pressures in the two actuator chambers, respectively. The instantaneous pressure in a given chamber was calculated using the ideal gas law,

$$P_i = \frac{m_i}{V_i M} RT, \text{ for } i = 1, 2 . \quad (5.3)$$

In Eqn. (5.3), V_i is the volume of the actuator, m_i is the mass of CO_2 in the chamber and pneumatic lines, M is the molecular weight of CO_2 (44 g/mol), R is the universal gas constant (8.314 J/(K·mol)), and T is the temperature of the gas (room temperature 298 K, constant due to isothermal assumption). The chamber volume can be expressed as a function of vane angle θ:

$$V_1 = B_{vane}\theta , \quad (5.4)$$

$$V_2 = B_{vane}(\pi / 2 - \theta) , \quad (5.5)$$

where B_{vane} is the volume-to-angle ratio for the rotary actuator.

The mass of CO_2 in each actuator chamber at a given time is calculated by integrating the mass flow rate $\dot{m}$ and is used to determine the pressures P_1 and P_2. The mass flow into and out of each actuator chamber was driven by pressure differentials within the system (P_{up} and P_{dn}) and was divided into two regimes (choked/non-choked) depending on the upstream and downstream pressures:

choked flow: $$\frac{P_{up}}{P_{dn}} > \left(\frac{k+1}{2}\right)^{\frac{k}{k-1}} = 1.832 ,$$

non-choked flow: $$\frac{P_{up}}{P_{dn}} < \left(\frac{k+1}{2}\right)^{\frac{k}{k-1}} = 1.832 ,$$

where $k = 1.3$ for CO_2, and P_{up} and P_{dn} are upstream and downstream pressure, respectively. Orifice plate flow theory was used to model the mass flow rate [68]. When the choked flow condition was satisfied, the mass flow rate was defined as,

$$\dot{m} = f(P_{up}, P_{dn}, A) = C_d A C_1 P_{up}, \quad (5.6)$$

where $C_1 = \sqrt{\frac{kM}{RT}\left(\frac{2}{k+1}\right)^{(k+1)/(k-1)}} = 0.00281$, C_d is the discharge coefficient, and A is the orifice cross-sectional area. When the non-choke condition was satisfied, mass flow rate was defined as

$$\dot{m} = f(P_{up}, P_{dn}, A) = C_d A C_2 P_{up}\left(\frac{P_{dn}}{P_{up}}\right)^{1/k}\sqrt{1-\left(\frac{P_{dn}}{P_{up}}\right)^{(k-1)/k}}, \quad (5.7)$$

where $C_2 = \sqrt{\frac{2kM}{RT(k-1)}} = 0.0124$. The mass flow rate for our system, Eqn. (5.7), was a function of upstream pressure P_{up}, downstream pressure P_{dn}, and the cross sectional area of flow restrictions [68, 69]. The coefficient A describes the equivalent orifice plate cross-section area and was the same for both Eqn. (5.6) and Eqn. (5.7). The mass flow in the PPAFO came from three main sources: from the power source through the valve into one side of the actuator chamber $\dot{m}_{in}$, leakage from one chamber to another (across the actuator vane) $\dot{m}_{leak}$, and flow out of the actuator from the second chamber $\dot{m}_{out}$. Relationships for these mass flows can be shown as:

$$\dot{m}_{out} = f(P_2, P_{atm}, A_{valve}), \quad (5.8a)$$

$$\dot{m}_{in} = f(P_{source}, P_1, A_{valve}), \quad (5.8b)$$

$$\dot{m}_{leak} = f(P_1, P_2, A_{leak}), \qquad (5.8c)$$

$$\dot{m}_1 = \dot{m}_{in} - \dot{m}_{leak}, \qquad (5.9a)$$

$$\dot{m}_2 = -\dot{m}_{out} + \dot{m}_{leak}, \qquad (5.9b)$$

where P_{source} is the pressure at the supply (CO_2 bottle), A_{valve} is the cross-section area of the fully opened proportional valve orifice (a different A_{valve} was used for the solenoid valve), and A_{leak} is the equivalent cross-section area of the leakage pathway across the actuator vane. In Eqns. (5.8a), (5.8b), and (5.8c), $\dot{m} = f(P_{up}, P_{dn}, A)$ has the corresponding values of P_{up}, P_{dn}, and A.

Finally, the friction torque T_f from Eqn. (5.1) can be expressed as,

$$T_f = \begin{cases} T_{f,static} & \text{if } \dot{\theta} = 0 \\ -sign(\dot{\theta}) \cdot T_{f,dynamic} & \dot{\theta} \neq 0 \end{cases}, \qquad (5.10)$$

where $T_{f,static}$ is the static frictional torque. $T_{f,static}$ is equal and opposite the net actuator torque as long as its value falls below the experimentally determined maximum torque, $T_{static,\max}$. Once the actuator torque exceeds $T_{static,\max}$, the vane starts to move and the dynamic frictional torque, $T_{f,dynamic}$, begins to oppose vane motion. The sign of the dynamic frictional torque, $sign(\dot{\theta})$, is determined according to the actuator direction of rotation.

5.2.2.2 Identification of PPAFO Model Parameters

Several model parameters in the above equations were identified from indirect and direct experimental measurements, 3D modeling software, and component data sheets. The actuator torque-to-pressure constant ($K_{actuator}$), the static and dynamic frictional torques of the actuator (

$T_{static,\max}$ and $T_{f,dynamic}$), and rotary damping ratio (β) were determined experimentally. To identify the parameter $K_{actuator}$, static force measurements were made using a digital scale (Berkley, IA, USA) over a 95 psig range. Three repetitions of measurements were made at increasing and decreasing 5 psig increments (Fig. 5.4 left panel).

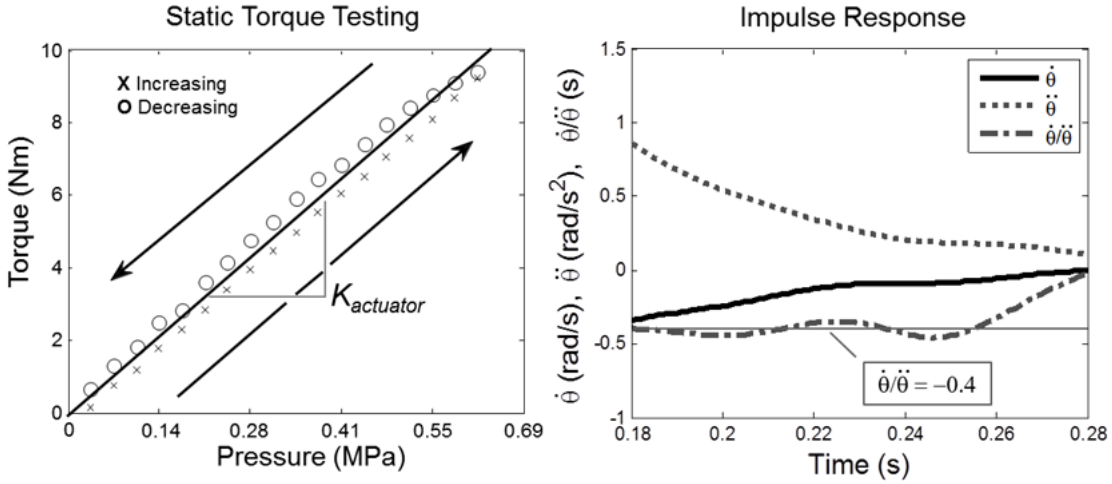

Figure 5.4 ***Left panel****: experimental determination of* $K_{actuator}$*. Measurements were taken as the pressure in the actuator chamber was increased by 5 psig (0.034 MPa) increments (denoted as* X*) to 90 psig (0.621 MPa) and then decreased by 5 psig increments back to 0 psig (denoted as* O*). The average of three sets of measurements was used to determine* $K_{actuator}$*.* ***Right panel****: experimental determination of rotary damping ratio* β*. The ratio between the angular acceleration and the angular velocity is proportional to* β*,* i.e., $\alpha/\omega = -\beta / I_{zz}$*, where* α *is angular acceleration and* ω *is angular velocity.*

The difference between the upward and downward measurements was a result of static friction. As pressure increased (denoted with an 'X'), static friction opposed vane motion reducing force measurements at the scale. The opposite effect occurred as pressure was decreased from 95 psig (denoted with an 'O') to 0 psig resulting in higher force measurements. The torque difference between data points at an equivalent pressure was twice the static frictional

torque of the actuator ($T_{static,\max} = 0.45$ Nm). The resulting nominal pressure torque (bold line) lies between the data points. The slope of this line was defined as the actuator torque-to-pressure constant ($K_{actuator} = 1.451 \times 10^{-5}$ m^3). Losses due to dynamic friction at velocities close to zero were then found using, $T_{f,dynamic} = -I_{zz}\alpha$, with $\alpha = 0.13$ rad/s^2 ($T_{f,dynamic} = 0.011$ Nm).

The PPAFO rotary damping ratio (β) was determined through a multi-step process. First, the system was positioned horizontally (with the ankle axis aligned with gravity) to minimize the impact of gravity. The parameters T_f, T_{ex}, and $T_{actuator}$ were all assumed to be equal to zero, which simplified the dynamics to

$$I_{zz}\ddot{\theta} + \beta\dot{\theta} = 0 . \qquad (5.11)$$

Next, an impulsive force was applied to the end of the footplate. The resulting angular motion was recorded using the AFO angle sensor and used to calculate the corresponding angular velocity and acceleration. The damping ratio, $\beta = 0.02$ kg·m^2/s, was approximated using the experimental data and the following equation:

$$\beta = -I_{zz} \cdot \frac{\ddot{\theta}}{\dot{\theta}} , \qquad (5.12)$$

where the moment of inertia, $I_{zz} = 0.0084$ kg·m^2, of the rotating components of the PPAFO system was calculated using 3D model software (Autodesk Inventor 2010, Autodesk, Inc. San Rafael, CA). The assumption of a constant ratio between the angular velocity and acceleration, $\dot{\theta}/\ddot{\theta} = -0.4$ determined at the end of the impulse response (Fig. 5.4 right panel), simplified the calculation.

Direct measurement of the fully open flow rate ($\dot{m}_{in} = 1.5$ g/s at 50 psig) through the valves was used to determine the parameters related to mass flow ($A_{valve} = 12.6$ mm^2 for the solenoid valve, $A_{valve} = 31.6$ mm^2 for the proportional valve, $C_d = 0.113$ s/m) used in Eqns. (5.9a) and (5.10). The parameter $A_{leak} = 0.3$ mm^2 in Eqn. (5.8c) was identified by directly measuring the mass flow rate across the vane. The mass flow rate of the leakage across the actuator vane was measured to be $\dot{m}_{leak} = 0.045$ g/s at 50 psig. Finally, the volume to angle ratio of the actuator vane ($B_{vane} = 51$ cm^3/rad) was taken from the actuator data sheet.

5.2.2.3 Simplified Model of the Leg

A simple planar two-link rigid body model was used to represent the shank and foot segment of the leg (Fig. 5.5). The motion of the model was confined to the sagittal plane, and two degrees-of-freedom were used to define allowable configurations: the segment angle of the shank (ϕ), and the ankle joint angle (θ). Note that θ describes the motion of both the PPAFO vane and the ankle joint angle.

The dynamics of the leg model were given using the well-known Euler-Lagrange formulation such that the dynamics can be expressed as,

$$\mathbf{M(q)}\ddot{\mathbf{q}} + \mathbf{C}(\dot{\mathbf{q}},\mathbf{q})\dot{\mathbf{q}} + \mathbf{G(q)} = \begin{Bmatrix} T_1 \\ T_2 + T_{ex} \end{Bmatrix}, \qquad (5.13)$$

$$\text{where, } \mathbf{q} = \begin{Bmatrix} \phi \\ \theta \end{Bmatrix}. \qquad (5.14)$$

In (5.13), $\mathbf{M(q)}$ is the inertia matrix, $\mathbf{C}(\dot{\mathbf{q}},\mathbf{q})$ is the damping matrix and contains the centrifugal and Coriolis terms, $\mathbf{G(q)}$ is the gravity vector, T_1 is the subject-generated knee joint torque, T_2

is the subject-generated ankle joint torque, and T_{ex} is the torque applied to the leg model from the PPAFO, also defined as the coupling torque in Eqn. (5.1) [70]. The physical parameters of the model are based on anthropometric measurements from a single subject: $l_{shank} = 0.46$ m, $l_{foot} = 0.18$ m, $m_{shank} = 4.5$ kg, $m_{foot} = 1.0$ kg, $I_{zzshank} = 0.1$ kg·m^2 and $I_{zzfoot} = 0.001$ kg·m^2. Experimental data from the same subject were used to calculate the shank segment states, ϕ and $\dot{\phi}$. Because the motion of the shank is prescribed, the knee joint torque (T_1) is also determined by the experimental data. Additionally, to further simplify the model, the ankle joint torque from the individual was assumed to be zero ($T_2 = 0$), simulating a 100% neuromuscular deficit. The PPAFO was used to control the motion of the foot through the applied torque T_{ex}. Equations (5.1) and (5.13) were then used to solve for θ.

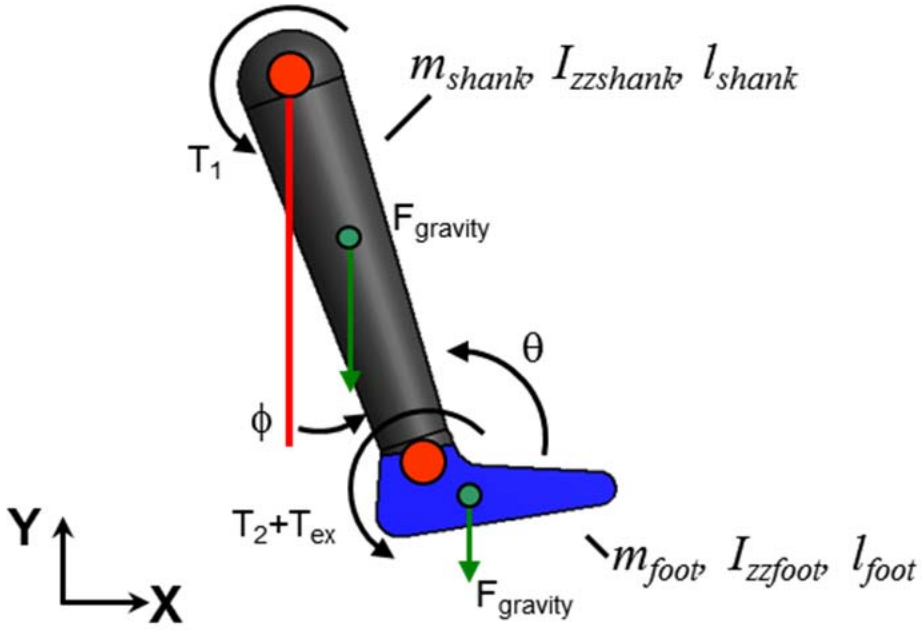

Figure 5.5 *The two-link rigid body leg model is coupled to the PPAFO through the applied external torque* T_{ex}.

5.2.3 PPAFO-Leg Model Validation

A step response was used to experimentally validate the coupled open-loop models of the system. Both hardware configurations were considered during the validation. A step response was selected because it is typical of the simplified functional tasks that will be used to evaluate system performance in Section 5.3.3. For both system configurations, the source pressure was set to 60 psig, and the PPAFO moved across the entire range of motion. The general trends seen in the experimental data for both the position and pressure response of the system matched the simulated results well. Representative results from the proportional valve are shown in Fig. 5.6.

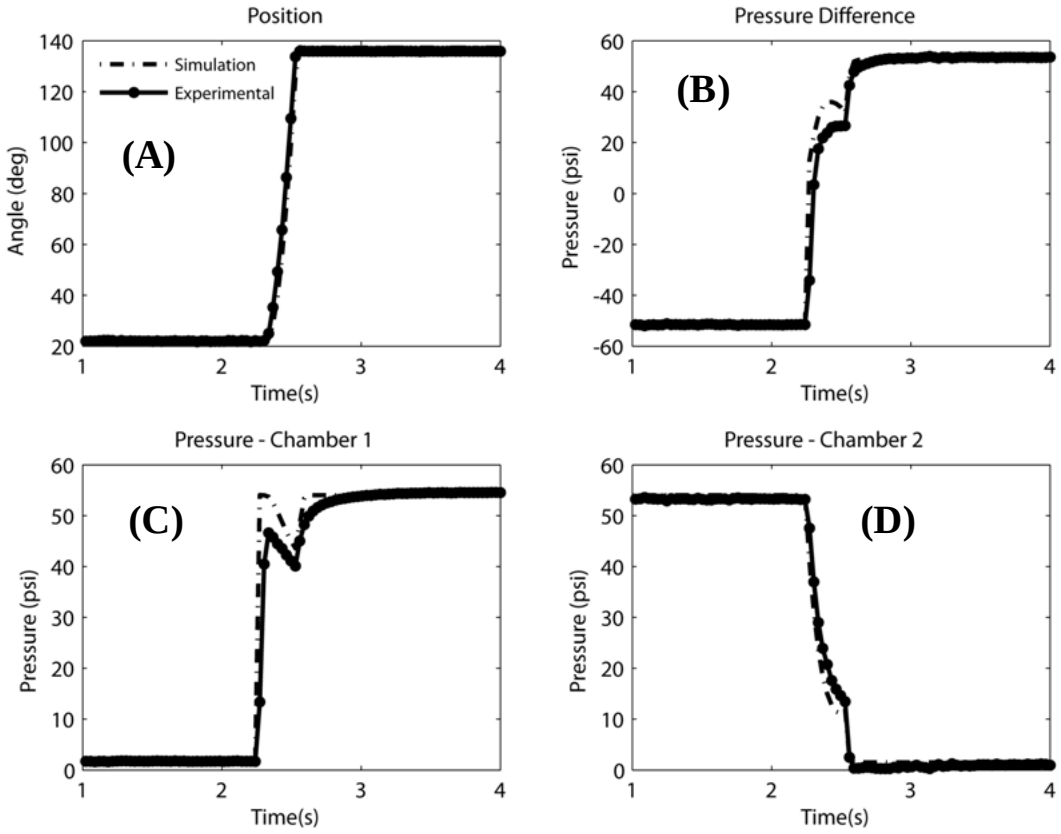

Figure 5.6 *Simulated and experimental open-loop coupled PPAFO-Leg system response to a step function with the proportional valve. (A) The vane angle increased through the actuator's full range of motion (110 deg); (B) the pressure differential driving the actuator; (C) the pressure response in the first chamber (P_1); (D) the pressure (P_2) in the second chamber fell as the vane rotated. Experimental and simulated results compare well.*

As can be seen from the figure, the pressure initially increased inside Chamber 1 until the vane's maximum static friction ($T_{static,\max}$) was exceeded and the vane began to move (Fig. 5.6 (A)). At this point, the pressure in Chamber 1 decreased as the volume, V_1, was increased by the moving vane. This lasted until the vane rotated to the other side of the actuator and stopped.

After the vane ceased moving, the pressure in Chamber 1 increased to the source pressure and stabilized (Fig. 5.6 (C)). On the other hand, the pressure in Chamber 2 (Fig. 5.6 (D)) began at the source pressure and fell when the valve was opened. As the vane moved, the rate at which the pressure was dropping briefly slowed. This rate reduction was due to the compression of the CO_2 in Chamber 2, which occurred briefly before equalizing to atmospheric pressure. The agreement between the model predicted results and the experimental results for the PPAFO are of particular note because they illustrate the fidelity of the model. Slight differences between the predicted and experimental response of the pressure indicate the potential presence of system dynamics that were not captured by the simplified model.

5.3 Model-Based System Analysis and Control Design

The models derived and validated in Section 5.2 were used to evaluate the new hardware configuration and control scheme (Fig 5.7) that seek to address performance and efficiency limitations in the current PPAFO system. Three simplified tasks that emulate ankle function during gait were selected to evaluate the performance and efficiency of the different system configurations.

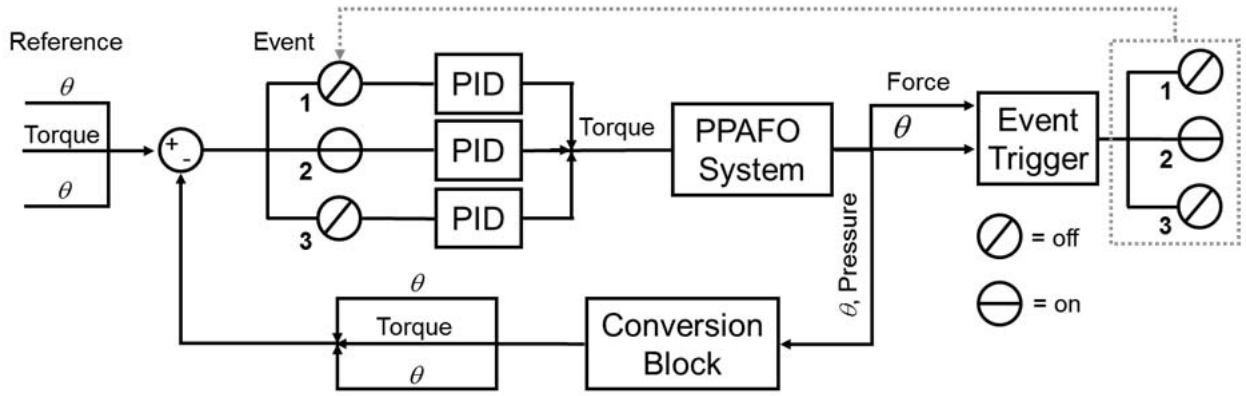

Figure 5.7 *Proposed control architecture that makes use of separate PID controllers to accomplish three functional gait tasks by tracking different variables.*

5.3.1 Description of Functional Tasks Required for Gait

5.3.1.1 Ankle Function during Gait

Walking consists of cyclic motion patterns that are divided into gait cycles beginning and ending at consecutive ground contacts (heel strikes) of the same limb. Each cycle can be further subdivided into phases corresponding to the functional tasks required for gait [1]. The ankle joint plays an important role in these functional tasks. At the initiation of the gait cycle, during loading response, the muscles that power the ankle are used to decelerate the foot to foot flat preventing foot slap [6]. During mid and terminal stance, plantarflexor torque generated at the ankle is used for forward propulsion [7, 8]. Finally, during swing, dorsiflexor muscles of the ankle joint are used to control the motion of the foot to maintain toe clearance, preventing foot drop, as the swing leg is advanced [1]. Lower limb pathology or injury that impairs the dorsi and/or plantarflexor muscles of the ankle joint has the potential to disrupt some or all of these functional

tasks. In the next section, the role of the ankle joint was simplified to three key functional tasks that were used to assess PPAFO performance.

5.3.1.2 Simplified Functional Tasks Used for System Comparisons

Three control objectives were defined for the PPAFO system: (1) motion control of the foot at heel strike to prevent foot slap, (2) torque control during stance to aid propulsion, and (3) position control during swing to prevent foot drop (Fig. 5.8 (A)-(B)). Experimental testing of the PPAFO was performed on a test fixture consisting of a rigid aluminum stand, and a mock leg and shank with rotational freedom at the ankle and knee joints. The inertial properties of the mock leg were based on anthropometric data from a healthy male subject and matched the parameters used with the simplified leg model presented in Section 5.2. A test fixture was used because it provided a more controlled environment for the system evaluation than a human subject.

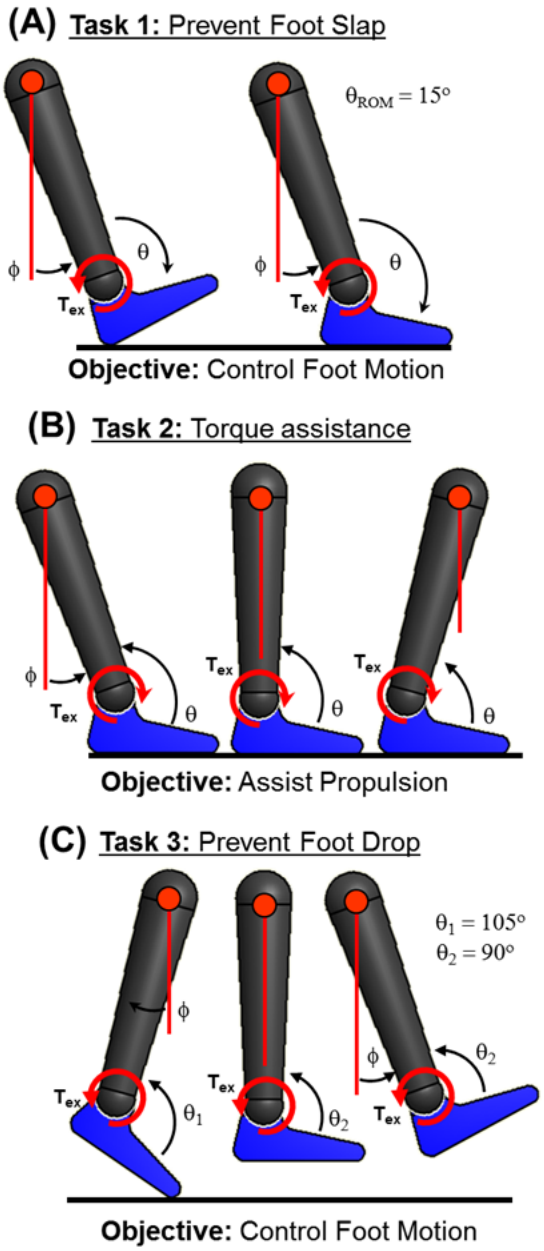

Figure 5.8 *The coupled model was used to compare the performance and efficiency of PPAFO hardware configurations and associated control algorithms during three functional tasks: (A) prevention of foot slap, (B) propulsive torque assistance, and (C) prevention of foot drop.*

In Task 1, the PPAFO was used to control the motion of the foot at initial contact (Fig. 5.8 (A)). Following ground contact at heel strike, the foot continues to rotate around the ankle

joint until it is flat on the ground. Joint impairment can lead to an uncontrolled motion that results in an audible slap when the forefoot contacts the ground (foot slap). During this task, the control objective was to track an angular position reference trajectory designed to bring the foot to the ground at a constant velocity. For simplification, the shank angle was assumed to be held at a constant angle.

In Task 2, the PPAFO provided assistive plantarflexor torque for propulsion assistance during stance (Fig. 5.8 (B)). In this task, the PPAFO was used to track a torque profile consisting of a ramp and a step function. This simplified profile emulated the behavioral trend seen in torque profiles from healthy walkers. For simplification, the entire foot segment remained in contact with the ground for the duration of the task.

The objective of Task 3 was to prevent the foot from dropping below neutral (90 degrees) during swing (Fig. 5.8 (C)). The foot was initially plantarflexed 30 degrees to correspond to an approximate configuration of the foot at the stance-swing transition. Next, the PPAFO was used to hold the foot at its neutral 90 degree position in order to prevent foot drop.

5.3.2 PPAFO Control Design

Having identified three key functional tasks, a control approach capable of achieving these tasks was designed. For simplicity and ease of implementation, PID controllers were used to control the proportional valve during the functional tasks. The controllers had the form,

$$C(s) = k_p + k_i \frac{1}{s} + k_d s\,, \qquad (5.15)$$

where k_p is the proportional gain, k_i is the integral gain, and k_d is the derivative gain. These gains were determined through heuristic tuning for each task. The control objectives in Task 1

included controlling the motion of the foot at initial contact, minimizing the tracking error between the PPAFO angle and the reference angle, and designing the system to meet specific performance requirements in terms of response time and overshoot of the PPAFO angle. In Task 2, the control objectives consisted of generating plantarflexor torque for propulsion assistance during stance and minimizing the root mean square (RMS) tracking error between the PPAFO torque and a desired reference torque. Lastly, the control objectives for Task 3 involved controlling the position of the foot during swing, minimizing the tracking error between the PPAFO angle and the desired angle, and meeting specific design requirements such as response time and overshoot of the PPAFO angle. Values for these heuristically-determined PID controller gains are given in Table 5.1. The same gains were used to generate both simulated and experimental results.

Table 5.1 *Proportional valve PID gains for the three task controllers.*

	K_p	K_i	K_d
Task 1	0.045	0.05	0.0052
Task 2	0.095	0.25	0.006
Task 3	0.045	0.05	0.0052

The solenoid valves were controlled in a binary manner. If the control signal (U) was greater than zero, dorsiflexor torque (T_o) was applied to the actuator. If the control signal was less than zero, plantarflexor torque ($-T_o$) was applied. T_o is the maximum torque that the actuator can generate at a given source pressure. This can be shown mathematically as,

$$T_{actuator} = \begin{cases} T_o & \text{if } U > 0 \\ -T_o & \text{if } U < 0 \\ 0 & \text{if } U = 0 \end{cases}. \qquad (5.16)$$

5.3.2.1 Performance Parameters

To compare the two valve configurations, as well as the modified PID control architecture, the following system performance parameters were examined: root mean square (RMS) errors between the reference and system outputs for assistive torque, angular position, and angular velocity of the PPAFO; response time and overshoot of angular position; and CO_2 consumption. After tuning the controllers to maximize system performance during the functional tasks, the system that consumed the least stored energy (CO_2) was considered the more efficient.

5.3.3 Experimental and Simulation Results

During the experimental analysis of the two system configurations, the functional tasks were each performed separately. The RMS tracking errors from the experimental results illustrated that the proportional valve significantly outperformed the solenoid valves in all three tasks, Table 5.2. This was especially apparent during Tasks 1 and 3 where the RMS errors for the proportional valve were decreased 91% and 86% over the solenoid valve, respectively. Additionally, the experimental CO_2 consumption was sizably smaller, up to 91%, across the three tasks, Table 5.2.

Table 5.2 *Performance of the proportional and solenoid valves during the three functional tasks.*

Functional Task	Valve Type	RMS Tracking Error	CO_2 Consumption
Task 1: Angular Reference	Solenoid	33.9 (deg)	2.0 (g)
	Proportional	3.0 (deg)	0.1 (g)
Task 2: Torque Reference	Solenoid	16.0 (Nm)	1.1 (g)
	Proportional	13.7 (Nm)	0.4 (g)
Task 3: Angular Reference	Solenoid	45.2 (deg)	6.5 (g)
	Proportional	6.3 (deg)	0.3 (g)

5.3.3.1 Task 1: Motion Control of the Foot to Prevent Foot Slap

The goal of Task 1 was to control the motion of the foot after heel contact. The solenoid valves showed poor performance throughout the task as illustrated by the 91% increase in experimental RMS error as compared to the proportional valve. The source of these errors can be seen in the top panel of Fig. 5.9 as oscillatory behavior, which was unable to track the reference trajectory. On the other hand, the use of the proportional valve resulted in improved tracking performance throughout the task (bottom panel of Fig. 5.9). An additional benefit of the proportional valve was the reduced CO_2 consumption. The proportional valve consumed approximately 95% less CO_2 than the solenoid valves.

While the use of a proportional valve significantly improved the system performance, there were a few disadvantages that should be discussed. Although the system did display a relatively slow setting time to steady-state, the main disadvantage of the proportional valve was the 0.2 s delay at the initiation of the ramp transition, Fig. 5.9 bottom panel. This delay could be due to either the slow sampling rate or a physical limitation of this particular valve. Further investigations must be conducted in order to determine the cause of this delay. It is worth noting that delays may also have been present in the response of the solenoid valves, but the oscillatory behavior of the system made this difficult to observe.

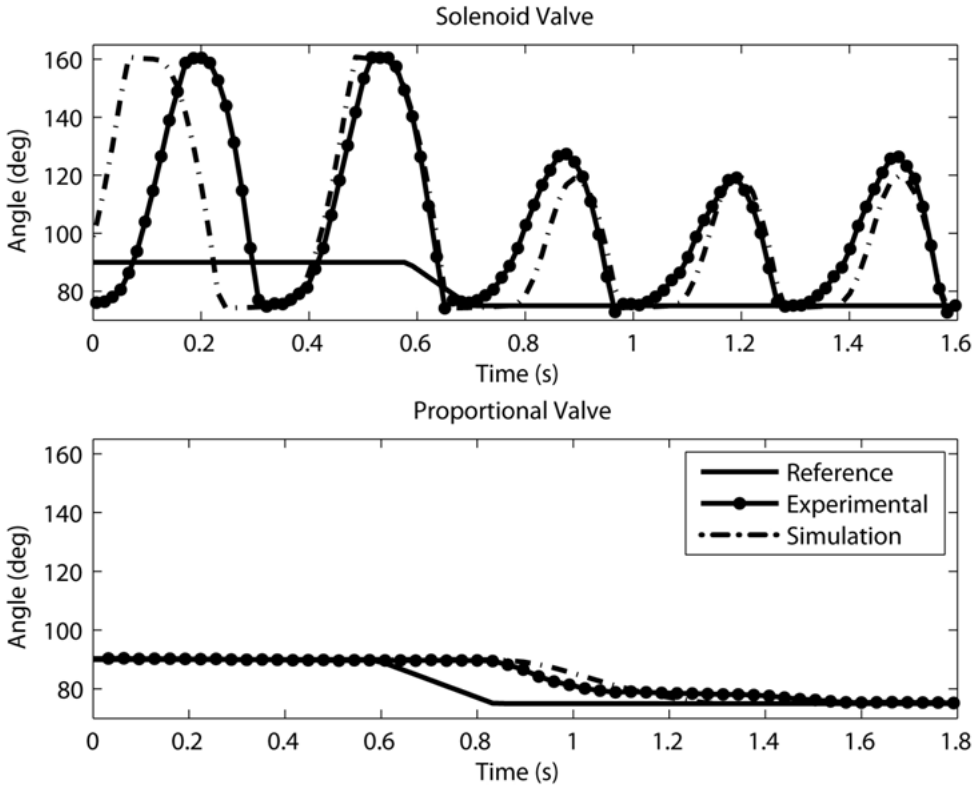

Figure 5.9 *Experimental and simulation results during functional task 1, motion control of the foot during initial contact to prevent foot slap. The proportional valve (bottom panel) significantly outperformed the solenoid valve (top panel) during this task. Note that simulated results capture the behavior of the system and are comparable to the experimental results.*

5.3.3.2 Task 2: Torque Assistance During Stance

In Task 2, the PPAFO was used to provide an assistive plantarflexor torque for propulsion assistance during stance. Although the 15% improvement in RMS tracking error was a smaller performance gain than seen in Task 1, the proportional valve still outperformed the solenoid valve. Additionally, the oscillatory behavior displayed by the solenoid valves during the initial ramp portion of the trajectory illustrated poor system performance that would not be desirable during actual implementation with an impaired subject, Fig. 5.10 top panel. The

experimental results also demonstrated that the proportional valves had lower CO_2 consumption (63% less) than the solenoid valve.

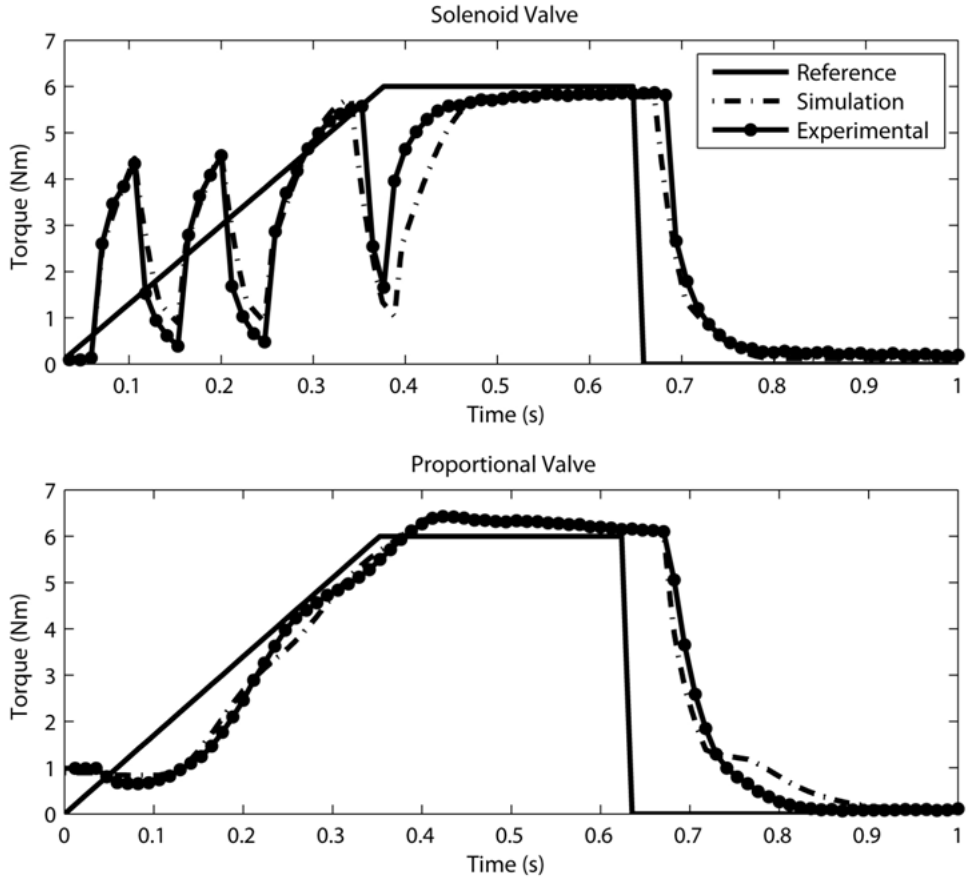

Figure 5.10 *Experimental and simulation results for both valve configurations during the second task, propulsive torque assist during stance. The system configured with the proportional valve (bottom panel) tracked the reference trajectory better than the solenoid valve (top panel), particularly during the initial ramp. The simulated results for both valve configurations agree well with the experimentally collected data.*

5.3.3.3 Task 3: Motion Control during Swing to Prevent Foot Drop

The objective during Task 3 was to control the position of the foot to maintain toe clearance during swing. The proportional valve was able to track the reference trajectory

reasonably well, while the solenoid valve once again displayed oscillatory behavior and failed to perform this task, Fig. 5.11.

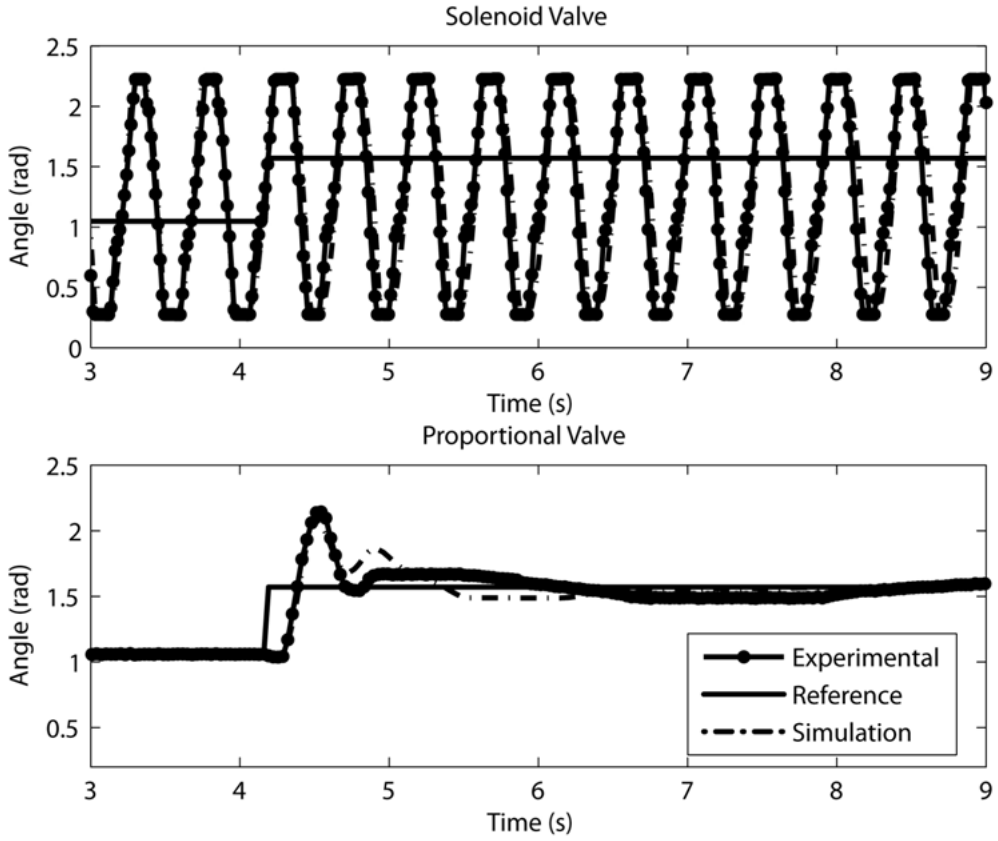

Figure 5.11 *Experimental and simulation results for the third functional task, motion control of the foot during swing to prevent foot drop. The solenoid valve (top panel) was not able to track this reference input. The proportional showed some difficulties, as evident by the large overshoot and long settling time, but had much better performance as compared to the solenoid valve. Both the modeled systems show good agreement with the experimental results.*

As with Tasks 1 and 2, the proportional valve tracked the reference better than the solenoid valves during the experimental trials with an 86% smaller RMS tracking error. Additionally, the proportional valve consumed 95% less CO_2 during this task. Although the proportional valve resulted in improved performance over the solenoid valves, it still displayed a

0.2 s delay, had an overshoot of 30 degrees, and required several seconds to settle to steady-state (Fig. 5.11 bottom panel). Again, delays may have been present in the response of the solenoid valves, but the oscillatory behavior of the system made this difficult to observe.

5.4 Discussion

Efficient and effective control of a powered AFO is crucial to maximizing the assistive benefit that an impaired user receives from the device. This work has emphasized that models that accurately approximate the behavior of an AFO system are central for effective control design. Additionally, this chapter again highlighted that accurate models facilitate the analysis of a system and its subsystems for use in improved system design.

Accordingly, the PPAFO system model derived in this work was used to design a new control architecture and to evaluate the performance of both the current and modified PPAFO hardware configurations. The implementation of a proportional valve and new control methodology in the modified PPAFO system addressed two critical limitations identified in the current system: (1) an inability to generate intermediate levels of torque for assistance and motion control, and (2) high pneumatic power consumption caused by inefficient actuation.

The simulated and experimental results demonstrated that limitations in the current hardware configuration prevented the system from meeting the control objectives of Task 1 and Task 3. Further, this configuration only marginally met the objectives defined for Task 2. The performance of the solenoid valves was severely limited by the component-driven 20 Hz switching frequency. The slow switching frequency introduced significant delays that resulted in oscillatory behavior during the tasks, particularly those that required positional reference tracking. While these performance results clearly indicated the inability of the solenoid valves to

provide fast enough modulation for accurate torque or position tracking, this valve was originally selected for use in the system due to its size and cost. Although the valve did show comparatively effective assistance with respect to the original control objective of providing constant torque during the gait cycle, these additional results indicated the need for improved hardware.

The performance benefits from the proportional valve were apparent in the simulated and experimental results of Tasks 1 and 3. Unlike the solenoid valves, the proportional valve has the functional capability to modulate the system torque in order to track a changing reference. The use of the proportional valve with the system resulted in significant improvements in RMS tracking error over the solenoid valve, up to a 91% decrease. The proportional valve was also significantly more efficient, consuming 91% less CO_2 over the course of the three tasks. While the simulated and experimental results demonstrated that the proportional valve addressed the limitations in the current system, these results also highlighted certain areas for improvement in the modified design. Specifically, the delay in the actuation of the proportional valve is of particular concern, Figs. 5.9-5.11. Lengthy system delays could be particularly problematic for an assistive device because of the potential for an incorrectly timed control action that could disrupt gait. Additional disadvantages of proportional valves are the current size and weight of the valves and the control electronics, which do not make this valve very conducive to a portable compact device.

5.5 Conclusion

This chapter addressed limitations in the performance and efficiency of the current portable powered ankle-foot orthosis (PPAFO) through the introduction of new hardware and

control schemes. Simulation and experimental results demonstrated that the use of a proportional valve, in place of solenoid valves, resulted in both significant performance and efficiency gains during three representative gait tasks. The improved system performance will increase the effectiveness of the PPAFO during gait assistance, while the enhanced efficiency will translate directly to increased duration of use. Improved performance and efficiency are crucial to transitioning the PPAFO system from a laboratory tool into a practical human assist device. Future work will seek to explore advanced control strategies for enhanced system performance in assisting impaired subjects.

Chapter 6
CONCLUSIONS AND FUTURE DIRECTION

6.1 Conclusions

Compact, lightweight, and efficient portable powered ankle-foot orthoses (PPAFOs) will expand treatment and rehabilitation opportunities for individuals with impairments to the ankle joint complex. For daily-wear applications, this improvement would result from the ability of the PPAFO to accommodate a variety of functional deficits by providing torque assistance at the joint; a need that currently prescribed passive ankle-foot orthoses (AFOs) cannot address. Additionally, using powered AFOs in a rehabilitation environment will increase the pool of people who can benefit from these devices; ranging from impaired individuals with permanent deficits to anyone recovering from an acute ankle injury. PPAFOs would also enable in-home rehabilitation. In-home rehabilitation allows a clinician to prescribe daily physical therapy routines that require use of the device at home rather than at a clinic, further expanding the potential benefits. Unfortunately, the current state-of-the-art designs for powered AFO systems include tethers that limit the operation of these devices to the labs or clinics in which they were developed. To address the need for portable powered AFOs, this dissertation focused on the development, characterization, modeling, and experimental validation of a novel portable powered AFO (PPAFO). The PPAFO developed in this work aimed to fill the gap in current

orthotic technology through the creation of an untethered assist device for flexible rehabilitation both in the clinic and at home.

Chapter 1 introduced and motivated the need for AFOs in the treatment of lower limb muscle impairments that affect gait functionality. This chapter also divided current AFO technology into three groups: passive, semi-active, and active AFO systems. A detailed review of state-of-the-art AFO systems was then presented in Chapter 2. This review served to highlight a gap in current AFO technology, the lack of a portable powered AFO, and identified technological challenges facing the development of such a system. Specifically, the design must minimize the size and weight of the device, while simultaneously increasing the efficiency of the power supply and actuators to meet assistance and longevity requirements. The conclusions from Chapter 2 motivated and directed the design of the PPAFO presented in Chapter 3.

Chapter 3 introduced the design of the novel assistive device and provided an initial characterization of system performance. The PPAFO uses fluid power combined with a portable power supply, a belt worn CO_2 bottle, to provide a flexible platform for gait assistance. The direction (dorsi or plantar), timing, and magnitude of assistance are modulated based on subject specific needs. Gait assistance requires high forces applied at a low velocity during a given cycle. This characteristic makes the use of a high-force low-velocity fluid power actuator particularly advantageous for this application. Additional benefits to using fluid power in place of an electro-mechanical solution are the ability to actuate a joint without a transmission and transport energy from the power supply with flexible lines. The fluid power lines provide increased flexibility for component placement and allow the power supply to be worn on the body, thereby reducing the weight at the shank and foot. In the pilot data presented in Chapter 3, results from both healthy walkers and an individual with plantarflexor impairment demonstrated

the device's functionality. The controlled torque from the PPAFO allows the orthosis to meet an individual's functional requirements, while the portability of the device expands its uses for rehabilitation.

Although this pilot data demonstrated that the PPAFO is capable of providing functional assistance, the quantification of the PPAFO's ability to assist gait requires further examination. To address this, additional data from 1 impaired and 2 healthy subjects were collected and presented in Chapter 4. This expanded data set was used to evaluate PPAFO performance during two walking scenarios: (1) a speed perturbation to the gait of healthy walkers, and (2) applied functional assistance for individuals with both plantarflexor and dorsiflexor impairments during level treadmill walking. These particular case studies provided insight about the sensitivity of the system to a common gait perturbation, such as changing walking speeds, and demonstrated the PPAFO's ability to provide a range of functional assistance. The performance of the PPAFO during the tasks was evaluated with traditional metrics such as time and distance measures and joint moments and powers, as well as new gait analysis techniques that quantify changes in bilateral symmetry, complexity, and variability during gait. These additional metrics offered increased insight into both kinematic and kinetic changes present in a subject's gait due to PPAFO assistance. The results from this chapter demonstrated that the PPAFO is capable of providing functional assistance for both dorsiflexor and plantarflexor impairments. However, these results also highlighted performance limitations associated with the hardware (e.g., the solenoid valve), as well as the use of a threshold for event detection. The solenoid valve, while inexpensive and easy to implement, resulted in the PPAFO's inability to efficiently and effectively meet the functional requirements for gait assistance.

In an effort to address the performance and efficiency limitations associated with the solenoid valves, Chapter 5 presented a model-based system analysis technique for new hardware configuration and improved control design. This chapter addressed two critical system limitations created by the solenoid valves from the current system: (1) an inability to generate intermediate levels of torque for assistance and motion control, and (2) high pneumatic power consumption caused by inefficient actuation.

Modeling and simulation results demonstrated that a proportional valve would enable the PPAFO to more effectively meet the control objectives required for functional gait assistance. Experimental results validated that the use of a proportional valve, in place of solenoid valves, resulted in both significant performance and efficiency gains during three representative gait tasks. The improved system performance increased the effectiveness of the PPAFO during the completion of the representative tasks, while the enhanced efficiency translated directly to increased duration of use for the portable system. The work in Chapter 5 highlighted the benefits of a system model that accurately approximates the behavior of the AFO system, particularly with regard to effective control design. Future work will continue to be directed towards transitioning this first generation system into a robust, viable device capable of meeting demanding system requirements during both rehabilitation (short term goal) and as an effective daily-wear assist device (long term goal). Along these lines, a patent application covering the technology embodied by the PPAFO described in this dissertation has been filed [71].

6.2 Future Work

Improved performance and efficiency are crucial to transitioning the PPAFO from a laboratory tool into a practical human assist device. The results from Chapter 5 demonstrated

that modifications to system hardware along with improved control schemes can result in both performance and efficiency gains. These results serve as a promising starting point and future work should continue to be focused on improvements to both system hardware and enhanced control algorithms. This section will detail potential avenues for future work and promising efforts along these lines that have already been initiated.

6.2.1 Improving the Efficiency of the Current System

In order to be used effectively as an assistance or rehabilitation tool, powered AFOs must be capable of continuous use for extended periods of time. In Chapter 3, the longevity of the current PPAFO configuration, with a 9 oz CO_2 bottle, was found to be ~40 min. To improve the viability of the PPAFO as a rehabilitation tool, the longevity of the system must be increased by identifying and addressing inefficiencies in the system. Along these lines, we have taken a systematic approach for the evaluation of the energy efficiency of the PPAFO [72]. Preliminary work presented in [72] identifies changes that can be made to system components, as well as how the PPAFO is operated. These changes have the potential to result in significant improvements to overall system efficiency. Future work should be directed towards implementing these changes on the actual system and evaluating the efficiency improvements during gait.

6.2.2 The Next Generation PPAFO System

Reducing the overall size and weight of the system will minimize the energetic impact on the wearer. To address this issue, the development of the second generation (Gen2) PPAFO is currently being conducted in parallel with the work presented in this dissertation. This work has been performed in conjunction with collaborators from the Center for Compact and Efficient

Fluid Power (CCEFP) and is focused on reducing the weight of the orthosis to less than 1 kg through integration and co-design of PPAFO system components. The Gen2 PPAFO system has been assembled and bench top testing is currently underway. Future work should be directed towards the experimental evaluation of the device with both healthy and impaired walkers.

6.2.3 Improved Control of the PPAFO

In this dissertation, control of the PPAFO during gait was divided into two parts: (1) gait event detection to determine the PPAFO control objects for different phases of the gait cycle, and (2) controlling the applied torque to meet the functional objectives from part (1). Continuing to improve the approaches used to address both parts of the control problem will result in improvements to overall system performance.

6.2.3.1 Improved Event Detection

Although control timing based on sensor detected gait events has been used both in this work as well as by others to control powered AFOs, additional improvements to event detection need to be explored [30, 31]. Utilizing techniques commonly applied in machine learning that leverage information available from both the AFO sensors and the cyclic nature of gait presents one promising avenue. Along these lines, work on the design of an event detection strategy during level walking that does not rely on direct sensor event detection has begun [73]. The approach described in [73] computes a state estimate that represents the location of the individual in the gait cycle based on PPAFO sensor measurements (two force sensors and an angle sensor). This approach takes advantage of a high degree of correlation between gait cycles in order to compute a state estimate based on maximizing the cross-correlation between a window of past sensor measurements and a reference model learned from training data. In the future, this

improved event detection strategy should be implemented during PPAFO subject testing to improve event detection and allow increased flexibility for the definition of boundaries that determine the functional objectives for the PPAFO.

6.2.3.2 Improved Control Design

Chapter 5 demonstrated potential performance and efficiency improvements from changes to both system hardware and control strategies during representative gait tasks on a testbed comprised of a representative replica of a shank and foot. Future work should be directed towards implementing these improvements during active walking with a human subject to validate these performance benefits. Additionally, advanced control schemes should be considered in order to improve overall system performance.

Improved feedback and feedforward controllers could be constructed to take advantage of inherent characteristics of gait. For example, the cyclic nature of gait with its high correlation between cycles would lend itself well to repetitive control schemes. Control algorithms could also be used to improve the robustness of the system to varying walking conditions and changes in patient behavior. Adaptive control strategies should be explored to improve system performance in the presence of these types of disturbances. The functional control objectives defined in this work all dealt with a single functional task, level walking. Future control algorithms must be able to accommodate different functional impairments and a variety of walking modes (e.g., level walking, ramp walking, stair walking) in a changing walking environment. Switched systems, gain scheduling, bumpless transfer, and model predictive control are some of the most relevant control methodologies that offer the potential to address these control needs.

6.2.4 Continued Subject Testing

The PPAFO was evaluated in a controlled laboratory environment during level walking. Continued testing outside of the lab is needed before the PPAFO is ready for in-home subject rehabilitation and treatment. Additional testing with impaired subjects should also be done. Assessing the quality of the functional assistance during experimental trials will continue to advance hardware and software design. Additionally, feedback from the user in terms of fit, weight, appearance, and overall impression of the device is very important for effective design refinements.

Logistical challenges related to the use of the PPAFO as an in-home rehabilitation device must also be considered. These challenges include, but are not limited to, devising an effective method for determining and implementing a subject specific AFO "prescription" for continued rehabilitation, replenishing empty CO_2 bottles on the fly, and evaluating whether the PPAFO is easy to use and robust enough for everyday use. Additional subject testing combined with a user-based design approach will help to guarantee the creation of a simple, robust, and user-friendly assist device.

LIST OF REFERENCES

1. Perry, J., *Gait Analysis: Normal and Pathological Function*. 1992, Thorofare, NJ: SLACK Incorperated.
2. Dollar, A.M. and H. Herr, *Lower extremity exoskeletons and active orthoses: challenges and state-of-the-art*. IEEE Transactions on Robotics, 2008. **24**(1): p. 144-158.
3. *Becker Orthopedic*. 2003 [cited 2009; Available from: http://www.beckerorthopedic.com/cenfab/cfp.htm.
4. Sadeghi, H., *Local or global asymmetry in gait of people without impairments.* Gait & Posture, 2003. **17**(3): p. 197-203.
5. Waters, R.L. and S. Mulroy, *The energy expenditure of normal and pathologic gait.* Gait & Posture, 1999. **9**(3): p. 207-231.
6. Ren, L., et al., *A phase-dependent hypothesis for locomotor functions of human foot complex*. Journal of Bionic Engineering, 2008. **5**(3): p. 175-180.
7. Neptune, R.R., S.A. Kautz, and F.E. Zajac, *Contributions of the individual ankle plantar flexors to support, forward progression and swing initiation during walking.* Journal of Biomechanics, 2001. **34**(11): p. 1387-1398.
8. Winter, D.A., *Biomechanics and Motor Control of Human Movement*. Third ed. 2005, Hoboken, New Jersey: John Wiley & Sons, INC.
9. Meinders, M., A. Gitter, and J.M. Czerniecki, *The role of ankle plantar flexor muscle work during walking.* Scandinavian Journal of Rehabilitation Medicine, 1998. **30**(1): p. 39-46.
10. Simon, S., et al., *Role of the posterior calf muscles in normal gait.* The Journal of Bone and Joint Surgery, 1978. **60**(4): p. 465-472.
11. Kepple, T.M., K.L. Siegel, and S.J. Stanhope, *Relative contributions of the lower extremity joint moments to forward progression and support during gait.* Gait & Posture, 1997. **6**(1): p. 1-8.
12. Nadeau, S., et al., *Plantarflexor weakness as a limiting factor of gait speed in stroke subjects and the compensating role of hip flexors.* Clinical Biomechanics, 1999. **14**(2): p. 125-135.
13. Barnett, S., A. Bagley, and H. Skinner, *Ankle weight effect on gait: orthotic implications.* Orthopedics, 1993. **16**(10): p. 1127-31.
14. Redford, J.B., *Orthotics etcetera.* 1986, Baltimore, MD: Williams and Wilkins.
15. Rose, G.K., *Orthotics: Principles and Practice*. 1986, London: Williams Heinemann.
16. Orthopedic, B., Becker online catalog: Troy, Michigan.

17. Yamamoto, S., et al., *Development of an ankle-foot orthosis with dorsiflexion assist, part 2: structure and evaluation.* Journal of Prosthetics and Orthotics, 1999. **11**(2): p. 24-28.
18. Teyssedre, H. and G. Lefort, *Dynamic orthesis*, E.P. Office, Editor. 2005: France. p. 1-9.
19. Kitaoka, H.B., et al., *The effect of custom-made braces for the ankle and hindfoot on ankle and foot kinematics and ground reaction forces.* Archives of Physical Medicine and Rehabilitation, 2006. **87**(1).
20. Yamamoto, S., et al., *Comparative Study of Mechanical Characteristics of Plastic AFOs.* Journal of Prosthetics & Orthotics, 1993. **5**(2): p. 59-64.
21. *Tamarack Variable Assist Joint - Ankle Brace - Ankle Orthotic*. 2008 [cited 2009; Available from: http://www.tamarackhti.com/joints/variable_assist.asp.
22. Chin, R., et al., *A pneumatic power harvesting ankle-foot orthosis to prevent foot-drop.* Journal of NeuroEngineering and Rehabilitation, 2009. **6**(19).
23. Hirai, H., et al. *Development of an ankle-foot orthosis with a pneumatic passive element*. in *The 15th IEEE International Symposium on Robot and Human Interactive Communication*. 2006. Hatfield, UK.
24. Yokoyama, O., et al., *Kinematic effects on gait of a newly designed ankle-foot orthosis with oil damper resistance: A case series of 2 patients with hemiplegia.* Archives of Physical Medicine and Rehabilitation, 2005. **86**(1): p. 162-166.
25. Takaiwa, M. and T. Noritsugu. *Development of pneumatic walking support shoes using potential energy of human*. in *7th JFPS International Symposium on Fluid Power*. 2008. Toyama, Japan.
26. Yamamoto, S., et al., *Comparative Study of Mechanical Characteristics of Plastic AFOs.* Journal of Prosthetics & Orthotics, 1993. **5**(2).
27. Novacheck, T.F., et al., *Quantifying the Spring-Like Properties of Ankle-Foot Orthoses (AFOs).* Journal of Prosthetics & Orthotics, 2007. **19**(4): p. 98-103.
28. Furusho, J., et al. *Development of shear type compact MR brake for the intelligent ankle-foot orthosis and its control; research and development in NEDO for practical application of human support robot*. in *IEEE 10th International Conference on Rehabilitation Robotics, 2007*. 2007. Noordwijk, the Netherlands.
29. Svensson, W. and U. Holmberg. *Ankle-foot-orthosis control in inclinations and stairs.* in *2008 IEEE International Conference on Robotics, Automation and Mechatronics.* 2008. Chengdu, China.
30. Blaya, J.A. and H. Herr, *Adaptive control of a variable-impedance ankle-foot orthosis to assist drop-foot gait.* IEEE Transactions on Neural Systems and Rehabilitation Engineering, 2004. **12**(1): p. 24-31.
31. Boehler, A.W., et al. *Design, implementation and test results of a robust control method for a powered ankle foot orthosis (AFO).* in *IEEE International Conference on Robotics and Automation*. 2008.
32. Hwang, S., J. Kim, and Y. Kim. *Development of an active ankle-foot orthosis for hemiplegic patients.* in *Proceedings of the 1st international convention on Rehabilitation engineering & assistive technology: in conjunction with 1st Tan Tock Seng Hospital Neurorehabilitation Meeting* 2007. Singapore
33. Pratt, G.A. and M.M. Williamson. *Series elastic actuators.* in *IEEE International Conference on Intelligent Robots and Systems.* 1995.

34. Hollander, K.W., et al., *An efficient robotic tendon for gait assistance*. J. Biomech. Eng. , 2006. **128**(5): p. 788-792.
35. Hitt, J., et al. *Dynamically controlled ankle-foot orthosis (DCO) with regenerative kinetics: incrementally attaining user portability*. in *2007 IEEE International Conference on Robotics and Automation*. 2007.
36. Weber, D.J., et al., *BIONic WalkAide for correcting foot drop.* IEEE Transactions on Neural Systems and Rehabilitation Engineering, 2005. **13**(2): p. 242-246.
37. Hausdorff, J.M. and H. Ring, *Effects of a new radio frequency–controlled neuroprosthesis on gait symmetry and rhythmicity in patients with chronic hemiparesis.* American Journal of Physical Medicine and Rehabilitation, 2008. **87**(1): p. 4-13.
38. Krebs, H., et al., *A paradigm shift for rehabilitation robotics.* IEEE Engineering in Medicine and Biology Magazine, 2008. **27**(4): p. 61-70.
39. Ferris, D.P., J.M. Czerniecki, and B. Hannaford, *An ankle-foot orthosis powered by artificial pneumatic muscles.* Journal of Applied Biomechanics, 2005. **21**(2): p. 189-197.
40. Ferris, D.P., G.S. Sawicki, and A.R. Domingo, *Powered lower limb orthoses for gait rehabilitation.* Topics in Spinal Cord Injury Rehabilitation, 2005. **11**(2): p. 34-49.
41. Ferris, D.P., et al., *An improved powered ankle-foot orthosis using proportional myoelectric control*. Gait & Posture, 2006. **23**(4): p. 425-428.
42. Noel, M., et al., *An electrohydraulic actuated ankle foot orthosis to generate force fields and to test proprioceptive reflexes during human walking.* IEEE Transactions on Neural Systems and Rehabilitation Engineering, 2008. **16**(4): p. 390-399.
43. Bharadwaj, K., et al., *Design of a robotic gait trainer using spring over muscle actuators for ankle stroke rehabilitation.* Journal of Biomechanical Engineering 2005. **127**(6): p. 1009-1014.
44. Krebs, H.I. and N. Hogan, *Therapeutic robotics: a technology push.* Proceedings of the IEEE, 2006. **94**(9): p. 1727-1738.
45. Roy, A., et al. *Measurement of human ankle stiffness using the Anklebot*. in *IEEE 10th International Conference on Rehabilitation Robotics, 2007. ICORR 2007*. 2007. Noordwijk, The Netherlands.
46. Esfahani, E.T., *Developing an Active Ankle Foot Orthosis Based on Shape Memory Alloys*, in *Mechanical Engineering*. 2007, University of Toledo: Toledo. p. 161.
47. Bar-Cohen, Y. *Electro-active polymers: current capabilities and challenges.* in *Proceedings of the SPIE Smart Structures and Materials Symposium,*. 2002. San Diego, CA.
48. Wax, S.G. and R.R. Sands, *Electroactive Polymer Actuators and Devices*, in *SPIE Conference on Electroactive Polymer Actuators and Devices*. 1999: Newport Beach, California.
49. Herr, H.M. and R.D. Kornbluh. *New horizons for orthotic and prosthetic technology: artificial muscle for ambulation.* in *SPIE's Smart Structures and Materials (EAPAD)*. 2004.
50. Yamamoto, S., et al., *Development of an ankle - foot orthosis with an oil damper*. Prosthetics and Orthotics International, 2005. **29**(3): p. 209 - 219.
51. Chin, R., E. Loth, and E. Hsiao-Wecksler. *Fluid-power harvesting by pneumatic bellow during human gait*. in *8th International Symposium on Fluid Power, ASME Fluids Engineering Conference*. 2008. Jacksonville, FL.

52. Durfee, W. and Z. Sun, *Fluid power system dynamics*. 2009, University of Minnesota.
53. Stansbury, L., et al., *Amputations in U.S. military personnel in the current conflicts in Afghanistan and Iraq*. Journal of Orthopaedic Trauma, 2008. **22**(1): p. 43-46.
54. Shorter, K.A., et al., *Technologies for Powered Ankle Foot Orthotic Systems: Possibilities and Challenges.* Transactions on Mechatronics, 2009.
55. Norris, J.A., et al., *Effect of augmented plantarflexion power on preferred walking speed and economy in young and older adults.* Gait & Posture, 2007. **25**(4): p. 620-627.
56. Cai, M., K. Kawashima, and T. Kagawa, *Power Assessment of Flowing Compressed Air*. Journal of Fluids Engineering 2006. **128**(2): p. 402-406.
57. Kram, R., et al., *Force treadmill for measuring vertical and horizontal ground reaction forces.* Journal of Applied Physiology 1998. **85**: p. 764-769.
58. Byrne, C.A., et al., *Effect of walking speed changes on tibialis anterior EMG during healthy gait for FES envelope design in drop foot correction.* Journal of Electromyography and Kinesiology, 2007. **17**(5): p. 605-616.
59. Dickstein, R. and Y. Laufer, *Light touch and center of mass stability during treadmill locomotion* 2004. **20**(1): p. 41-47.
60. Siler, W.L., A.L. Jorgensen, and R.A. Norris, *Grasping the handrails during treadmill walking does not alter sagittal plane kinematics of walking.* Archives of Physical Medicine and Rehabilitation, 1997. **78**(4): p. 393-398.
61. Shorter, K.A., et al., *A Portable-Powered-Ankle-Foot-Orthosis for rehabilitation.* Journal of Rehabilitation Research & Development, Accepted 2010.
62. DiBerardino Iii, L.A., et al., *Quantifying complexity and variability in phase portraits of gait*. Clinical Biomechanics, 2010. **25**(6): p. 552-556.
63. Shorter, K.A., et al., *A new approach to detecting asymmetries in gait.* Clinical Biomechanics, 2008. **23**(4): p. 459-467.
64. Griffin, M.P., O. S.J., and I.D. McBride, *Role of symmetry in gait performance of stroke subjects with hemiplegia.* Gait Posture, 1995. **3**(September): p. 132-142.
65. Vaughan, C.L., B.L. Davis, and J.C. O'Connor, *Dynamics of Human Gait*. Second Edition ed, ed. K. Publishers. 1999, Cape Town, South Africa.
66. Becker, P., et al., *Gait asymmetry following successful surgical treatment of ankle fractures in young adults.* Clinical orthopaedics and related research, 1995(311): p. 262-269.
67. Richer, E. and Y. Hurmuzlu, *A High Performance Pneumatic Force Actuator System: Part I—Nonlinear Mathematical Model*. Journal of Dynamic Systems, Measurement, and Control 2000. **122**(3): p. 416-426.
68. Munson, B.R., D.F. Young, and T.H. Okiishi, *Fundamentals of Fluid Mechanics*. 1990, New York: Wiley.
69. Shen, X., et al., *Nonlinear averaging applied to the control of pulse width modulated (PWM) pneumatic systems.* Journal of Dynamic Systems, Measurement, and Control 2006. **128**(3): p. 7.
70. Spong, M., S. Hutchinson, and M. Vidyasagar, *Robot Modeling and Control*. 2006: John Wiley & Sons.
71. Hsiao-Wecksler, E.T., et al., *Portable Active Fluid Powered Ankle-Foot Orthosis.* 2010: United States.

72. Li, Y., et al., *Energy Efficiency Analysis of A Pneumatically-Powered Ankle-Foot Orthosis*, in *IFPE*. 2010: Las Vegas.
73. Li, Y., et al., *Estimating System State During Human Walking with a Powered Ankle-Foot Orthosis.* IEEE/ASME Transactions on Mechatronics, Submitted.